# Numerical computation of fluid properties at nano/meso scales.

Dyson, Peter

University of Wales, Swansea
Civil and Computational Engineering Centre

# Numerical Computation of Fluid Properties at Nano/Meso Scales

Peter Dyson

Supervisor: Rajesh Ransing

Submitted to the University of Wales, Swansea in fullfilment of the requirements for the degree of Doctor of Philosophy of Engineering

Swansea, 2006

*To my loving family and friends*

# Abstract

Engineering systems are increasingly being developed with dimensions within the micro to nano scale. Mature simulation schemes are available for large scale systems ($> 0.5\mu m$) in the form of continuum mechanics, and for small scale systems ($< 50nm$). However, there is to simulation scheme that covers the middle, meso scale, range between them. The work presented in this thesis focuses on the development of a computational framework focused on fluid systems on the nano-meso scale, with characteristic dimensions between 50nm and 500nm. Existing methods approach the meso scale either with approximated molecular behaviour from the 'top down', or directly modelling molecular physics from the 'bottom up'. Top down approaches have the disadvantage of only including known behaviour with some statistical variations to approximate chaotic behavior. Bottom up approaches model the fluid from a molecular physics model, but fail to capture bulk fluid behaviour and are computationally expensive.

The approach developed in this thesis, covers the middle ground between continuum and molecular simulation scales. A molecular physics model is used to govern the behaviour of the fluid, and is surrounded by a set of meso scale boundary conditions, providing an accurate and efficient fluid model. Bulk fluid behaviour is extracted in the form of ensemble property distributions in a versatile grid-like implementation, allowing the fluid properties to be calculated from first principles accurately and efficiently.

Each part of the developed method is validated separately. The physics model is compared with published results of simulations at molecular scales, as there is insufficient information for meso scale fluid systems. The bulk ensemble property collection scheme is fully explored by means of a parametric study.

Case studies are presented to highlight how bulk fluid properties, such as velocity, temperature and pressure, can be examined as distributions in time and space over the flow field in channel flow systems.

The approach developed in this thesis opens the door to accurate and efficient meso scale fluid simulation. This work has also identified the next step to widen and improve the abilities for meso scale fluids to be fully investigated.

# Declaration and Statements

### Declaration

This work has not been previously accepted in substance for any degree and is not being concurrently submitted in candidature for any degree.

Signed_____ (Candidate)

Date 15/12/06

### Statement 1

This thesis is the result of my own investigations, except where otherwise stated. Where correction services have been used, the extent and nature of the correction is clearly marked in a footnote(s).

Other sources are acknowledged by footnotes giving explicit references.
A bibliography is appended.

Signed_____ (Candidate)

Date 15/12/06

### Statement 2

I hereby give consent for my thesis, if accepted, to be available for photocopying and for inter-library loan, and for the title and summary to be made available to outside organisations.

Signed_____ (Candidate)

Date 15/12/06

# Contents

# List of Figures

# List of Tables

# Acknowledgements

Firstly, I would like to gratefully acknowledge the enthusiastic supervision of, Dr. Rajesh Ransing. I could not have imagined having a better advisor and mentor, providing me with expert knowledge support and enthusiasm throughout this research.

A thanks to all my friends who have helped and supported me throughout my time at Swansea, both in and around Swansea and back in Surrey. You have all been a constant source of encouragement and support. A special thanks to Jon, Sam and Dima for their support and technical discussions.

A very big thankyou goes especially to my Parents and to David and Heather, for their constant enthusiasm, patience, love, and support.

# List of Symbols and Abbreviations

The following notation will be used unless otherwise stated.

| Abbreviation | Description |
|---|---|
| $A$ | Area |
| $a$ | Acceleration |
| $E$ | Energy |
| $E_{KE}$ | Kinetic energy |
| $E_{PE}$ | Potential energy |
| $F$ | Force |
| $f$ | Tangential momentum accomodation coefficient |
| $g$ | Gravitational acceleration |
| $H$ | Height |
| $h$ | Smoothing length |
| $Kn$ | Knudsen number |
| $k_b$ | Boltzmann constant |
| $l$ | Characteristic length |
| Ł | Mean free path |
| $L_s$ | Slip length |
| $m$ | Mass |
| $N$ | Number of molecules |
| $n$ | Number of moles |
| $P$ | Pressure |
| $P_c$ | Critical Pressure |
| $Pr$ | Prandtl number |
| $p$ | Momentum |
| $Q$ | Volume flow rate |
| $R$ | Universal Gas Constant |

| Abbreviation | Description |
|---|---|
| $Re$ | Reynolds number |
| $r$ | Radius |
| $T$ | Temperature |
| $T_c$ | Critical Temperature |
| $t$ | Time |
| $U$ | Applied velocity |
| $U$ | Potential energy |
| $u$ | Velocity |
| $V$ | Volume |
| $v$ | Speed |
| $w(r)$ | Weighting function |
| | |
| $\alpha$ | Polynomial constants |
| $\beta$ | Boltzmann factor |
| $\gamma$ | Strain |
| $\epsilon$ | Well depth |
| $\theta$ | Characteristic angle |
| $\lambda$ | Order parameter |
| $\mu$ | Dynamic viscosity |
| $\xi$ | Thermostat parameter |
| $\pi$ | Ratio of the circumference to the diameter of a circle |
| $\rho$ | Density |
| $\sigma$ | Collision diameter |
| $\tau$ | Shear stress |
| $\tau$ | Molecular frequency scale |
| $\nu$ | Dynamic viscosity |
| $x, y, z$ | Cartesian coordinates |
| $\bar{x}$ | Average value |
| $\langle v \rangle$ | Ensemble average |
| $x_{x,y,z}$ | Cartesian components |
| $x_{i,j,k}$ | Identifiers |
| $\hat{v}$ | Unit vector |

# Chapter 1

# Introduction

The overall aim of this work is the following:

> *"To develop a computational framework with the ability to capture and characterise fluid flow properties in terms of useful engineering quantities from molecular to continuum scales (50nm to 500nm)"*

## 1.1 Background

Fluid simulation at nano/meso scale ($100nm$-$1\mu m$) presents a current stumbling block for the numerical modelling community. The traditional consideration of fluids assumes that the influence of molecular interactions is negligible, however, at nano/meso scales this is not the case. The aim of the work presented in this thesis is to develop a simulation method with the ability to capture and characterise fluid flow properties in terms of useful engineering quantities from continuum to molecular scales ($1\mu m$ to $50nm$ ).
Current advances in nano and micro technology have allowed for engineering to take place at smaller and smaller scales. For example, Ghosh *et al.* [1] have developed a device to generate electrical current from the flow of water/blood to power pacemakers and other bio-electronic devices. Other advances include cooling channels etched into the surface of micro/nano chips, and nanofluidic transistors [2] , flow through membranes used in controlled drug delivery [3] and other fluid devices [4]. In the design of devices at such small scales, it is critical to be able to simulate their behaviour accurately, especially as experimental measurement becomes prohibitively expensive at these scales. Un-

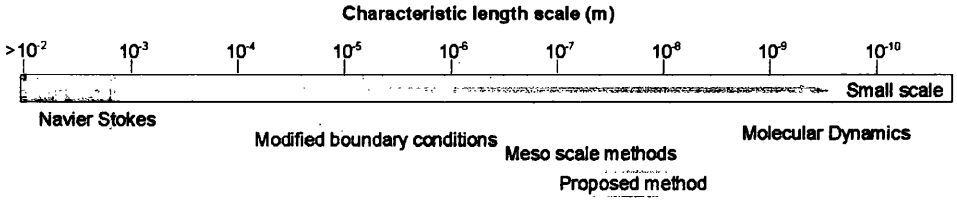


Figure 1.1: Length scales of simulations, showing the targeted location of the method proposed in this thesis

fortunately, it is precisely at this meso-scale that the conventional continuum simulations become less effective, as they fail to capture all the key physical interactions. Figure 1.1 shows the regimes of simulation methods over a range of scales, existing meso scale methods such as Lattice Boltzmann (LB) [5] and Dissipative Particle Dynamics (DPD) [6] tackle problem at the high end of the meso scale region. This work focuses on the lower end of the meso scale where molecular physics play a larger part.

All fluid is constructed of molecules under continuous motion and it is the arrangement of these molecules that defines the bulk behaviour of a fluid. For example, a fluid flowing over a solid boundary displays layers of fluid of different velocities at varying distances from the boundary. At a molecular level, the constant molecular interchange between fluid layers causes slower layers to exert a net drag force on faster layers, and vice versa. This causes a velocity profile which can be used to quantify this molecular exchange effect in terms of the macroscopic quantity of viscosity.

At meso scales, fluid displays macro scale effects such as viscosity, laminar and turbulent flow regimes, boundary layers, etc. but at such small scales, the number of molecules and molecular interactions is no longer effectively infinite and the conventional continuum laws are not able to adequately describe them. The continuum laws are unable to include the localised molecular physics which dominates the behaviour of the fluid at this scale.

Even though the conventional continuum laws do not apply in the meso scale regime, modelling engineering problems at these scales require us to quantify the macro scale effects resulting from the molecular interactions as these properties are key to characterising fluid behaviour in engineering systems. Addressing this challenge forms the kernel of this thesis, which is to be met by looking at meso scale systems in terms of both bulk and molecular scale physics.

## 1.2 Scope of Work and Research Contributions

The work in this thesis presents a first step into mesoscopic modelling of fluid from elementary principles of fluid behaviour. The aim of this research is to develop a meso scale method with an appropriate physics model and the ability to characterise fluid in terms of quantities relevant to the meso scale. The main research activities were:

- Understand the basics of fluid motion, and methods for modelling fluid on the extremes of the meso scale to appreciate the relevant issues for simulation in this region. This includes reviewing existing methods for meso scale simulation and methods for coupling continuum and molecular scale methods.

- The main focus of this work is on the development of a method of extracting mesoscopic properties from the molecular model. Various methods were reviewed to aid in the development of a robust meso scale method that would accurately predict the behaviour of systems at the lower end of the meso scale region.

- Implementation of computationally efficient methods into a meso scale molecular model. Modelling meso scale systems requires an accurate description of the physics of the system. Molecular boundary conditions were simplified and simulated pressure gradients were assumed at input and output boundaries so that the computational effort was focused on modelling the fluid physics in the region of interest.

- A study of the performance of the molecular model was performed at molecular scale dimensions to develop an understanding of the issues that affect computational performance of the model.

- The developed method was applied to a large slit pore system at meso scale to examine the behaviour of the fluid model.

Within these research tasks, the following research contributions were made:

- Development of a novel meso scale method for simulating systems between $50nm$ and $0.1\mu m$. The focus of the development of this model

was to describe meso scale systems in terms of useful engineering properties that could not be adequately described by continuum mechanics equations. The developed method contains two components:

  - *Meso scale molecular model.* A simplified molecular physics model was developed with simplifications made for boundary conditions to allow the focus of the computational effort to be on the fluid physics.
  - *Bulk property characterisation.* For systems within the meso scales, bulk fluid effects are present and observable from molecular mechanics. However, due to the presence and importance of molecular effects that cannot be characterised within the continuum governing equations, these properties are manifested from the molecular model. A method has been developed within this thesis to extract these properties from the fluid model to allow these bulk properties to be characterised. A full parametric study of the developed method is presented in order to develop further insight into the proposed methodology.

- A performance study has also been presented in this thesis that highlights the issue of the number of molecules used in the simulation particularly characterising the effect of density on system performance.

## 1.3 Outline of Thesis

This thesis is divided into eight chapters. The following is a synopsis of each.

- *Chapter One.* This chapter provides an introduction to the research area and provides an outline of the thesis. An overview of the work presented and research contributions made is also presented.

- *Chapter Two.* A discussion of fluid flow behaviour on scales between the continuum and molecular scale is presented. This chapter presents a background in the continuum view of fluid, and how it can be described and modelled at these scales. The discussion then moves to the molecular scale, and how fluid at these scales differs from the continuum model. The basic outline of the construction of molecular simulation

models is given and conditions when molecular scale effects dominate the behaviour of fluid systems are discussed.

- *Chapter Three.* A review of existing meso scale modelling schemes is presented in two sections, 'top down' and 'bottom up' approaches. Top down methods operate by adding molecular information into a continuum simulation, this includes a discussion of the limits and breakdown of the continuum laws. Bottom up approaches tackle meso scale problems by using molecular physics, which are simplified in regions of low activity.

- *Chapter Four.* A meso scale simulation method is developed based on a 'bottom up' approach. This chapter shows the implementation of the molecular model and the ups scaling of information to characterise the bulk properties of the fluid system.

- *Chapter Five.* The developed method is extended to deal with flowing fluids with the implementation of a flow generation method, balanced by additional thermodynamic controls. Case studies are presented in two sections, sampling and gradient studies. The sampling case studies explore the parameters of the bulk property characterisation and explain their use. The gradient studies show examples of use with thermally driven and pressure driven flows, validated against published results.

- *Chapter Six.* The developed method is applied to a molecular scale flow through a slit pore to demonstrate the depth of information that this method can extract from a the meso scale molecular model by looking only at the distribution of velocity across the pore. Different flow regimes are examined and shown to exhibit similar behaviour to laminar/turbulent flow.

- *Chapter Seven.* The developed meso scale method is applied to large scale systems containing between 20,000 to 100,000 molecules. An investigation is also performed to examine the behaviour of the method in terms of performance with large numbers of molecules.

- *Chapter Eight.* Original research contributions are summarised, along with recommendations for future work.

# Chapter 2

# The Nature of Fluid Flow

## 2.1 Introduction

The fundamentals of fluid flow on a wide range of scales are introduced in this chapter. The characterising properties of a fluid and their relevance at large scales (kilometre to millimetre scale) and small scale (nanometre and angstrom scale) will be discussed. The continuum approach to describing the behaviour of a fluid will be presented along with the methods of simulation at the continuum scale. In contrast, the molecular scale is considered along with fluid structure and simulation methods used at this scale. Examples of the change in physics and fluid behaviour that occur as the scale is reduced are presented, concentrating on the effect of confinement on a fluid.
This chapter highlights the special requirements of meso scale systems. Elements from both the continuum scale and the molecular scale are needed to fully model and describe a fluid system.

## 2.2 Basics of Fluid Motion

The basic characteristic property that defines a fluid, is viscosity. Fluid, unlike solids is unable to offer any permanent resistance to a shearing force. The fluid will continue to deform as long as the force is applied, taking the shape of any solid boundary it touches. The deformation of a fluid occurs from shearing forces acting tangentially to any solid surface. The fluid can be considered as layers parallel to a surface, which slide over each other as shown in Figure 2.1.

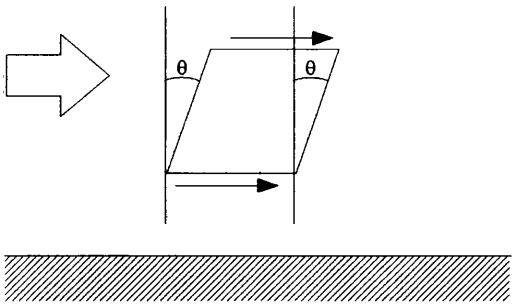


Figure 2.1: Internal shear between fluid layers

Each fluid layer applies a shear force to the next, and is in turn sheared by those it touches.

The ability to deform continuously under an applied force makes fluids behave differently from solids. Solid bodies are capable of maintaining an unsupported shape and structure, and can resist finite shear.
Fluids themselves fall into two categories liquids and gasses. To a fluid dynamicist, who is interested in flows at macro scale there are two characterising differences between them:

- Liquids have densities an order of magnitude larger than gasses
- Liquids and gasses respond very differently to changes in pressure and temperature

Gasses can also be expanded and compressed much easier than liquids due to the lower density and spacing between molecules. The motion of all fluids relies on the interaction and internal shear between fluid layers, but the actual interaction between layers occurs from collisions between many molecules on the molecular scale ($\sim 10^{-9}m$). In fact all fluid effects and properties occur from molecular interactions, but at macroscale ($\sim 10^{-4}m$) the detailed molecular physics of this behaviour can be neglected as the number of molecules within the characteristic length can be considered as sufficiently large. At these scales the fluid can be viewed as having physical properties corresponding to the statistical averages of the underlying molecules and are known as continuum or bulk properties. Molecular physics, manifested in a continuum framework have the ability to be defined as continuous functions of time and space.

### 2.2.1 Continuum/Bulk Properties

Bulk or continuum properties such as velocity, density and pressure remain constant at a point and changes due to molecular motion are assumed to be negligible. These properties are also assumed to vary smoothly from point to point with no jumps or discontinuities. This assumption is correct as long as the characteristic distance of the system is of an order of magnitude greater than the distance between molecules.
This assumption of bulk physical properties allows the behaviour of fluid systems to be approximated by a set of deterministic equations, that represent the underlying infinite chaotic molecular motion on a much larger scales.
The definition and basis of these bulk properties will be of significant importance in later discussions, so it is necessary to explain the origin of some of these bulk properties to clarify concepts.

#### Density

The density of a fluid is defined as the mass contained within a unit volume. It is computed as a function of mass ($m$) and volume ($V$) of a sample as follows:

$$\rho = \frac{m}{V} \tag{2.1}$$

This expression of density is represented in terms of mass per unit volume ($Kg/m^3$). Other expressions of density used are specific weight (weight per unit volume, $N/m^3$), relative density (relative to another density, *dimensionless*), and specific volume (reciprocal of density, $m^3/Kg$). Density can also be computed from molecular properties, in terms of sample volume, $V$, containing $N$ molecules of individual mass, $m_{molecule}$ [7].

$$\rho = \frac{N m_{molecule}}{V} \tag{2.2}$$

This expression also has units of $\frac{Kg}{m^3}$ and can be defined from $N = 1$ to $N = \infty$.

#### Temperature

The temperature ($T$) at any point in a fluid is derived from the internal kinetic energy of the underlying, $N$, molecules, each with velocity, $v_i$ and mass, $m$ [8].

$$E_{KE} = \sum_{i=1}^{N} \frac{1}{2} m v_i^2 \tag{2.3}$$

At continuum or bulk scales the number of molecules is assumed to be infinite, but the distribution of the velocity of this (almost) infinite number of molecules can be assumed to follow the Boltzmann distribution, which in one dimension appears as

$$f(v) = \sqrt{\frac{m}{2\pi k_b T}} e^{\frac{-mv^2}{2k_b T}} \tag{2.4}$$

Where $k_b$ is the Boltzmann constant. This distribution can then be used to calculate the average squared velocity in the system to relate the velocity distribution to the kinetic energy,

$$\langle v^2 \rangle = \sqrt{\frac{m}{2\pi k_b T}} \int_{-\infty}^{\infty} v^2 e^{\frac{-mv^2}{2k_b T}} dv \tag{2.5}$$

which gives

$$\langle v^2 \rangle = \sqrt{\frac{m}{2\pi k_b T}} \frac{\sqrt{\pi}}{2} \left[\frac{2k_b T}{m}\right]^{\frac{3}{2}} = \frac{k_b T}{m} \tag{2.6}$$

The equation for the translational kinetic energy of the molecules can now be related to the temperature of the system in one dimension.

$$E_{KE} = \frac{1}{2} m \langle v^2 \rangle = \frac{k_b T}{2} \tag{2.7}$$

For three dimensions, this simply becomes

$$\frac{1}{2} m \langle v^2 \rangle = \frac{3}{2} N k_b T \tag{2.8}$$

which describes the temperature of a local system of $N$ molecules.
In terms of bulk properties, where locally $N \to \infty$, the temperature is considered constant and varies smoothly from over the whole domain.

### Pressure

The pressure is explained by kinetic theory as arising from the force exerted by colliding gas molecules onto the walls of the container [9]. To explain the mechanics of pressure, consider a single molecule with velocity, $v$ along the $x$ direction contained within two walls perpendicular to its direction of travel,

and separated by length, $l$, as shown in Figure 2.2.

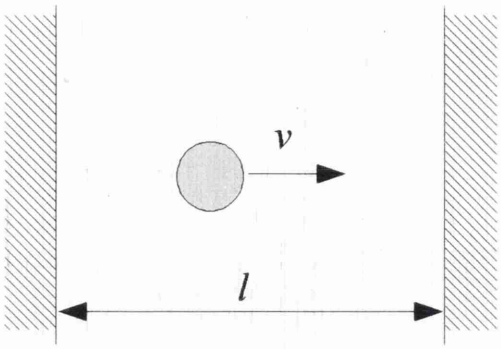


Figure 2.2: Single molecules oscillating between two walls

By considering the collision between the molecule and one of the walls, the momentum lost by the molecule and the wall is

$$\Delta p = p_{initial} - p_{final} = mv_x - (-mv_x) = 2mv_x \tag{2.9}$$

The time between successive collisions on this particular wall will be

$$\Delta t = 2\frac{l}{v_x} \tag{2.10}$$

Force is the rate of change of momentum, so the force on the wall from the single molecule is

$$F = \frac{\Delta p}{\Delta t} = \frac{2mv_x}{\frac{2l}{v_x}} = \frac{mv_x^2}{l} \tag{2.11}$$

For a large number ($j$) of molecules and collisions with the wall, this becomes

$$F = \frac{m\sum_j v_{jx}^2}{l} \tag{2.12}$$

Now, by adding in collisions with walls in all six directions we obtain

$$F = 2\frac{m}{l}\sum_j \left(v_{jx}^2 + v_{jy}^2 + v_{jz}^2\right) \tag{2.13}$$

For equilibrium conditions and a sufficiently high collision rate with the walls, the force on all six walls can be assumed to be the same, therefore the force

on a single wall becomes

$$F = \frac{1}{6}\left(2\frac{m\sum_j v^2}{l}\right) = \frac{m\sum_j v^2}{3l} \tag{2.14}$$

Where $v_j$ is the velocity of molecule $j$ in three dimensions. It is now possible to talk in terms of the average velocity of the molecules, $\left(\frac{1}{N}\sum_j v_j^2\right)$, which can be represented by $\bar{v}^2$

$$F = \frac{Nm\bar{v}^2}{3l} \tag{2.15}$$

This can then be divided by the area, $A$, of the wall to give the pressure

$$P = \frac{F}{A} = \frac{Nm\bar{v}^2}{3lA} \tag{2.16}$$

The cross sectional area multiplied by length yields a volume, $Al = V$, which when combined with Equation 2.2 yields

$$P = \frac{1}{3}\rho\bar{v}^2 \tag{2.17}$$

thereby describing pressure as a function of density and kinetic energy of molecules which, as shown in Equation 2.8 is in turn directly related to the temperature of the system. As with temperature, at continuum scales the number of molecules tends to infinity, and any fluctuations or statistical differences become approximately zero. In this case both pressure and temperature may be considered as constant at any point in the fluid domain.

### Viscosity

Viscosity quantifies the resistance put up by a fluid undergoing finite shearing forces and can commonly be perceived as internal fluid friction, or resistance to pouring. This effect occurs from the drag forces occurring between adjacent fluid layers moving and different velocities. The concept of viscosity is best demonstrated by example.

Figure 2.3 shows a fluid trapped between two parallel plated separated by distance $H$. The top plate moves with constant velocity $U$, and the bottom plate is at rest. The fluid in between them adheres to both plates, so that the fluid layers at each of the plates has the same velocity at the plate.

The velocity of the fluid changes linearly in this case, so the velocity at any

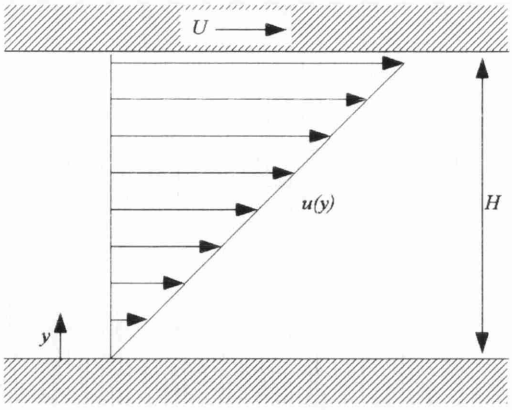


Figure 2.3: Viscous flow between parallel plates, the bottom plate is at rest, and the top plate moves with velocity $U$

point between the plates can be computed as follows,

$$u(y) = \frac{y}{H}U \tag{2.18}$$

It is known from experiments that for Newtonian fluids, frictional force per unit area, $\tau$ is proportional to the difference in velocity between the two plates, and inversely proportional to the separation $H$. Together, this is interpreted as the frictional force being proportional to the velocity gradient, $\frac{du}{dy}$,

$$\tau = \mu\frac{du}{dy} \tag{2.19}$$

with the proportionality factor being fluid parameter $\mu$, which characterises the drag between fluid layers and known as the dynamic viscosity. This is known as Newtons law of viscosity, where a linear relationship between velocity gradient and shear stress is assumed. Whilst this is valid for most simple fluids such as water and most gasses, non-Newtonian fluids such as plastics and pseudo plastics, exhibit a more complex relationship and Newtons law does not apply.

To obtain the coefficient of viscosity, $\mu$, for a Newtonian fluid, the situation shown above in Figure 2.3 is used. The coefficient is then extracted by comparing the applied $U$, and the drag force on the opposite plate, $\tau$.

The concept of kinematic viscosity is described in fluid systems where frictional and inertial forces interact. It is defined as the ratio of dynamic viscosity, $\mu$,

to the fluid density, $\rho$

$$v = \frac{\mu}{\rho} \tag{2.20}$$

**Causes of viscosity** Viscous effects occur due to internal friction between fluid layers, and it is important to consider the nature and cause of this drag. The molecules in a fluid are continuously moving and have little, if any, structure. Consequently, they are in constant molecular exchange between fluid layers. This exchange occurs via two mechanisms, the transfer of mass, by a fluid molecule physically crossing between fluid layers, and the transfer of energy via inter-layer collisions/potential energy interactions.
This constant exchange occurring over a sufficiently large number of collisions causes energy and momentum to propagate smoothly throughout the fluid at a rate governed by the physical properties of the molecular interactions, and the conditions of the fluid. However, the condition of the fluid in terms of pressure and temperature causes different effects in liquids and gasses.

**Viscosity of Gasses** In a gas, the molecules are widely spaced, and interact relatively little, so an increase in temperature increases the kinetic energy of the molecules and viscosity increases as a result of increased mass transfer between layers.
According to the kinetic theory of gasses [9], the viscosity is proportional to the square root of the absolute temperature. This however, is an exact solution to an approximate model and in reality, the rate of increase of viscosity is much higher [7].
In gasses viscosity is found to be independent over the normal range of pressures, with the exception of extremely high pressure.

**Viscosity in Liquids** In liquids, which have much higher densities, the distance between molecules is much shorter and the cohesive/attractive forces between them increases the viscous effect. The response to an increase in temperature, and hence kinetic energy, decreases the effect of these cohesive forces which reduces the viscosity. However, the increased molecular interchange between fluid layers increases the viscosity [7]. The net result is that liquids show a reduction in viscosity for an increase in temperature.
Due to the close packing of the molecules in a liquid, high pressures also affect

the viscosity. At high pressures, the energy required for the relative movement of a molecule is increased, causing an increase in viscosity.

### 2.2.2 Continuum Approximations

At over distances in and above the micro-scale, approximately $\geq 10^{-6}m$, the number of molecules in the system can in the order of millions! In these cases, the number of molecular interactions occurring over length and time scales is also huge. Because of this, it can be considered acceptable to assume that the influence of any individual molecular exchange/interaction is negligible as the number of molecules in any volume tends to infinity. The continuum assumption considers an infinite number of molecules in a domain, and neglects their individual contributions. The interpretation of continuum is given as;

> *Continuum A continuous thing, quantity, or substance; a continuous series of elements passing into each other [10].*

If a fluid is considered as a continuum, then each part is considered as identical (ie. fluid is homogenous) to the next and infinitely divisible, the molecular structure of fluid is ignored. This means that the fluid is assumed to have the same properties even if the domain dimensions are $100nm$, $1mm$ or $1km$.
By making the continuum assumption, molecular scale effects are neglected and the bulk properties are defined by the physical observable relationships between them. These properties can then be used to characterise fluid flows, as done in experiments by Reynolds [11] whose number, the Reynolds number, presents a criteria for dynamic similitude.

$$Re = \frac{\rho u L}{\mu} \tag{2.21}$$

The Reynolds number is the ratio of inertial $(u/\rho)$ to viscous $(\mu/L)$ forces, where $L$ is the characteristic length, of a flow with speed $u$. This can be used to both for determining kinematic and dynamic similitude for comparing scale models to real applications, and can also be used to characterise the point of transition between laminar and turbulent flow (critical Reynolds number).
A large Reynolds number indicates that the inertial forces dominate the system, with a low viscosity causing the small scales of fluid motion to be relatively undamped. Whereas a high Reynolds number flow has high viscous forces, which damp out small scale motion.

The Reynolds number represents simple characterisation of the behaviour of a fluid system. To look more in depth at the measure and description of fluid behaviour, a set of continuum governing equations are used. However, before these are considered it is important to set out the rules for the fluid mechanics interpretation of a continuum, these are known as the continuum assumptions/approximations.

### Continuum approximations

- **Infinitely divisible.** The characteristic length of the fluid should be several orders of magnitude larger than molecular diameters, such that the number of molecules in the system is large enough to be considered as approximately infinite. By assuming an infinite number of molecules, the fluid is considered homogenous at all scales, and can be divided up/decomposed into a infinite number of identical sections. If the fluid was considered in terms of a finite number of molecules, when it is divided up even in a finite number of sections, some will contain mass (a molecule) and energy and some will not (Figure 2.4).

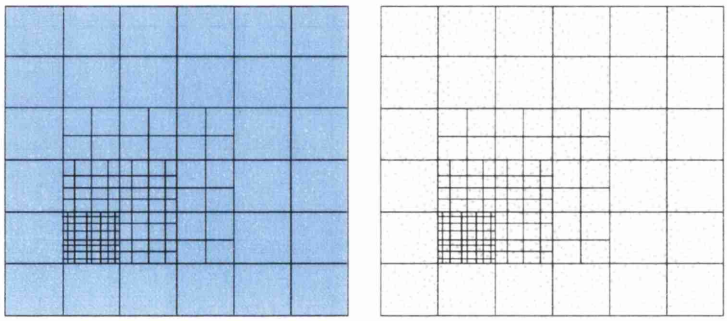

Figure 2.4: Left: Continuous and infinitely divisible Right: Finite number of molecules, mass and energy localised and not continuously distributed.

- **Thermodynamic equilibrium** To maintain the assumption of continuum mater with an infinite number of molecules, there must also be an approximately infinite number of inter molecular interactions occurring over length and time scales in the system. This means that an continuous propagation of energy throughout the system. Discontinuities cannot occur as the fluid is continuous (infinitely divisible) and an infinite number of infinitely small intermolecular energy exchanges smooth

out and propagate fluid properties and energy through the system.
This is also essential to maintain the linear relationship between stress and strain rate, and heat flux and temperature gradient. The thermodynamic equilibrium condition also states that there are sufficient interactions or collisions to smooth out any statistical variations occurring from the molecular scale (Figure 2.5).

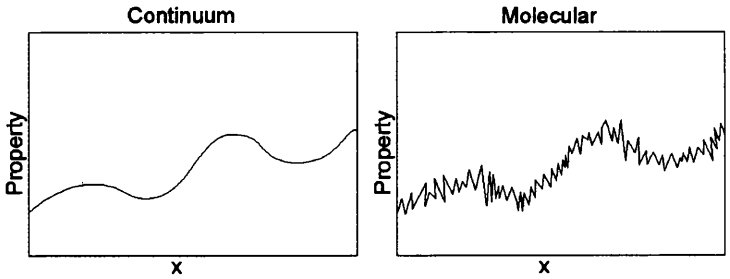


Figure 2.5: Statistical variations in properties arising from finite number of molecules in the system

If these conditions are met, the fluid system can be considered as a continuum. This is an important classification, as it means the flow can be approximated using continuum laws.
The continuum laws can be applied in both simple analytical form, as in the Bernoulli equation(inviscid flows),

$$\frac{P}{\rho} + \frac{v^2}{2} + gh = constant \tag{2.22}$$

or for more complex situations that require numerical solution. For cases such as simple pipe flows, the Bernoulli equation can be of use where little information is required. However in complex systems or geometries, a more detailed analysis and interrogation is required. In this case, fluid behaviour can be simulated using a set of conservative governing equations solved numerically as shown in Figure 2.6. These simulation, based on the continuum assumptions and continuum scale observations and laws, provide a detailed and accurate model of fluid behaviour, where experiments are difficult, expensive, or a greater amount of information is needed.

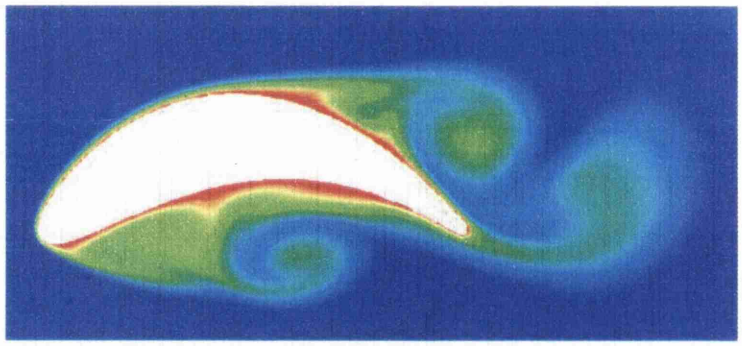

Figure 2.6: Simulation of complex fluid system [12]

### 2.2.3 Continuum Scale Simulation

Both simple and complex fluid systems can be investigated, within the limits of the continuum assumptions, by sets of governing differential equations that describe fluid behaviour. The mathematical solution of these equations throughout a fluid domain is known as *Computational Fluid Dynamics* (CFD). The governing equations describe the mathematical representation of a physical model that is derived from experimental flow measurements and observations. These representative equations are then replaced with an equivalent numerical description, which are solved using numerical techniques for the dependant variables of velocity, density, pressure and temperature. One of the most widely used sets of governing equations are the Navier-Stokes equations.

#### Navier-Stokes Governing Equations

The Navier-Stokes equations are a set of governing equations that describe the behaviour of fluids in terms of continuous functions of space and time. They state that changes of momentum in the fluid are based on the product of the change in pressure and internal viscous dissipation forces acting internally.
The scheme works by not considering instantaneous values of the dependant variables, but their flux, which in mathematical terms is interpreted as the derivative of the variables. The equation set is separated into three conservation laws for mass, energy and momentum.

**Mass** The conservation of mass, known as the continuity equation, is obtained by considering the mass flux into and out of any elemental control volume within the flow field. In the cartesian coordinate system, $x$, $y$, $z$, with

fluid velocities along those directions being $u$,$v$,$w$ respectively. The continuity equation then becomes

$$\frac{\delta\rho}{\delta t} + \frac{\delta(\rho u)}{\delta x} + \frac{\delta(\rho v)}{\delta y} + \frac{\delta(\rho w)}{\delta z} = 0 \tag{2.23}$$

The first term accounts for any change in density over time, while rest of the terms describe the change in density in the $x$, $y$, and $z$ directions.

**Energy** The expression for the conservation of energy in a fluid system is

$$\begin{aligned}\frac{\delta(\rho e)}{\delta t} + \frac{\delta(\rho u e)}{\delta x} + \frac{\delta(\rho v e)}{\delta y} + \frac{\delta(\rho w e)}{\delta z} = \\ \rho Q + \frac{\delta}{\delta x}\left(k\frac{\delta T}{\delta x}\right) + \frac{\delta}{\delta y}\left(k\frac{\delta T}{\delta y}\right) + \frac{\delta}{\delta z}\left(k\frac{\delta T}{\delta z}\right) \\ - P\left(\frac{\delta u}{\delta x} + \frac{\delta v}{\delta y} + \frac{\delta w}{\delta z}\right) - \varphi\left(\frac{\delta u}{\delta x} + \frac{\delta v}{\delta y} + \frac{\delta w}{\delta z}\right)^2 \\ + \mu\left\{2\left[\left(\frac{\delta u}{\delta x}\right)^2 + \left(\frac{\delta v}{\delta y}\right)^2 + \left(\frac{\delta w}{\delta z}\right)^2\right]\right. \\ \left. + \left(\frac{\delta v}{\delta x} + \frac{\delta u}{\delta y}\right)^2 + \left(\frac{\delta w}{\delta y} + \frac{\delta v}{\delta z}\right)^2 + \left(\frac{\delta u}{\delta z} + \frac{\delta w}{\delta x}\right)^2\right\}\end{aligned} \tag{2.24}$$

where $\varphi$ is the bulk viscosity, $Q$ is the heat added per unit mass, $k$ is the thermal conductivity, and $e$ is the internal energy

**Momentum** The conservation of momentum equation is as follows:

$$\begin{aligned}\frac{\delta(\rho u)}{\delta t} + \frac{\delta(\rho u^2)}{\delta x} + \frac{\delta(\rho u v)}{\delta y} + \frac{\delta(\rho u w)}{\delta z} = \\ \rho X - \frac{P}{x} + \frac{\delta}{\delta x}\left[\mu\left(2\frac{\delta u}{\delta x} - \frac{2}{3}\left(\frac{\delta u}{\delta x} + \frac{\delta v}{\delta y} + \frac{\delta w}{\delta z}\right)\right)\right] \\ + \frac{\delta}{\delta y}\left[\mu\left(\frac{\delta u}{\delta y}\frac{\delta v}{\delta x}\right)\right] + \frac{\delta}{\delta z}\left[\mu\left(\frac{\delta w}{\delta x}\frac{\delta u}{\delta z}\right)\right]\end{aligned} \tag{2.25}$$

$$\frac{\delta(\rho v)}{\delta t} + \frac{\delta(\rho vu)}{\delta x} + \frac{\delta(\rho v^2)}{\delta y} + \frac{\delta(\rho vw)}{\delta z} = \rho Y - \frac{P}{y} + \frac{\delta}{\delta y}\left[\mu\left(2\frac{\delta v}{\delta y} - \frac{2}{3}\left(\frac{\delta u}{\delta x} + \frac{\delta v}{\delta y} + \frac{\delta w}{\delta z}\right)\right)\right] + \frac{\delta}{\delta z}\left[\mu\left(\frac{\delta v}{\delta z}\frac{\delta w}{\delta y}\right)\right] + \frac{\delta}{\delta x}\left[\mu\left(\frac{\delta u}{\delta y}\frac{\delta v}{\delta x}\right)\right] \quad (2.26)$$

$$\frac{\delta(\rho w)}{\delta t} + \frac{\delta(\rho wu)}{\delta x} + \frac{\delta(\rho wv)}{\delta y} + \frac{\delta(\rho w^2)}{\delta z} = \rho Z - \frac{P}{z} + \frac{\delta}{\delta z}\left[\mu\left(2\frac{\delta w}{\delta z} - \frac{2}{3}\left(\frac{\delta u}{\delta x} + \frac{\delta v}{\delta y} + \frac{\delta w}{\delta z}\right)\right)\right] + \frac{\delta}{\delta x}\left[\mu\left(\frac{\delta w}{\delta x}\frac{\delta u}{\delta z}\right)\right] + \frac{\delta}{\delta y}\left[\mu\left(\frac{\delta v}{\delta z}\frac{\delta w}{\delta y}\right)\right] \quad (2.27)$$

where $X$, $Y$ and $Z$ are components of body force.
Equations 2.23 to 2.27 represent the Navier-Stokes set of conservation equations used to numerically compute fluid properties. For these properties to be used in to simulate a fluid system, then need to be localised at discrete points within the flow domain before they are solved using a numerical scheme.

### Solving Continuum Equations

There are a number of schemes for solving the fluid conservation equations in a simulation environment, such as the finite difference, finite volume, finite element, boundary element, etc.. However, the three most developed and widely used of the bunch will be considered, the finite difference method, the finite element method and the finite volume method.

**Finite Difference Method (FDM)** The finite difference method is a simple and efficient method for solving the continuum governing differential equations. Instead of derivatives being computed over infinitesimal elements, increments of finite width are used as an approximation. There are three varieties of finite difference, the forward, backward and central difference, which are highlighted in Figure 2.7 and are calculated as follows for parameter, $p$ at point $P$:

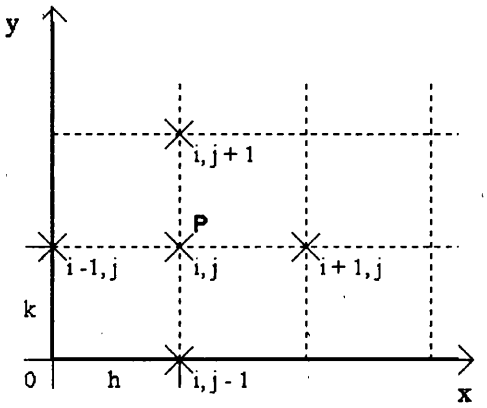


Figure 2.7: Illustrating the Finite Difference Methods calculations at point $P$

Forward difference:

$$\left(\frac{\partial p}{\partial x}\right)_{i,j} = \frac{p_{i,j+1} - p_{i,j}}{h} \tag{2.28}$$

Backward difference:

$$\left(\frac{\partial p}{\partial x}\right)_{i,j} = \frac{p_{i,j} - p_{i,j-1}}{h} \tag{2.29}$$

Central difference:

$$\left(\frac{\partial p}{\partial x}\right)_{i,j} = \frac{p_{i,j+1} - p_{i,j-1}}{2h} \tag{2.30}$$

Using this method the partial differential equations can be replaced with simple algebraic equations that can be solved either iteratively or by matrix inversion. This can be implemented for fluid flow simulations to yield the values of the flow variables at discrete points in the flow field. Due to the structures of the FDM, problems are limited to problems with simple boundaries where a structured mesh can be used. For more complex problems, the finite element method allows for more versatility but is much more complex.

**Finite Element Method (FEM)** The aim of the finite element method is to determine the values of the dependant variables of the conservative flow equations. FEM achieves this by dividing the flow domain into a finite number of cells or elements, each containing a small portion of the continuous fluid. At points placed at the corners or sides of these elements, points which are known

as nodes, the governing equations are evaluated. Instead of working with the

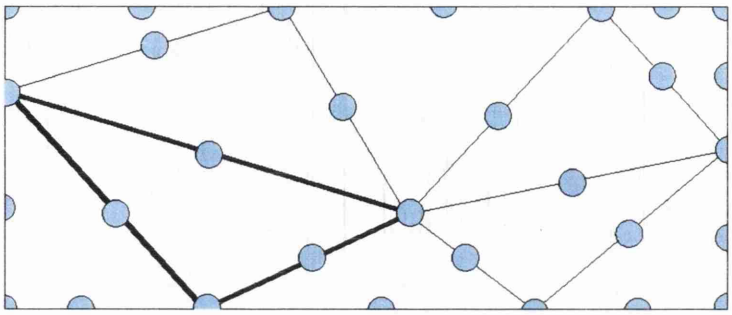

Figure 2.8: Governing equations evaluated at nodes surrounding fluid elements

differential equations directly, the FEM uses these nodes to discretise and evaluate the governing equations in an integral form using weighting functions.

**Finite Volume Method (FVM)** Similar to the Finite Element Method, FVM discretises the flow domain into elemental control volumes surrounding a node. Flow parameters are then treated as fluxes between control volumes, and conservation is maintained in each element. This allows for better treatment of flows with discontinuities such as shock waves.

### Advantages

Continuum simulations are able to provide an accurate model for fluid behaviour in a wide range of applications and systems. The division of the flow field into discrete elements allow for complex geometries to be simulated and smaller elements can be used to refine the solution in areas of high gradient, or where a greater accuracy is needed.

By approximating the fluid as a continuum, and ignoring the underlying molecular behaviour saves a great deal of computational effort and accuracy has been proved to be sufficient in many applications. The molecular information can be approximated at these scales, as the molecular motion cancels out to yield only bulk properties at this scale.

Continuum simulations also have the flexibility to prescribe a wide variety of boundary conditions capable of replicating almost any system, whist still maintaining global conservation laws.

#### Limitations

Continuum mechanics however, has its drawbacks. It is dependant on the generation of the mesh of elements and nodes it uses in the approximation. The generation of these meshes can be almost as time consuming and challenging as the actual simulation. These meshes can also have a significant effect on the solution, either through resolution or the distribution of nodes, and must be generated with consideration for the system of interest.
The scale of the system is also limited by the continuum approximations. Because of the continuum approximations, the matter of interest must be uniform throughout and infinitely divisible. This removes the ability to deal with discrete objects, such as, at the top of the scale extreme planetary systems, and at the lower end molecules. As the continuum governing equations are approximate relationships which are approximated in their solution, careful validation and testing must also be performed , which is true of any simulation method. Particular care must also be taken close to the continuum limit.
The breakdown of these approximations in the meso scale region between the continuum and molecular scales was studied in detail and the transition from continuum to molecular scale effects is explained in depth in later sections.

## 2.3 Molecular Mechanics

At very small scales ($\leq 10^{-8}$), the mechanics of fluid take on an entirely different form. The continuum approximations and laws are not valid as the number of molecules in the system is of the order of tens to thousands. At this scale the molecular interactions dominate the physics of the fluid, and it is debatable whether fluid is an accurate description as it is better described as a molecular flow.

### 2.3.1 Molecular Properties

The properties at a molecular scale ($\sim 10^{-9}$) are very different from those considered at the bulk/continuum scale. At this scale, the characteristic length of the flow is comparable to the diameters of individual molecules. There is no concept of bulk properties, and fluid-like motion is in the form of the motion of individual molecules. The fluid is now not continuous, as the molecular centres represent discontinuities in both density and energy.

The molecular chemistry of the making or breaking of bonds or changes to the internal structure of molecules is not considered in this research, although it is important to understand the mechanisms by which molecules interact in a chemically stable fluid.

A molecule is formed of an aggregate of two or more atoms bonded together by special bonding forces. The examination of interactions between bonded molecules was first undertaken by a Dutch chemist Johannes Diderik van der Waals whose studies into noble gasses lead to the characterisation of the forces between molecules [13]. The Van de Waals force was originally considered to describe the force between all molecules,

$$U(r) = \frac{Ae^{br}}{r} - \frac{C_6}{r^6} \tag{2.31}$$

Where $A$, $b$, and $C_6$ are characterising parameters for the molecules, and $r$ is the distance from the molecule centre. However it is now mainly used to describe the polarisation of molecules into dipoles.

The interaction forces are characterised in two parts, a long range attractive force, $\frac{C_6}{r^6}$, and a short range, but strongly repulsive force, $\frac{Ae^{br}}{r}$, as shown in Figure 2.9.

The repulsive forces, or London forces [14], named after the physicist Fritz

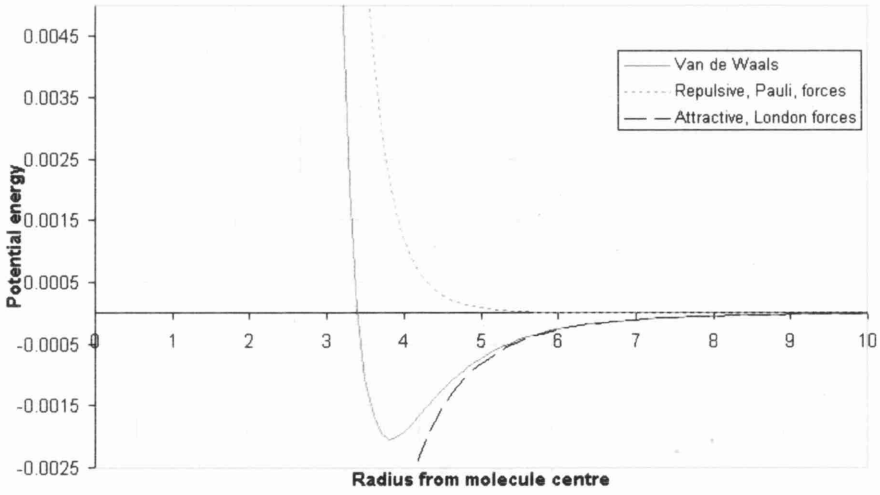


Figure 2.9: Van de Waals potential, as the sum of attractive, London, and repulsive, Pauli, forces.

London, represent the weak forces that occur between transient dipoles/multipoles. This occurs from an uneven distribution of electrons surrounding the nucleus

of the molecule, creating a temporary multipole.
The electron density in a molecule's electron cloud varies due to the finite number of electrons orbiting the atom, but the variation of density in the cloud created hotspots of high charge, creating a temporary multipole that attracts hotspots of opposite charge on other molecules. A molecule with a temporary multipole can also attract/repel electrons from neighbouring molecules, thereby propagating the multipole effect. These short term multipoles produce the net affect of a weak attractive force between neutral molecules such as nitrogen, methane and many others.
The London forces are higher for larger molecules with more dispersed electron clouds.
The attractive part of the potential comes from the strong short range repulsive forces between two the overlap between negatively charged electron clouds, based on the Pauli principle [15]. The Pauli principle states that as the clouds of electrons of the two interacting particles intersect, the energy increases dramatically.
The behaviour of a molecular system is defined by the properties of a system of molecules. However, the individual properties of molecules can be combined together to describe the state, or global properties of the system or region. An analogy can be found with the macro scale ideal gas equation of state, which relates the pressure, $P$, volume, $V$, and temperature, $T$, of an idea gas of $n$ moles,

$$PV = nRT \tag{2.32}$$

The Van de Waals equation of state [16] describes a similar relationship for molecular system

$$P = \frac{RT}{V-b} - \frac{a}{v^2}nRT = \left(P + a\frac{n^2}{V^2}\right)(V - nb) \tag{2.33}$$

where $n$ is the number of moles, and the gas law is corrected for the internal volume of the molecules using correction factor $b$, and adjusted with parameter $a$, which characterises the cohesion/attraction between molecules.
Parameters $a$ and $b$ can also be obtained from the critical properties of the fluid [17],

$$a = \frac{27R^2T_c^2}{64P_c} \tag{2.34}$$

$$b = \frac{RT_c}{8P_c} \tag{2.35}$$

The equation of state approaches the ideal gas law as these correction factors approach zero. This allows the description of the fluid in terms of state of the fluid, rather than as a large number of chaotic molecules. The Van de Waals equation is best suited to low temperature and pressure systems, however there are other equations of state that can be applied to other situations, e.g. Lennard-Jones equation, Clausius equation, etc.

### 2.3.2 Molecular Simulations

Molecular simulations play a vital role in science today by providing a framework on which to investigate theories and solutions in a relatively low risk and low cost environment. At molecular scale, investigations and experiments are very costly to perform, and in some situations it is not possible with current technology. Because of this, molecular simulations are often thought of as blurring the line between experiment and simulation, as they can be used to investigate theories that otherwise could not otherwise be tested.
Molecular simulation is the study of material/fluid by considering the individual interactions of atoms or molecules, as will be described in detail in Chapter 3. General simulation schemes involve representative molecules interacting with some sort of boundary, and each other to achieve a change in position and momentum. There are many different forms of simulation methods and techniques that can be applied to many different situations, each offering different advantages. The basic mechanism behind almost all molecular simulations is relatively basic, relying on a system of particles that represent atoms or molecules that interact using Newton's law,

$$F = ma \tag{2.36}$$

where the force acting on a particle, $F$, is equal to its mass, $m$, multiplied by its acceleration, $a$. The force acting on any one of the many particles in the system is determined by the movement of those around it. There are two branches of molecular simulation, stochastic and deterministic. The deterministic approach is in the form of Molecular Dynamic (MD) simulation, where the outcome could theoretically be worked out. Stochastic methods, such

as the Monte Carlo simulation method, have an element of unpredictability and chance and the result cannot be exactly calculated in advance, these will be discussed in more detail later. Despite the deterministic approach of standard molecular dynamics, it remains a statistical mechanics method, as system property values are developed from ensemble averages over the system.

Molecular simulations rely on representative molecules interacting with each other, so each molecule must possess individual properties that determine how it will move in the next time step; these are position, $r$, and momentum, $p$, applied in the number of dimensions present in the simulation. It is from these properties that interactions and collisions are found and evaluated, thus proceeding the simulation. Given that the state of the whole system is governed by a function of the properties of all the individual particles, we can introduce the concept of 'Phase Space'. At any time in the simulation, the state of the system can be defined by a single point in a $6N$-dimensional 'Phase Space', where $N$ is the number of particles in a 3-dimensional system. Each 3-dimensional particle contains information about its momentum ($p_x$, $p_y$, $p_z$) and position ($x$, $y$, $z$) in each of the three dimensions, so for $N$ particles, there are $6N$ variables. As the simulation progresses, the phase point will move throughout phase space, sampling more of the regions accessible without violating any of the rules set at the start of the simulation, such as constant energy, pressure or temperature.
In the following sections the basics behind simulations of molecular systems, and then proceed to how it applies to real fluid flow problems and situations is described.

## 2.4 Types of Simulation

The above sections have described the general form of molecular simulations used to explore the constant energy surface of a system. However, the simulation so far can describe the positions and momentum of the molecules in the system. These properties are useful within the simulation, but cannot be compared with a real situation because such information is not available. Available system properties such as temperature, entropy, pressure, etc. are the result of the motion of many particles and not properties of individual molecules. Such bulk properties are extracted from the simulation data with

the use of statistical mechanics, by averaging the properties of a large number of molecules over a specified period of time.
This method of property evaluation relies on Boltzmann's ergotic hypothesis [8]. The hypothesis assumes a quantum description of the system of particles, and for any system there are $i$ different possible energy states conforming to a constant energy $E$ (proportional to system volume). Over a sufficiently long period of time the hypothesis assumes that the phase space trajectory will sample almost all of these energy state configurations resulting in an average value, known as the ensemble average and considered to be representative of the system (over all state configurations, see Figure 2.10). The ergotic hypothesis therefore states that over a sufficient period of time, the ensemble average is equal to the statistical average obtained by simulation. This is a reasonable assumption for most cases, however it does not apply when considering meta-stable phases or glasses.

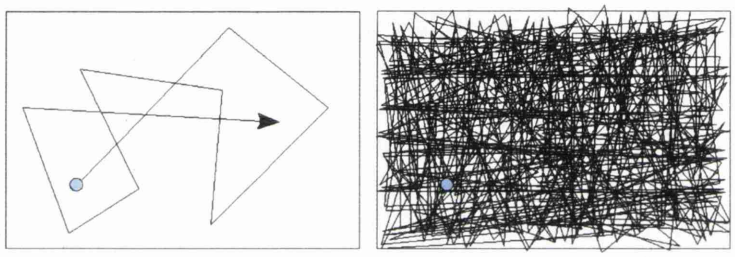

Figure 2.10: Left: poor phase space sampling Right: Excelent phase space sampling, resulting in excellent ensemble averages of bulk properties

The ergotic hypothesis leads to the construction of many different conservation laws that can be applied to simulate different properties and situations. These groups sample different ensemble averages and conserve different properties in molecular simulations, the most common of which are listed below.

- **Microcanonical Ensemble (NVE)** Constant number of particles, volume and energy. It is also common to control the temperature of the simulation during the equilibrium stage so that the target system temperature is reached within a suitable number of time steps. The simplest form of temperature control is to periodically scale the velocities, however this is not a truly isothermal method and must be removed before the properties are collected.

Although energy is considered to be conserved, there will be slight fluctuations and the possibility of a small drift due to truncation and rounding errors from the calculations.
This type of ensemble is useful for predicting thermodynamic response functions.

- **Canonical Ensemble (NVT)** Constant number of particles, volume and temperature. As in the microcanonical ensemble, during the initialisation stage the velocities are scaled to the desired value for the set temperature. Although useful for initialisation, velocity scaling is not suitable to use as a control for a simulation as it is crude and not a truly isothermal method. Therefore, other thermostatic methods must be used to apply the temperature control, which will be explained in detail in Chapter 4. This ensemble is used to perform conformational (spatial arrangements of a molecule) searches of models evaluated in a vacuum without periodic boundary conditions. Even when periodic boundary conditions are used, this ensemble can be useful if pressure is not a significant factor, as the constant temperature and volume provides less perturbation due to the absence of pressure coupling.

- **Isobaric-Isothermal Ensemble (NPT and NST)**

  - NPT Constant number of particles, pressure and temperature Temperature is controlled using one of the thermostatic schemes detailed in Chapter 4, and the pressure is controlled by varying the volume of the system using the Berendsen, Anderson or the Parrinello-Rahman schemes [18]. The Berendsen and Anderson schemes work by varying the size of the system, while the Parrinello-Rahman scheme is also capable of varying the shape of the system.
  - NST Constant number of particles, stress and temperature This is an extension to the constant pressure ensemble, which adds extra control on the stress components $xx$, $yy$, $zz$, $xy$, $yz$, and $zx$.

  Both methods are mainly used in structural applications. NST can be used to evaluate stress/strain relationships and NPT is generally used when the correct pressure, volume and temperature are important.

- **NPH and NSH**
  - NPH Constant number of particles, pressure and enthalpy. This ensemble is similar to the NVT ensemble, only the size on the cell is allowed to vary.
  - NSH Constant number of particles, stress and enthalpy. The control of the stress of the system implies the use of one of the variable volume schemes, of which the Parrinello-Rahman scheme is used to vary the size and shape. This ensemble can only be used in fully 3D periodic systems.

  In both ensembles, enthalpy, h, is conserved but it is also common, as with many of these methods, to use temperature scaling in the initialisation and equilibration stages to stabilise the system.
  NPH and NSH are commonly used to investigate natural response functions such as specific heat (at constant temperature), thermal expansion, adiabatic compressibility, and adiabatic compliance tensors.

- **Grand Canonical Ensemble ($\mu$VT)** Simulations with constant chemical potential $\mu$, volume and temperature is used widely to investigate capillary phenomena, and other chemically driven effects.

These ensembles are used within statistical mechanics, both for stochastic and deterministic approaches to investigate different environments and systems.
The Monte Carlo molecular simulation method represents the stochastic approach, which incorporates an element of randomness in the molecular model.

### 2.4.1 Monte Carlo Simulation

The Monte Carlo simulation method is a powerful tool for integrating complex equations using a relatively simple probability theory [19]. This is best illustrated by a simple example:
In this example, the value of $\pi$ is calculated using a brute force approach to Monte Carlo integration. To approach this problem, first consider an arc with radius $R$, within a square domain of side $l$, as shown in Figure 2.11

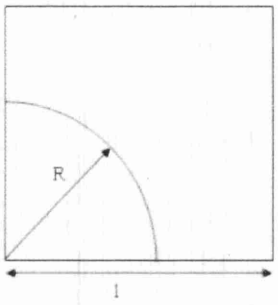


Figure 2.11: Monte Carlo integration

The domain is probed using a number of test points, randomly distributed over the area, as shown in Figure 2.12

The area of inside the arc is then estimated by the ratio of the number of

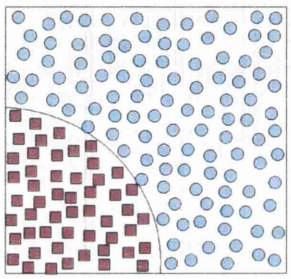

Figure 2.12: Monte Carlo integration, domain is interrogated by random points, some lie within the arc

points inside its constraints (Red squares) and the total number of points (Red squares + blue circles).

$$\frac{squares}{circles + squares} = \frac{\text{area of arc}}{\text{area of square}} \tag{2.37}$$

which becomes:

$$\text{Area of arc} = \frac{\text{No. squares}}{\text{No. circles + No. squares}} \times \text{Area of square} \tag{2.38}$$

The equation for the area of an arc is known as $\pi R^2$, so this becomes,

$$\frac{\pi R^2}{4} = \frac{\text{squares}}{\text{circles + squares}} \times l^2 \tag{2.39}$$

Rearranging for $\pi$ gives:

$$\pi = \frac{\text{squares}}{\text{circles} + \text{squares}} \frac{4l^2}{R^2} \tag{2.40}$$

Equation 2.40 relates the ratio of particles within the arc to the value of $p$. The accuracy of the estimation is mainly dependant on the number of points used to probe the domain. This approach is known as the brute force approach, and is the less sophisticated form of Monte Carlo integration, where there is an equal probability for a sample point to be taken from anywhere within the domain.
Monte Carlo simulation uses elements from this technique to move the molecules in the system in the following way.

1. A molecule is selected at random from the system
2. The molecule is then moved a random distance in a random direction
3. The resulting change in potential energy of the whole system is then evaluated and if it is reduced, the move is accepted
4. Some failed moves are also accepted according to a probability value, $P$, completely rejected moves are ignored

The distance a particle is moved is often scaled to alter the acceptance ratio of moves making the simulation more efficient.

When applied to molecular simulation there is a need to improve computational efficiency by making certain approximations for solving equations on relatively inactive regions. It is at this point Importance Sampling techniques are introduced into the Monte Carlo method, as described by Metropolis et al [20].
The Metropolis Monte Carlo method biases the contribution of each move to the statistical average based on the Boltzmann factor. The probability of a particle being selected is also influenced by the Boltzmann factor as follows.

1. The overall system energy is calculated, $E_i$
2. From the system, one molecule is picked out. The probability of selection for each particle is determined by the probability parameter $A$

3. The molecule is assigned a small perturbation, such as a small displacement in position, and the new system energy is calculated $E_j$

4. If the new system energy is smaller than the old system energy, accept the addition of the perturbation

5. If the new system energy is greater than the old system energy, accept the perturbation with probability: $B = e^{-\frac{E_j - E_i}{k_b T}}$ (note that $\beta = e^{-\frac{E}{k_b T}}$ is the Boltzmann factor)

6. Repeat steps 1-5

This gives the probability value that an added perturbation will be accepted as, $A$ multiplied by $B$. By allowing a small proportion moves that increase the system energy to be accepted, provides a limited amount of protection against meta-stable configurations and quasi-equilibrium conditions. By doing this, the system is pushed towards the configuration that is most likely to occur, thus speeding up the simulation run time.
Another modified form of the Monte Carlo technique, is the force biased method [21]. This adds some extra calculation overhead into each molecule evaluation to determine the resultant force acting on the particle by its neighbours, biasing the random move performed within the simulation. This also improves the computational efficiency as statistical averages need to sample fewer configurations.
Additional information on the Monte Carlo simulation method and its different ensembles can be found in the book by Gould *et al.* [22]. Gould provides examples of Monte Carlo methods, focusing on its advantages at simulating phase changes, which has been used to good effect by Levesque [23] applied to hydrogen storage in carbon nanotubes.

### 2.4.2 Molecular Dynamics

Molecular dynamic simulations model fluid in two ways, with molecules being represented as hard or soft spheres. Modelling with hard sphere models provides a relatively simple approach to approximating a system of molecules but still has valid applications, such as looking into the liquid-gas phase transition, diffusion and hard sphere fluids have a well defined critical point. The drawbacks are mainly to do with the discontinuous nature of the model. The

collisions are performed instantaneously and spheres only interact repulsively, where as real systems have some form of attraction between particles. Because of this, it is also used for gas simulations where the distances between molecules are far greater than their diameter, and inter-molecular interactions occur rarely. Despite these disadvantages, the model is still widely and successfully used, but care must be taken to ensure it is appropriate to the situation being simulated.

A more realistic, but more complex and computationally demanding approach, is the soft sphere model. In this model, the long range attractive and repulsive forces are modelled as a continuous function of the separation between pairs of molecules. The use of a continuous interaction function improves the accuracy of the simulation at the cost of increasing the computational load.

### 2.4.3 Introduction to the Physics of MD Simulations

Molecular dynamic simulations work on the same basic principles regardless of the actual interaction laws (hard or soft spheres) and rely on the following three steps, initialisation, equilibrium and production. These stages are detailed below following the example of a molecular scale cubic cell suspended in a fluid away from any physical boundaries, as shown in Figure 2.13

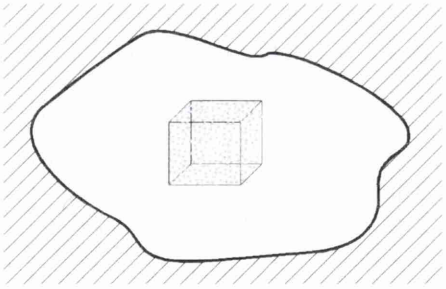

Figure 2.13: Control volume of fluid suspended away from any solid boundaries

#### Initialisation

When the simulation is run, the first task preformed is to define the problem, this is known as initialisation. This stage of the simulation accounts for only one time step in the simulation and is used to create the system of spheres based on a set of user defined parameters. In the example used, a control

volume suspended in a fluid of set volume and density is simulated (Figure 2.13). The initialisation stage is where the dimensions of the considered volume of the system are defined and representative molecules are placed within. Therefore a method is needed to position $N$ spheres within the system. If the spheres were to be randomly assigned positions, there is a quite high probability that some of them may overlap, creating extremely high interaction forces, disrupting the system with unnatural forces. It is therefore more practical to assign positions based on a lattice or crystal structure.

However, this creates a problem, as fluid molecules do not conform to a static lattice, but move constantly within the domain. This means that the fluid molecules need to break out of the initial lattice structure and find a natural, randomised, equilibrium position. A degree of randomisation is added to the molecules to allow them to break out of this structure. This can either be done by adding a degree of randomisation to the initial molecular positions, or to assign random initial velocities. Randomised positions, however are generally used for very large systems to reduce the simulation time taken to settle into a random 'cloud'.

By assigning random initial velocities to the molecules it is also possible to control the initial temperature of the system by assigning velocities based on the Boltzmann velocity distribution (Equation 2.4).

Once all of the initial positions and velocities for the all the spheres have been defined, the forces on each of the atoms must be evaluated giving the overall force on the particle. The force calculations are used to perform changes to the dynamics of the particles in the system, but these changes are performed with in the time loops of the simulation. There are two time loops within the simulation, one in the equilibrium stage and one in the production.

### Equilibration

The simulation time allotted to the equilibrium period immediately follows the initialisation stage. This provides a buffering/settling time for the particles to mix themselves up and reach a maintainable equilibrium state that is sufficiently randomised. Once a stable, but randomised situation is reached, the production stage can proceed, which provides all the useful information about the run.

While the simulation is proceeding, there needs to be some way to measure

how well randomised the simulation has become and whether or not an equilibrium state has been reached.

**Monitoring** Initially, the positions and velocities of all the molecules in the system are defined, both of which need to be relaxed before the production phase can take place. To ensure this has been completed, there needs to be ways of detecting the state of the simulation. The state of the dynamics of the particles are measured against the Maxwell-Boltzmann velocity distribution, while the breakdown of the positions is evaluated using the Order parameter.

The Maxwell-Boltzmann velocity distribution is strongly linked to the Boltzmann Factor, derived from the kinetic theory of gasses. By looking at a small change in height of the atmosphere, and relating the pressure to kinetic theory, the Boltzmann factor is derived from the change in pressure and can be found as follows:

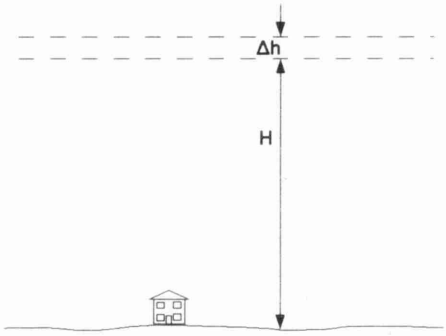


Figure 2.14: Boltzmann factor derived from elemental change in height in the atmosphere

**Boltzmann Distribution** The force exerted on the boundary of a fluid is described as $n$, the number density (no. of molecules divided by volume) multiplied by the volume and the weight of each molecule (force due to momentum exchange at collision at boundary)

$$F = mgAn\Delta h \tag{2.41}$$

so pressure becomes

$$\Delta P = -\frac{F}{A} = -\frac{mgAn\Delta h}{A} \tag{2.42}$$

$$\Delta P = -mgn\Delta h \tag{2.43}$$

The ideal gas law can be rearranged for $n$,

$$Pv = Nk_bT, \qquad n = \frac{N}{V} = \frac{P}{k_bT} \tag{2.44}$$

which when substituted into the expression for $\Delta P$ to give

$$\Delta P = -\frac{mg\Delta h}{k_bT}P \tag{2.45}$$

So for $h \to 0$

$$\int \frac{1}{P}dP = -\frac{mg}{k_bT}\int dh \tag{2.46}$$

gives,

$$P = P_0 e^{-\frac{mgh}{k_bT}} \tag{2.47}$$

Where $e^{-\frac{mgh}{k_bT}}$ is known as the Boltzmann factor. This form of the Boltzmann factor has been derived from potential energy, and as potential energy can be written as $mgh$, we can re-write the factor as

$$\beta = e^{-\frac{E_{PE}}{k_bT}} \tag{2.48}$$

where $E$ is the energy. A similar derivation can be performed using kinetic energy, resulting in a Boltzmann factor of

$$\beta = e^{-\frac{E_{KE}}{k_bT}} \tag{2.49}$$

This describes the probability that a molecule is a certain energy level for a prescribed temperature, $T$. By normalising probability values so they add to a unit value, the Boltzmann factor can be evaluated over a range of speeds to obtain the Maxwell-Boltzmann distribution for speeds. Where speed $v = \sqrt{v_x^2 + v_y^2 + v_z^2}$

$$f(v) = 4\pi \left(\frac{m}{2\pi RT}\right)^{\frac{2}{3}} v^2 e^{-\frac{m\mathbf{V}^2}{2RT}} \tag{2.50}$$

This velocity-probability distribution (Figure 2.15) can therefore be used to asses the dynamics of a simulation, by comparing the distribution of the resultant velocity of molecules with this distribution.

This is an important test as even for systems at steady state, as the velocity of individual particles does not remain constant, as they are constantly interacting and colliding with each other. It is sensible to consider the overall

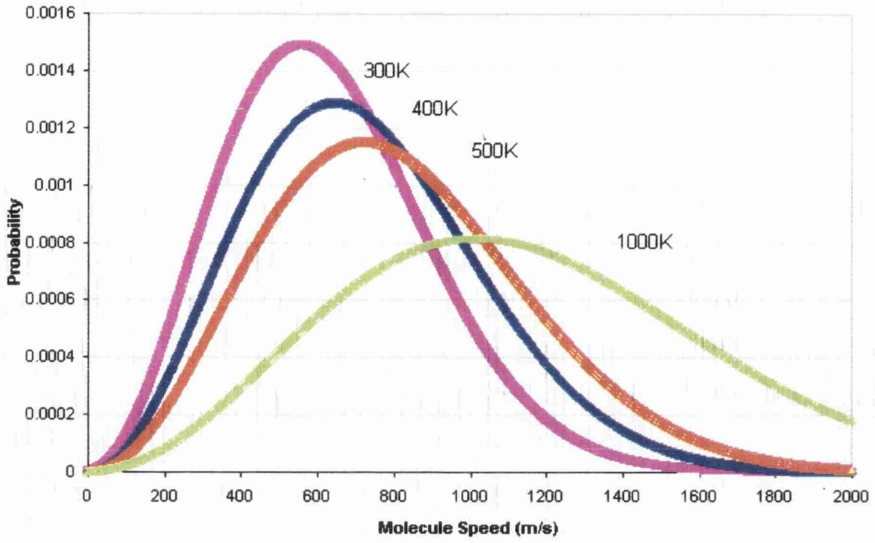


Figure 2.15: Maxwell distribution of velocity for temperatures of 300K, 400K, 500K and 1000K

distribution of velocities within the system to get a view of how the system is behaving and how it is approaching equilibrium.

By monitoring the distribution of velocities and its resemblance to the Maxwell-Boltzmann distribution, a measure of the approach to equilibrium is developed. It is then used to identify stability in the simulation. If the simulation is not stable, the temperature would fluctuate and the system would not be in equilibrium. It is therefore necessary to observe the development of the distribution over a period of time, ensuring that it converges with minimal oscillations. The graphs below (Figure 2.16) show the examples of the distribution at different temperatures.

The variations occur from statistical noise occurring from the finite number of molecules in the simulation. The greater the number of molecules, the lower the noise in the extracted distribution. For an infinite number of molecules, the distribution would be followed perfectly, the possibility of a continuum description.

Other measured thermodynamic properties, such as pressure and density are also sensitive to the state of the system. By looking at these properties and seeing how they behave is another tool in the identification of equilibrium, and smooth running of the simulation. Properties are averaged over a period of time, and need time to adjust themselves to the correct, stable value. If

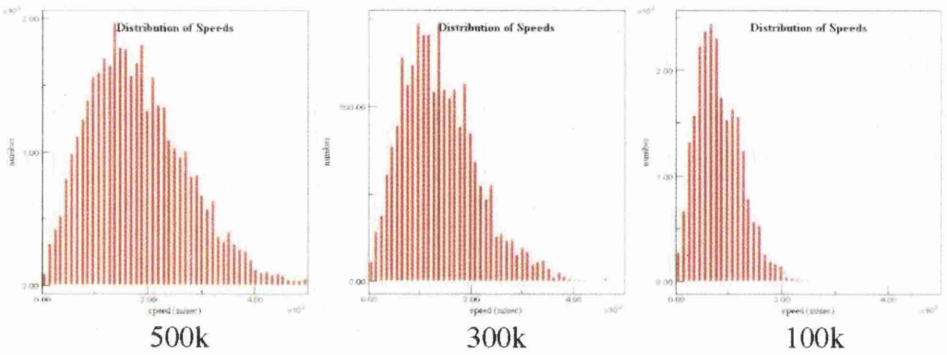


Figure 2.16: Maxwell distributions at 500k, 300k and 100k which show the shape of the distribution and how it changes at different temperatures [24]

some instabilities are present and the properties are not converging, the system cannot be in a steady state.
The stability of a property does not just imply that the value remains approximately constant, but it should also be able to recover its value after a small amount of perturbation, such as a temperature adjustment.

**The Order Parameter** The order parameter gives an indication of the randomisation of the positions of the particles within the system. There are many formulations of this parameter relating to different initial structures, but only an example of an FCC lattice is considered here.
First, the system of particles is broken down and the three Cartesian coordinates are considered independently. The form of the order parameter must be such that it is possible to detect when a particle is on or near an original lattice site.

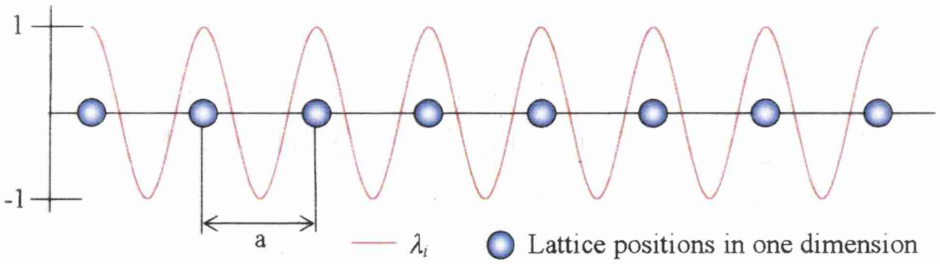


Figure 2.17: Order parameter relative to lattice positions

The form of such a function is described for a single particle as:

$$\lambda_i = cos\left(\frac{4\pi x_i}{a}\right) \tag{2.51}$$

where $a$ is the spacing between lattice sites, and $x_i$ is the position of molecule $i$. By summing this over all particles the average value can be calculated for all molecules, for each of the three directions:

$$\lambda_x = \frac{1}{N}\sum_{i=1}^{N} cos\left(\frac{4\pi x_i}{a}\right),\ \lambda_y = \frac{1}{N}\sum_{i=1}^{N} cos\left(\frac{4\pi y_i}{a}\right),\ \lambda_z = \frac{1}{N}\sum_{i=1}^{N} cos\left(\frac{4\pi z_i}{a}\right) \tag{2.52}$$

The overall value can then be calculated from the three directional components:

$$\lambda = \frac{1}{3}\left(\lambda_x + \lambda_y + \lambda_z\right) \tag{2.53}$$

This is the order parameter for the system. After the initialisation of the simulation, the order parameter can be used to confirm the lattice has been constructed correctly, if $\lambda$=1, all lattice sites are occupied. During the run the particles move from their initial position, which alters their individual order parameter to a value between -1 and 1 (Figure 2.17). for a fully randomised simulation, the parameter should be approximately zero, indicating an even distribution of particles between the bounds of the simulation. The order parameter can also be used to determine the point of solidification and the quality of the lattice, as used by Radhakrishnan and Gubbins [25]

A successfully equilibrated system should be sufficiently randomised and have reached a stable equilibrium point from which the production phase can begin. The stable point should have the same global properties regardless of the initial positions of the molecules, and can be tested us by applying random noise to the positions of the molecular lattice and examining several equilibration phases. A fully equilibrated system will have the following properties:

- Stable levels of kinetic, potential and total energy. Variations in energy levels are to be expected, but there should be no drift in average values of energy.
- Order parameter should be zero, indicating the molecules have sufficiently randomised.

- Velocities of all molecules should conform to velocity distributions for the set temperature for the system.
- Stable state which is independent of initial positions of molecules.

Although the above criteria help identify equilibrium there is still a chance for undetected instabilities to be present, so care must be taken to be certain that steady state has been reached. After sufficient randomisation, the production phase of the simulation can begin.

#### Production

After the successful randomisation of the system of molecules, the production phase can take place. This is basically an extension of the equilibrium phase to calculate the properties of the stable system over a set period of time. As the system is assumed to be sufficiently equilibrated, some of the controlling factors and adjustments are removed to allow the simulation to progress freely. Although the controls are removed, the parameters such as the order parameter and velocity distribution are still monitored to check for anomalies. At the end of the equilibration phase, all property averages are reset to zero so that when the production phase starts, the properties are not affected by the approach to equilibrium, and are the result of the production phase only.
This is the stage of the simulation where the interrogation and investigation of the system may start. There are two main types of dynamic models used in simulation to describe molecular dynamics, hard sphere and soft sphere. They differ in the way they handle interactions between particles. The hard sphere model considers interactions as binary collisions, whereas the soft sphere approach considers the molecules to be continually interacting via long range potential functions with their neighbours.

### 2.4.4 Hard Sphere Model

Hard sphere simulations only interact by colliding with one another and exchanging linear momentum in a perfectly elastic way. The forces present in the hard sphere model are relatively simple and easy to calculate. As there are no long range interactions, spheres only interact when they are colliding. The hard sphere models are generally event driven, where the simulation time

only steps forward to the next event, or collision. This is based on the assumption that all spheres have an initial position and velocity, and that sphere travels along the same direction at a constant speed (as there is no acceleration), such that the position at any time can be calculated as follows [8]:

$$r_i(t) = r_i(t_0) + (t - t_0)v_i(t_0) \tag{2.54}$$

Where $r_i$ and $v_i$ are the position (of the centre of the sphere) and velocity of particle $i$, $t_0$ is the start time and $t$ is the new time. As all molecules move in this way the time until two spheres overlap, i.e. when a collision occurs, can be predicted, highlighting the deterministic nature of the molecular dynamics approach.

At any collision between two spheres each with diameter $\sigma$ , the distance between the centres will be $\sigma$, therefore a collision occurs between two molecules with position at time $t$, of $r_1(t)$ and $r_2(t)$, when:

$$|r_1(t) - r_2(t)| = \sigma \tag{2.55}$$

which can be calculated as:

$$(r_1(t) - r_2(t))^2 = \sigma^2 \tag{2.56}$$

At this time, $t$, a collision is occurring, and in a simulation of $N$ molecules the molecules that are colliding next need to be determined. By substituting 1.3.1 for $r_1$ and $r_2$ in Equation 2.54 and rearranging for $t$ , gives the time at which the two spheres will collide:

$$t_c = t_0 + \frac{\left((-v_{12} \cdot r_{12}) \pm \sqrt{(v_{12} \cdot r_{12})^2 - v_{12}(r_{12}^2 - \sigma^2)}\right)}{v_{12}^2} \tag{2.57}$$

where

$$v_{12} = (t_c - t_0)v_1 - (t_c - t_0)v_2 \tag{2.58}$$

$$r_{12} = r_1(t) - r_2(t) \tag{2.59}$$

This gives the collision time, $t_c$, for two spheres providing they are moving towards each other. Therefore, before $t_c$ is calculated, the state of the collision for the colliding pair must be determined.

For example, take molecule number one from our simulation and consider the

possibility that it may collide with molecule 37. There are two basic possibilities, either they are moving towards each other or away. Mathematically, this is described by the projection of the velocity difference along the line of the centres of the spheres by finding the product of $v_{12}$ and $r_{12}$. If the result is less than zero, the spheres are moving together:

$$v_{12} \cdot r_{12} > 0 \tag{2.60}$$

If the spheres satisfy this condition, they are said to be moving toward each other but this does not guarantee a collision. To determine if they will collide we need to consider the limiting case where they come in contact as they pass each other.

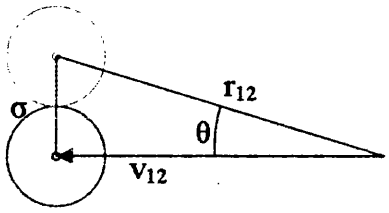


Figure 2.18: Hard Sphere Collision detection

By considering the one sphere to be fixed and the other to have velocity equal to the velocity difference, the above figure shows the limiting case for collision. It can be seen that there must be a limiting value of $\theta$ that if exceeded, no collisions occur and the spheres pass each other [8].

This collision test is evaluated for every possible colliding pair within the system by looping over all molecules, and calculating the next collision time for each. From these times, a table of collision times is created containing predictions for when each sphere will have its next collision. The calculation of this table is the last step in the initialisation stage.

The table can then be used and updated in the equilibrium and production stages to advance the simulation and evaluate the next collision.
Collisions are modelled as binary interactions, occurring instantaneously, where the molecules exchange linear momentum.

### Time Steps

The first task in the time step loop is to look at the table of predicted collision times and find which collision will occur next. The first collision to happen

is the only reliable prediction as the collisions afterwards may occur in a different order. The simulation is then progressed by advancing to the time of this collision and moving all spheres using a similar form of Equation 2.61

$$r(t + \Delta t) = r(t) + v(t)\Delta t \tag{2.61}$$

The new position for each sphere, $r(t+\Delta t)$ is calculated from the old position, $r(t)$ by adding the distance travelled at constant velocity, $v(t)$, during $\Delta t$. When all spheres have been moved, the two that are colliding will be in contact and the momentum exchange can take place. As the masses of the spheres are the same, the mass terms can be cancelled out of the momentum equation completely leaving just an exchange of velocity. The velocities of the two spheres are projected along the line of their centres, as in the two dimensional example in Figure 2.19. At the collision, the component of velocity along the

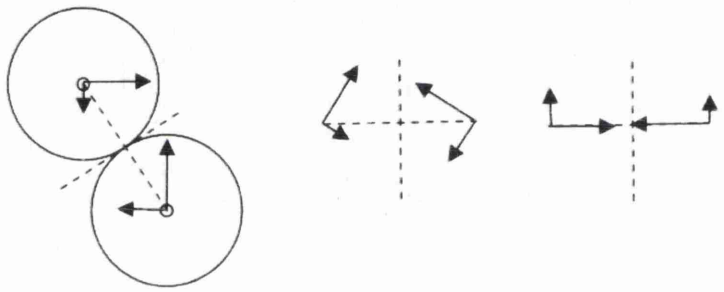

Figure 2.19: Hard Sphere collision evaluation, momentum is transformed from physical coordinates, along the line between the centres of the molecules, along which they exchange momentum

line connecting the two centres is exchanged, while the component of velocity perpendicular to this line, remains the same for both spheres. The velocities of both spheres are updated and can be used to update the prediction table for the next collision time for the pair. There is no need to update the table for all the molecules, as only the colliding pair experience a change in velocity. The updated tables can then be used to predict the time step to the next collision.

### 2.4.5 Soft Sphere Model

The soft sphere model of molecular interactions, considers molecules to interact by exerting a force on each other relative to the distance between them.

These interactions occur continually, with each molecule having a 'zone' in which, any other molecule present is influenced. Hard spheres will only interact when contact is made.

The initialisation stage starts as stated above, where the initial positions and velocities are been defined for all molecules in the system. Force calculation for soft sphere models is more complex due to the addition of long-range interactions. Particles in the system continually attract and repel their neighbours through a predefined potential function as opposed to the instantaneous and perfectly elastic collisions of the binary collisions described above.

This is best described with the use of the Figure 2.20 below, where the centre particle is interacting with particles within a set radius $R_C$. The most common potential used is the Lennard-Jones 12-6 potential, which provides an approximation of the attractive and repulsive forces experienced by non bonded molecules.

The potential functions are continuous and become weaker as the distance

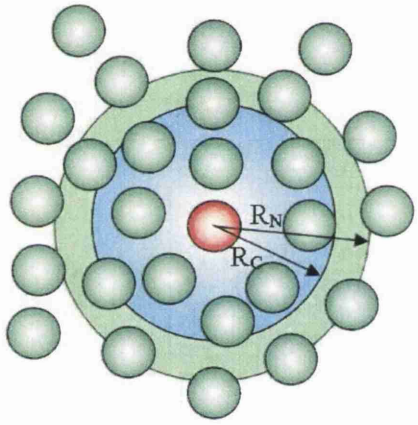


Figure 2.20: Soft sphere interaction detection

between molecules increases, so it is therefore convenient to set a limit to the 'zone of influence'(typically around 2-3 times the interaction radius of the molecules) of any one molecule (outside which the potential is approximately zero). This finite limit prevents molecules the simulation form including unnecessarily small interactions which can be approximated by long range correction factors [8], hence the simulation time is reduced. Despite this streamlining, the process of finding a particles neighbours is time consuming and there needs to be an effective method of storing the lists of neighbouring particles for each sphere.

Soft sphere molecular dynamics provides an accurate model for molecular scale fluids and generally used for dense fluids, where the cohesive part of the inter molecular interaction plays a more important role. Travis and Gubbins [26], and Tuzun *et al.* [27] show good examples of general molecular simulations. Other applications include chemical gradient driven flows [28], and studies of pore roughness [29] on flow parameters.

## 2.5 Effects at Molecular Scale

In this section, the effect of scale on the mechanics of a fluid at molecular scale are discussed along with the different mechanisms that are present which cannot be modelled on a continuum scale. The most obvious effects are present in highly porous media, where there is a high mix of fluid and solid molecules.

### 2.5.1 Phase Change in Confined Systems

The process of changing phases is in some cases modelled relatively well with hard spheres, however with soft sphere models when thawing, the melting temperature is often over estimated by up to 30% [30]. The melting temperature is the point at which solid and liquid can coexist, however for there to be liquid present, there needs to be a section within the simulation domain where the structure starts to break down (nucleation of the new phase). At any phase change a good indication is a jump in caloric curve relating to the adsorption of latent heat.

If the system comes close to a temperature and pressure at the phase boundary, the dynamics of the system can change quite substantially, and this needs to be taken into consideration. The change between liquid and gas is not as drastic as the change between liquid and solid, where the molecules fall into or out of a structured formation. As the temperature of the molecules is lowered, molecules posses less energy and do not interact with each other as strongly, and consequently they move less and less. The kinetic energy of the particles then reaches a point where, for a given density, they.are kept in the same position by all the other particles. At this point, the particles do not possess enough energy to break out of their position, due to the proximity of other molecules. During a phase change, energy is absorbed or discharged in the form of latent heat at constant temperature, this is the extra amount of

energy needed by the molecules to break out of the lattice and start moving around the container.

Phase change is a well understood mechanism, but the molecules behave slightly different when the solid/fluid is confined. Simulations of hard sphere fluid confined between hard walls were found to exhibit quasi-one dimensional motion near the wall [31], where the molecules near the walls were pushed up against the container, and could only move approximately parallel to the wall. This effectively creates different phase behaviour parallel and perpendicular to the boundary. The compressibility factor parallel and perpendicular was measured using the Radial Free Space Distribution Function (RFSDF) [32] within a Monte Carlo simulation of hard spheres. The study showed that as the distance between the plates was reduced from a separation to sphere diameter ratio of 21 to 3, the difference between the compressibility factors was increased between the parallel and perpendicular directions (with respect to the wall). This indicates that there is also a difference in pressure between the two components.

The RFSDF has components from both the compressibility factor and the order parameter, so by looking at the order parameter the phase of the fluid can be determined as a function of distance from the wall. Molecules away from the walls are still in the liquid phase and are free to move, but molecules closer to the wall are trapped between a non moving boundary and the moving particles colliding against them.

The quasi-one-dimensional motion combined with the difference in pressure results in the phenomena of anisotropic phases, where close to the wall, molecules are in the solid phase perpendicular to the wall and in the liquid phase parallel to the wall. Taking this quasi-one-dimensional theory one step further, and constraining a fluid within a cylindrical pore only two molecular diameters wide (between centres of molecules within the wall) freezing of the fluid is not observed to occur. The study by Peterson et al [33] showed that no phase transitions are observed in a single nano pore with diameter of twice the molecule diameter (between centres wall molecules), right down to absolute zero. However Radhakrishnan and Gubbins [34] showed that phase change was possible when the nanotubes were arranged in a cluster, due to correlation effects. Using a Grand Canonical Monte Carlo (GCMC) simulation (Constant chemical potential, volume and temperature) they firstly showed that a phase change was not observed in a single pore, however this also highlighted the problem

of fluctuations in thermodynamic properties due to the limited number of particles in the system. The investigation then turned to simulating a hexagonal cluster of pores, and the same cluster surrounded by periodic images of its self. The walls were oxygen molecules and the transported molecules were methane, and the periodic pore model showed that clusters of pores do show evidence of freezing at a temperature of about 40K. The simulation also replicated the hysteresis effect of regular phase change, but highlighted the importance of the correlation effect between pores.

In a Monte Carlo simulation of water, Meyer and Stanley [35] investigated the coexistence of two liquid phases of water within a strongly confined geometry shown if Figure 2.21. The theory of this is based on the fact that amorphous

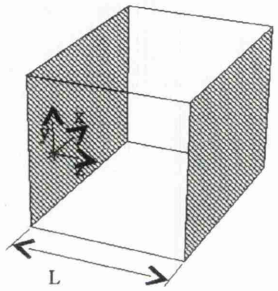


Figure 2.21: Confined geometry for simulation of liquid-liquid phase coexistence, L=10.95, periodic boundary conditions along x and y axes. Two parallel plates in the $xy$ plane are separated by length $L$ in the $z$ direction

solidified water displays two distinct phases, one with a lower density than the other and by extrapolating the transition line to a higher temperature to the meta-stable liquid region, there is a possibility of two liquid phases being present. This has been shown for bulk liquids, so Meyer and Stanley [35] investigated the same theory, when the geometry is confined as above. It was found that the pressures normal and parallel to the wall were different and furthermore, at temperatures below 230K the pressure parallel to the wall was found to become density independent, typical of the coexistence of phases of different densities in constant volume simulations [36]. The pressure normal to the wall however, remained density dependant right down to absolute zero. They concluded that it was possible for these high and low density phases to coexist within the simulation.

A combination of these works was looked at by Gatica et al [37] to investigate the adsorption of fluids within carbon nanotubes. As with the work

above, adsorbed fluid was expected to exhibit one-dimensional or quasi-one-dimensional behaviour. The study found the corrugation experienced by an adsorbed molecule to be much less when compared to planar graphite [37,38], leading to fluid adsorbed on to the wall showing what is known as a cylindrical shell phase. When the density within the nanotube is increased significantly, the cylindrical shell phase solidifies and becomes similar to the incommensurate monolayer solid film on graphite which is well known and studied [39]. At some point there must be a transition between the solid and fluid and at this threshold, there must also be the possibility of coexistence of the two phases. The solid 'axial phase' is recognised when the fluid becomes confined close to the axis of the tube as the number of molecules in the system is increased (hence increasing the density of the fluid). This axial phase transition operates in a similar way to Capillary Condensation and Layering Transition. The layering transitions are known to occur at higher temperature, however the one dimensionality of the system limits the transition to occur at T=0°C.It has also been shown that a bundle of adsorbing tubes exhibit correlation effects, which raises the transition temperature above zero [36, 40]

Radhakrishnan and Gubbins [25] work agrees with the above discussion of confined phase change, but applied to slit shaped pores. As with the cylindrical pores, fluids confined within slit shaped pores showed strong evidence of a third phase close to the walls. They investigated the effect of the wall-fluid interaction strength on the phase change, varying it from strongly attractive to repulsive, with respect to the fluid-fluid interaction strength.
Previous work by Miyahara and Gubbins [41] had already found that the strength of the interaction affects the hysteresis loop of the freezing temperature, relative to bulk material. However, Maddox and Gubbins [42] also found that the reduced confinement of the fluid in slit pores, as opposed to cylindrical pores, leads to higher freezing temperatures.
The study found that for strongly attractive walls the layer of particles nearest the wall froze at a higher temperature than those in the middle of the pore, similar to many of the examples described above for cylindrical pores. However, as the interaction swings the other way, becoming repulsive, the freezing effect also switches so that the centre of the pore freezes before the layer in contact with the walls. This implies that there must be a level of attraction or repulsion where the fluid freezes at one temperature, making the intermedi-

ate shell phase meta-stable, or disappear completely. The attractive/repulsive interaction potentials at the walls represent the difference between graphite carbon/silica walls, as carbon walls are strongly attractive and silica walls are weakly repulsive, however most silica based porous materials have cylindrical pores.

Kim and Steele [43] also looked at phase change at solid boundaries, studying the effect corrugation had on the monolayer of methane on graphite. Their small scale simulations of 289 molecules showed that increased corrugation leads to pre-transitional effects that are not present in solidification against smooth walls.

### 2.5.2 Adsorption/Desorption in Pores

Adsorption is the process by which a fluid adheres in a thin film to a solid or liquid with which it has contact. As an example, the following will discuss the effect of the conditions for filling and emptying of a silicate nanotube, as studied by Gelb [44]. The first thing to remember, is that classical statistical mechanics laws do not allow a first order phase transition to take place within short range one dimensional systems, even for the case of meso-scale pores which, despite their three-dimensionality. Bundles of pores or tubes, add to the systems dimensionality which alters the behaviour due to the long-range interactions. This can result in a first order change of phase within such a cluster due to the presence of neighbouring tubes. These inter pore effects are difficult to characterise in real materials and are therefore not, at present, widely investigated by simulations [34]. The filling of a pore involves three basic components, a high density phase representing the filled part of the pore, a low density part representing the multi-layer adsorption, and interface between the two, as shown in Figure 2.22.

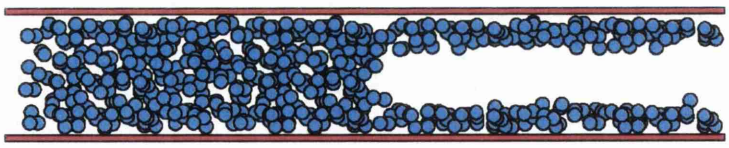

Figure 2.22: Phase regions for adsorption filling of pore.

As would expected from continuum scale observations of surface tension, the interface between the 'wet' walls of the pore and the 'filled' region is almost

hemispherical. Higher temperature adsorption results in a thicker layer at the walls through the adsorption layer, resulting in a lower surface tension and an increase in the number of interfaces within the pore. The effect of inhomogeneity of phases along the length of a pore, becomes negligible when there is no hysteresis present between adsorption and desorption, and leads to a rounding off of the phase transition, similar to the effect of periodic boundaries on bulk fluid [44]. It is therefore acceptable to think of the phase transition within nano-scale pores as almost first-order and apply standard transition thermodynamics, as long as the temperature does not approach the critical point and the distance between phase interfaces is comparable to the pore diameter. The term critical point used in capillary confined fluids has a different meaning to that of bulk fluid, and is used to describe the point at which adsorption/desorption hysteresis disappears. As a consequence of the inhomogeneity along the pore, it is not possible to observe a critical point in the bulk fluid sense, or its associated properties. At lower temperatures, the adsorption layer is thinner and the interfaces are further apart so small, periodic cells are used whereas for very high temperatures, the adsorption layer grows to such an extent, and the interfaces are so close together, that only one phase is present. The hysteresis, with respect to chemical potential during filling and emptying, is present in both experiment and simulation, however its effects are more pronounced in simulation, possibly due to the short time scale accessible. Longer pores have more capacity to exhibit inhomogeneity along their length which can present differences in nucleation on new phases and hysteresis loops. Pores with closed ends, can have the effect of the closed end acting as an already nucleated dense phase while filling and affect the hysteresis loop.

The simulations performed by Gelb [44], were for adsorption of Xeon on silica. A simplified model for silica was used, with the surface molecules modelled by oxygen. Silicone molecules are not present on the surface of silica, and are weakly interacting, and were therefore removed from the model. The pore was created by defining a box, 5.4nm square at one end and a length varying from 8nm to 108nm, full of a standard configuration of oxygen atoms for silica, and removing a cylindrical volume of atoms from the centre to create the desires pore geometry (Figure 2.23). A small amount of relaxation was applied to the system after the removal of the cylinder, to remove some of the translational symmetry experienced by the use of smooth continuum walls.

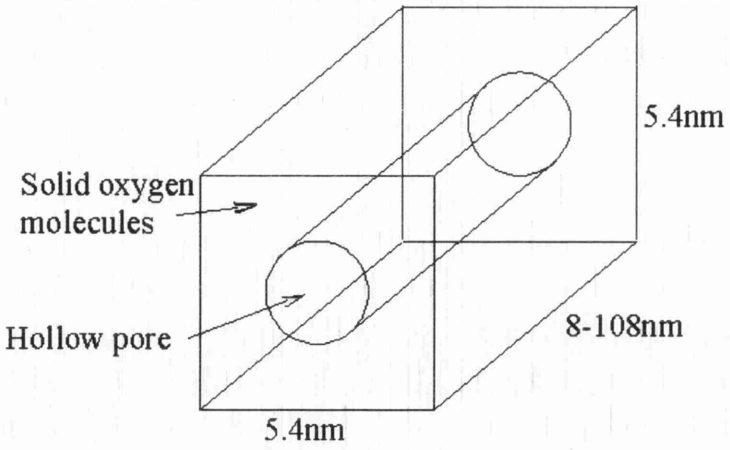


Figure 2.23: Cylinder oxygen atoms removed from system to create pore

Although this was done at the cost of increasing the computational load of the simulation. Three geometries were explored in this investigation, a finite pore with two open ends, an infinite pore with periodic boundary conditions, and a single ended pore. The geometries were also modified in diameter and length for further comparison. The simulations were based on a Grand Canonical Monte Carlo (GCMC) Method (constant chemical potential, volume and temperature) as it samples the correct ensemble for adsorption/desorption simulations and has been found to be reliable, despite inaccuracies when dealing with transport to and from the interface.

During the filling and emptying of long pores (108nm) it was noted that equilibration became extremely slow at the top of capillary rise and the bottom of desorption drop and required up to thirty times as many more moves than usual. During the desorption of the long open ended pore, the interface between the two phases moves steadily away from the open end, and there was no evidence on nucleation of either phase away from the interface. Desorption within an open ended pore often results from the nucleation of the low density phase within the high density region, resulting in 'bubbles' forming. But in this case, the interface also moves at an almost constant velocity.

The filling of the single ended pore shows the reverse happening, the closed end acts as an already nucleated phase and the interface moves up the pore, toward the open end at a relatively steady rate. Open ended 'infinite' pores do not have the 'head start' of the closed end and must nucleate the start of the high density phase before the filling process can properly begin. This means that capillary rise occurs at a higher chemical potential than closed ended

pores. Because of this higher potential, the closed ended pore has a smaller width hysteresis loop than the open ended tube, this also reduces the temperature at which hysteresis disappears. It was also found that the reduced hysteresis loop found with the single ended pore occurs at a chemical potential almost exactly in the middle of the larger loop of the open ended pore. Gelb also noticed that at the ends of the pore, weaker repulsive interactions could be affecting the stability of the simulation as the interface approached the ends of the tube.

Open ended and infinite pores were also compared using two different pore diameters, 4nm and 3nm. Although the hysteresis loop for the open ended


Figure 2.24: Infinite vs. Open pore

pore was smaller than for the closed ended pore, it is still smaller than the loop for the periodic pore. The effects of the open ended pore are more dramatic for the 4nm diameter, as much higher chemical potential is needed to induce nucleation of a new phase making the presence of the open end more important. The hysteresis experienced by the open ended pores for both diameters, is mainly on the desorption drop and not on the adsorption side, however the capillary rise occurs at a slightly higher chemical potential, indicating that the open ends may be stabilising the low density phase at the ends.

The final investigation performed by Gelb looked into the effect of changing the length of the pore cell for the periodic/infinite pore. Three lengths were tested, $8nm$, $16nm$ and $108nm$, and it was found that as the length was increased, the width of the hysteresis loop was reduced. This was attributed to the fact that the longer pores contained more density fluctuations, leading to a higher probability of nucleation of a new phase. This however, could have been due to poor sampling resolution as the difference is fairly small and is most pronounced at a reduced temperature of $\tilde{T} = 0.927$. There was a fairly close agreement between the two longest pores, the 8nm and 108nm, which could indicate that the difference in the hysteresis loops is not affected when the length becomes significantly greater than the pore diameter.

Gelb's [44] observations have been summarised below:

- Pore Length has little effect on the adsorption/desorption hysteresis despite added probability of nucleation, but the effect is greatest when the length is close to the pore diameter.
- Open ends on pores show much less desorption hysteresis for 3nm diameter pores than 4nm diameter pores.
- Single ended pores show almost no hysteresis due to the nucleation of phases at the end of the pores. Density also fluctuates greatly at pressures near condensation.
- Inter-pore correlation effects could yield a 'novel type of phase transition in two dimensions'.

The effect of the length of the tube is a fairly expected result. As long as the tube is long enough to separate the effects of the ends of the tube, the middle section shows little variation along its length. The difference in desorption hysteresis between pore sizes is mainly due to the nucleation of the ease of progression of the new phase which is made easier by the effectively larger particles, due to the narrower pore. The lack of hysteresis shown in single ended pores is mainly due to the closed end acting as a dense phase, giving a good start to phase nucleation.

## 2.6 Summary

In this chapter a general overview of fluid behaviour on continuum and molecular scales was presented. The bulk, or continuum, properties have been discussed along with their origins from molecular mechanics. Several methods for solving for these continuum properties were presented in terms of the governing equations which quantify the relationships between them.
On the molecular scale, the origin of intermolecular forces and interactions has been presented, and a wide variety of molecular simulation schemes have been discussed from the deterministic molecular dynamics, to the stochastic Monte Carlo method. Finally, the importance of these methods has been highlighted by considering the molecular examples in Section 2.5.
This chapter has shown the different approached to fluid simulation that are needed as the scale of the system changes. The meso scale lies in between the continuum and molecular scale and must use elements from both to correctly

capture the correct physics (from the molecular scale) and provide a description in terms of useful fluid properties (as characterised on the continuum scale).

# Chapter 3

# Fluid Physics at Meso Scales

## 3.1 Introduction

The focus of this chapter will be to present and discuss methods for combining information and physics from the continuum and molecular scales. The discussion begins with methods that couple continuum with molecular simulations. From this, two basic methods will emerge, where molecular simulations are used either to couple to the continuum region as a boundary condition (and vice versa), or by the molecular information being used to modify or enhance the continuum solution in a particular region.

Many of these methods consider solid systems or sparse gas dynamics, both of which can access larger length scales with molecular simulation than dense gasses or liquids, due to the dynamics and distance between molecules.

Existing meso scale methods will then be discussed, such as dissipative particle dynamics and the lattice Boltzmann method. The meso scale methods commonly used present a 'top down' approach, the benefits of which, and applications will be discussed.

The final section will discuss direct schemes from upscaling information from the 'bottom up' approach, to look at schemes for extracting bulk properties from molecular dynamics, with a view to not only extract the properties, but the property distributions throughout the molecular domain.

## 3.2 Top down Approach for Meso Scale Computation

The meso scale region is defined as a scale in between the micro scale and molecular scale (approximately between $10^{-6}m$ and $10^{-8}m$). The meso scale exists to cover the change in physics between the continuum approximated view, and the discontinuous molecular description. Hence, the upper limit of the meso scale is set by the point at which the continuum approximating laws are violated. This can occur at a range of scales, depending on the state and properties of the fluid, for example a sparse gas invalidates the continuum laws at larger scales than a solid.

### 3.2.1 Continuum Limit

For the fluid to be considered a continuum, the laws described in Section 2.2.2 are summarised as follows:

- Continuous and infinitely divisible fluid
- Fluid is in thermodynamic equilibrium

Because of the dependance of the continuum laws on the state of the fluid characterised by the rarefaction and energy of the molecules, the point of failure of these laws must be considered carefully. Travis *et al.* [45] show a comparison between Navier-Stokes hydrodynamics and molecular simulation, which displays different behaviour in terms of velocity profile and heat flux profile. Due to the differences in density and kinetic theory, it is however necessary to consider the continuum to molecular transition separately for liquids and gasses.
Gasses have a very well developed kinetic theory, and consequently are better able to describe the transition from continuum mechanics to fully molecular flow.

#### Gas Flows

To asses the validity of the continuum or molecular model for a gas, it is necessary to obtain a measure of the rarefaction of the gas at the scale of interest.

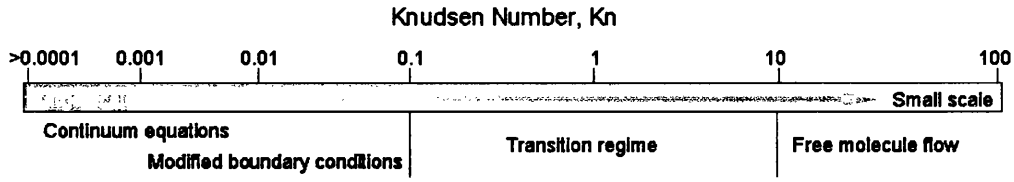


Figure 3.1: Range of Knudsen Numbers for Gas systems

To do this, the concept of mean free path is introduced. The mean free path is the average distance travelled by a molecule before it collides/interacts with another molecule. For an ideal hard sphere gas, the mean free path, Ł is a function of pressure, $P$, and temperature, $T$, as follows.

$$Ł = \frac{k_b T}{\sqrt{2}\pi P \sigma^3} \tag{3.1}$$

This provides a measure of the rarification of the gas. This can then be compared with the characteristic length of the flow field, $l$, which can either be taken as the characteristic dimension, or the gradient of a bulk property, such as density

$$l = \frac{\rho}{|\frac{d\rho}{dx}|} \tag{3.2}$$

The ratio of the characteristic length to the mean free path of the gas is known as the Knudsen (Kn) number

$$Kn = \frac{l}{Ł} \tag{3.3}$$

The value of which is used as a measure of the rarefaction of a gas with respect to the scale of the system, in order to test the validity of the continuum approximations. Typical values are shown in Figure 3.1 from the large scale continuum to molecular systems. A very small Kn number ($< 0.001$), describes a system that is well within the continuum laws, but as the Kn increases the small scale effects of the fluid become more pronounced [?].

The first stage of the breakdown of the continuum approximations occurs at a Knudsen number of greater than 0.001 where areas of high gradient, such as boundaries, cannot maintain the continuous distribution of macroscopic properties. This is a result of the deviation from thermodynamic equilibrium, where there are insufficient collisions in the system for the energy to propagate smoothly in areas of high gradient such as at the boundaries. The low number of molecular interactions with the boundary means that the velocity

and temperature of the solid and fluid are no longer the same at the interface, causing a violation of the no-slip condition (similarly the no jump in temperature condition) that is assumed in continuum mechanics [46].

To account for this initial deviation from the classical equations, the linear Navier boundary condition [47] describes the slip and no-slip conditions by relating the difference in velocity between the wall and fluid, $(u_{fluid} - u_{wall})$, to the strain rate at the wall, $(\partial u/\partial y)_{wall}$

$$u_{fluid} - u_{wall} = L_s \left(\frac{\partial u}{\partial y}\right)_{wall} \tag{3.4}$$

With $L_s$ being the slip length. This slip condition can be included in the continuum approximations as long as slip length $L_s$ is known or obtained via molecular simulation or experiment. For normal large scale continuum simulations $L_s$ is so small that the fluid and wall move at the same speed (no-slip condition), but as the Knudsen number of the system increases above a value of 0.001, the slip effect becomes more pronounced. The amount of slip that is allowed depends on the roughness of the surface over which the fluid is flowing and the interaction rate between the fluid and solid molecules.
A similar equation for the slip at the boundary, that includes temperature discontinuities, was presented by Smoluchowski [48]

$$u_{gas} - u_{wall} = \frac{2-\sigma_v}{\sigma_v} Ł \left(\frac{\partial u}{\partial y}\right)_{wall} + \frac{3}{4}\frac{\mu}{\rho T_{gas}} \left(\frac{\partial T}{\partial x}\right)_{wall} \tag{3.5}$$

$\sigma_v$ is the momentum accommodation coefficient, and Ł is the mean free path from above. The first term is the modified Equation 3.4 with the slip length being replaced by a description of roughness and scale, $\frac{2-\sigma_v}{\sigma_v}$Ł. The second term represents the thermal creep, responsible for slip in the direction of increasing temperature along the surface [49]. Similarly, the equation to account for temperature discontinuities at boundaries is,

$$T_{gas} - T_{wall} = \frac{2-\sigma_T}{\sigma_T} \left[\frac{2\gamma}{\gamma+1}\right] \frac{Ł}{Pr} \left(\frac{\partial T}{\partial y}\right)_{wall} \tag{3.6}$$

where $T_{gas}$ and $T_{wall}$ are the temperatures of the fluid and wall respectively, $\gamma$ is the specific heat ratio and $Pr$ is the non dimensional Prandtl number. $\sigma_T$ is the thermal accommodation coefficient, similar to the momentum coefficient

of Equation 3.6, $\sigma_T$ characterises the material properties of the interface.
These equations can apply modifications to the continuum governing equations, but the violation of the no-slip condition is only the initial sign of the failure of the continuum laws and the approach to the limit of the continuum laws. However, Bing-Yang *et al.* [29] demonstrated that the Maxwell slip model fails as the surface roughness of the wall approaches the mean free path of the fluid for gas systems.
For higher Knudsen numbers, the violation of the continuum laws becomes more serious, as the effect finite numbers of molecules affects the propagation of macroscopic properties further away from boundaries and wider areas of high gradient. Also the localisation of mass and energy at molecular sites, starts to bring statistical variations into the fluid properties. This type of breakdown occurs in the transition region between the continuum and molecular regions.
A transition region where continuum approximations cannot accurately predict the system behavior is between Knudsen numbers 0.1 to 10. In this region, the mean free path and characteristic length of the gas are comparable, indicating the importance of the underlying molecular physics of the system. In these systems, the continuum equations cannot be applied, even with boundary modifications.
For Knudsen number greater than Beyond a Kn of 10, the mean free path of the gas is more than 10 times greater than the characteristic length of the system, and the fluid is well within the limits of, and can only be described by molecular physics.

### Liquid Flows

The transition between the continuum and molecular region for liquids, goes through the same stages as for gasses, however there is no parameter to act as a guide throughout the transition. The Knudsen number cannot be defined, as there is no concept of mean free path for liquid flows and molecules are in a constant state of collision and move over much shorter distances [49,50]. The kinetic theory for liquids is not as well advanced as for dilute gasses, making the transition difficult to measure, however Loose and Hess [51] showed that thermal equilibrium, and therefore Newtonian behavior, stops as the strain

rate $\dot{\gamma}$ exceeds twice the molecular frequency scale, $\tau$.

$$\dot{\gamma} = \frac{\partial u}{\partial y} \geq 2\tau^{-1} \tag{3.7}$$

where the molecular time scale is derived from molecular properties of mass, $m$, well depth, $\epsilon$ and collision radius, $\sigma$, as,

$$\tau = \sqrt{m\sigma^2/\epsilon} \tag{3.8}$$

Where $u$ is the longitudinal velocity normal to $y$, $\sigma$ and $\epsilon$ are the characteristic length and energy scales for molecules of mass, $m$. However, under standard conditions the extremely small molecular time scale for liquids such as water, puts the continuum/Newtonian limit extremely high.
Other studies by Pfahler *et al* [52] showed the breakdown of the continuum description by comparing experimental data for the friction factor in a micro-channel liquid flow, with the continuum description. They varied the speed and depth of the channel ($100\mu m$ wide by $0.8\mu m$ and $1.7\mu m$ deep) and plotted the friction factor as a function of the Reynolds number, comparing the results with those of Navier-Stokes predictions. They concluded that there was a well defined point at which the behaviour of the liquid deviated form the predictions.
Liquid flows however, remain difficult to classify in terms of the deviation from the continuum description. However, when compared to gasses, the breakdown occurs at smaller length scales, due to the closer packing of the molecules.
Equations 3.5 and 3.6 are also valid for fluids but, as described above, the exact point at which they apply is difficult to determine.

The discussion above shows that there is a limit at which the continuum approximations can no longer be considered accurate. Beyond this point it is necessary to include information from the molecular scale. Methods for the inclusion of this information will now be presented.

### 3.2.2 Top-Down Meso Scale Methods

This method of domain coupling has been mainly applied to structural problems where the particles of the molecular region are frozen with a near zero mean square displacement. In the region of the interface, a finite element

mesh is scaled to dimensions which coincide with the molecular lattice. The boundary between the two regions must ensure that there is a connection between the degrees of freedom of in the continuum and molecular models that maintains all dynamic and conservation laws. The thickness of the interface is as small as possible so that the number of parameters linking the two domains is kept to a minimum. The domain coupling must also maintain the thermodynamics, static elastic, and dynamic elastic responses of the material.

One method of coupling length scales in this way was developed to deal with crack propagation was by Rafii-Tabar and coworkers [53] and resembles an iterative variation of the serial approach (Figure 3.2) applied to crack propagation problems. With this approach, the continuum region is used to

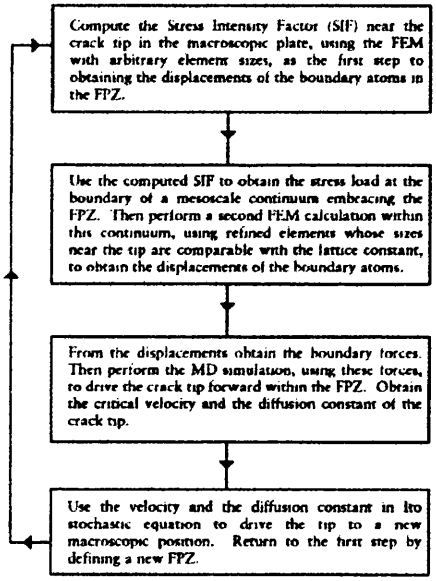


Figure 3.2: Iterative Procedure for Hybrid Coupling of Length Scales [53]

calculate the boundary conditions for the molecular region, which calculates the effective stochastic diffusion coefficient and growth at the crack tip for a short time interval, using a zero temperature molecular simulation. The average velocity that the tip travels is also calculated and all the molecular information is fed back into the continuum simulation for the next iteration. This approach uses a form of Langevin dynamics at the crack tip and FE simulation for the continuum with the molecules at the interface between the two representing the boundary conditions for the molecular region and have

no dynamics and are thermally insulating. So far this method has been limited to two-dimensional simulations with an molecular region not around 5000 molecules.
This approach was also used by Ayton *et al.* [54], who used this approach to simulate flow through biological membranes.

A similar coupling scheme was also described by Abraham [55] in the MAAD program. In this method, finite element and molecular dynamic regions are linked by defining a region between the two called the handshake region with a Hamiltonian described by finite element cells and two/three body interactions crossing the boundary, each contributing half weight. The displacements in the finite element region are updated by a molecular dynamic algorithm so ensure seamless transmission of displacements.

The Hybrid models are very computationally efficient and give almost seam-

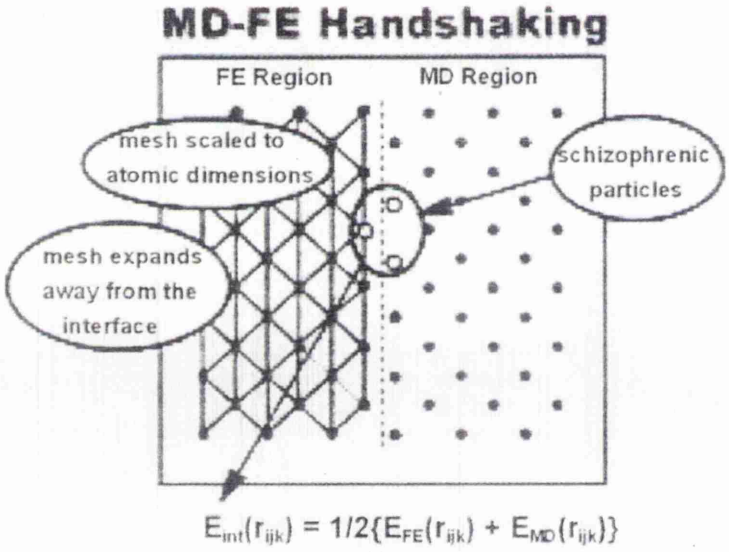


Figure 3.3: MAAD Handshake Region (FE/MD) [55]

less coupling between areas of different length scales. However, direct coupling between molecular sites and continuum meshes is not suitible for fluids, as the molecular sites in a fluid move constantly throughout the domain (thermal motion/diffusion) even if the fluid is at rest. Coupling between fluid domains requires an interface between the two that allows for the movement of molecules. For solids, the validity of the continuum equations can be extended, as the molecules are within a rigid structure and they move little, if at all, allowing the continuum laws to be valid at smaller scales. In fluids

however, the dynamic molecular structure cannot be treated in the same way. Garcia *et al* [56] developed the coupling between the Navier-Stokes equations and DSMC (Direct Simulation Monte Carlo) models for dilute gasses by using a Chapman-Enskog velocity distribution based current generation scheme. This model considers only the scattering of molecules due to collisions and it is the diffusion that is vital to the model, as opposed to the simulation of cracks and solid systems, where diffusion is negligible and position is important. The method they developed is based around an adaptive mesh and algorithm refinement (AMAR) base, where they use DSMC is used to enhance the accuracy of the final stage of refinement. The simulation is detailed as follows. The continuum region covers the whole domain of the simulation, even over laying the DSMC region. The DSMC region is contained within a number of these cells, and surrounded by buffer cells. Buffer cells are controlled by the

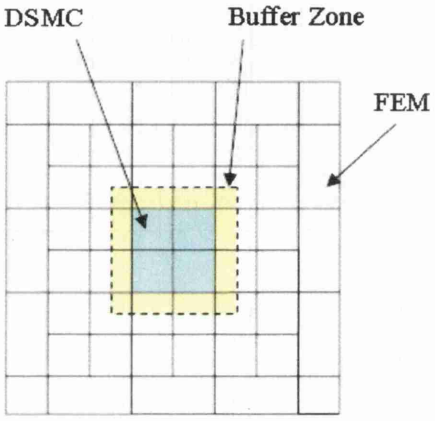


Figure 3.4: Direct Simulation Monte Carlo used as the finest stage in an adaptive mesh and algorithm refinement method [56]

continuum solution at the end of a molecular time step, the molecules within the buffer zone are deleted and a new set of molecules are created using the hydrodynamic parameters of the continuum solution. The buffer cells are used by the continuum part of the solution for two reasons, the first is to monitor the flux through the boundary between the DSMC and continuum region, and the second is to influence the DSMC region by assigning the density and velocity of the created molecules. The time steps used are not the same in the DSMC and continuum solutions, as this would lead to instabilities, however they must both progress at the same rate. There are in general four molecular time steps, $t_{part}$, to every one continuum time step, $t_{cont}$, meaning that the

DSMC simulation must perform four steps for every one of the continuum. The method follows the following routine.

1. Continuum region performs one step in time, $t_{cont}$, through all cells including those covering the DSMC region.

2. Molecules in the buffer region are replaced with particles determined by the hydrodynamic gradients (density/velocity/temperature) of the continuum cells that cover them. Molecules places are given a velocity assigned by a distribution, as in the initialisation stages of molecular dynamics, which is determined by the form of the continuum solver. If the simulations are based on the Euler equations, the Maxwell-Boltzman distribution is used, and for Navier-Stokes equations the Chapman-Enskog distribution is used.

3. Momentum and energy corrections are made to all other particles, determined by their overlying continuum cells.

4. DSMC advances one molecular time step, $t_{part}$. Particles are allowed to pass freely in and out of the buffer zone

5. Particles crossing the boundaries between cells contribute to a correction of the inter-cell flux between the continuum cells.

6. Repeat DSMC time steps (4-6) until continuum time step, $t_{cont}$, is reached

7. Conserved quantities, such as density, are used to correct continuum values.

8. Simulation then repeats steps 1-8 until total time is reached

This method uses molecular simulation overlaid over the continuum mesh to refine the continuum solution. As the molecules are created in the buffer zone at each time step, this causes problems of relaxation of the molecules at the beginning of each molecular iteration, which could influence the results, as the boundary conditions are essential to the solution of such a problem
A similar approach was developed by Nie *et al.* [57], where a navier-stokes region was coupled to a molecular region to evaluate a channel flow with a fixed obstacle. The molecular region was placed around the obstacle.

The approach to the meso scale has been attempted in many ways, the most publicised way is to couple continuum approximations with molecular information. This allows for the minimum volume considered by molecular simulation, thus improving the overall efficiency of the simulation. There are however, some distinct problems associated with coupling these two simulation schemes. Firstly, the continuum and molecular simulations have a different frame of reference. That is to say that the continuum region models the fluid in a steady state picture where variables like velocity, pressure and density take values relative to fixed positions in the system (Eulerian approach), where as the molecular model considers the dynamics of the molecules withing a fixed region (Lagrangian approach). This presents a barrier to the coupling of the two schemes that can be overcome, as will be shown, but can be especially tricky for dynamic fluid systems.
Secondly, as there is a substantial gap in the between effective length scales considered by continuum and molecular simulation, especially for dense gasses and liquids. Consequently, the majority of coupling schemes have been developed for solid and fracture mechanics, which present a simpler problem as molecules are fixed to lattice sites, allowing for a much simpler integration between molecular and finite element approximation. Other schemes work with relatively rarefied gasses, with low Knudsen numbers, that allow the molecular simulation to operate at to continuum dimensions, as the computational effort of molecular methods scale with the number of molecules in the system.
Another branch of 'top down' simulations methods are those which define new systems of governing equations which include a higher degree of molecular physics. These will be considered next.

### Dissipative Particle Dynamics

A similar approach is known as Dissipative Particle Dynamics (DPD) introduced by Hoogerbrugge and Koleman [6]. This is effectively similar in concept to molecular dynamics, where the particles used move using newtons laws, but the interaction laws are different from those used in molecular dynamics. Here, a single particle represents a group of molecules moving throughout the domain, and to account for the internal degrees of freedom of each 'area' of fluid, the interactions have fluctuating and diffusive components. DPD is typically used for simulating colloids [58] and complex fluids [59, 60], as its particle structure allows for the easy integration of large fluid particles and suspen-

sions.
Dissipative particle dynamics was originally derived from a molecular dynamic framework, but the bulk particle interaction laws are closer to continuum equations and include modification to represent the molecular physics. This method is widely used mainly for simulations in the high end of the meso scales. Because of its representative particle approach, this method allows easy coupling with continuum particle methods such as Smooth Particle Hydrodynamics.

### Lattice Boltzmann Method

The LB method considers for the flow domain by solving the Boltzmann equation over a discrete lattice/mesh. In this method, molecules exist as numbers possessed by each cell and flow is considered as the flux of molecules between cells. These lattice based methods are mainly used to solve highly porous and complex geometries [5, 61] at meso scale and for multi-component flows [62]. Lattice Boltzmann simulations are best suited to simulations of sparse gas systems where molecular interactions rarely occur. A similar approach using the Boltzmann equation was developed by Naris *et al.* [63] which implemented a simplification for the collision integral.

The Lattice Boltzmann and Dissipative Particle Dynamics methods have been combined with Smooth Particle Hydrodynamics to construct the DL MESO [64] package. This combination of methods has been very successful at modelling within the higher end of the meso scale. These methods allow fluid to be modelled at meso scales, however they have their limitations. The LB and DPD methods make assumptions about the distribution of the molecular physics occurring within their elements/particles, and the actual internal molecular interactions are approximated. The molecular degrees of freedom are removed to save computational load.

An alternative approach to investigating fluid behaviour and capture fluid properties at meso scale is from first principles of molecular interactions, or the 'bottom-up' approach. By directly modelling the molecular interactions within a fluid, it is possible to model a fluid in an environment that is closer to experimentation than simulation.

## 3.3 Bottom Up Approach for Meso Scale Computation

As has been demonstrated in the previous section, the continuum approximations begin to fail within the meso scale region ($\leq 10^{-6}$m). However, although the continuum assumptions fail, the bulk properties are still observable and have significant impact and meaning when a meso scale fluid is considered. This section demonstrates how meso scale fluid systems can be modelled from a 'bottom up' approach, by considering the fluid physics from first principles of molecular interactions. These molecular simulations also demonstrate bulk behaviour, modelling the continuum properties from their molecular origins, as described in Section 2.2.1.

### 3.3.1 Molecular Dynamics Model

Molecular dynamic simulations model the individual molecules of a fluid by representing each individual molecule as a coordinate point in space, with a set of molecular properties attached to it which describe its mass, size and interaction strength. The general scheme for molecular dynamics is presented in Section 2.3 and this section will focus on the details of the simulation and its relevance to meso scale systems.

#### Molecular Potential Model

The most commonly used potential model used in molecular dynamics is the Lennard-Jones potential. Inter-molecular potentials are used as a simplified model of all the interactions that are present in real systems. The approximation is derived in different ways, either by experiment or derived from first principles of molecular dynamics. Experimental based potential models are generally based more on realism than provable mathematics. The actual potential model represents, in general, the short range repulsive (Pauli/Coulomb forces), and long range attractibe (Van de Waals/London) interactions however in all Lennard-Jones models electronic degrees of freedom are neglected. There are two basic parts of the Lennard-Jones potential, an attractive part

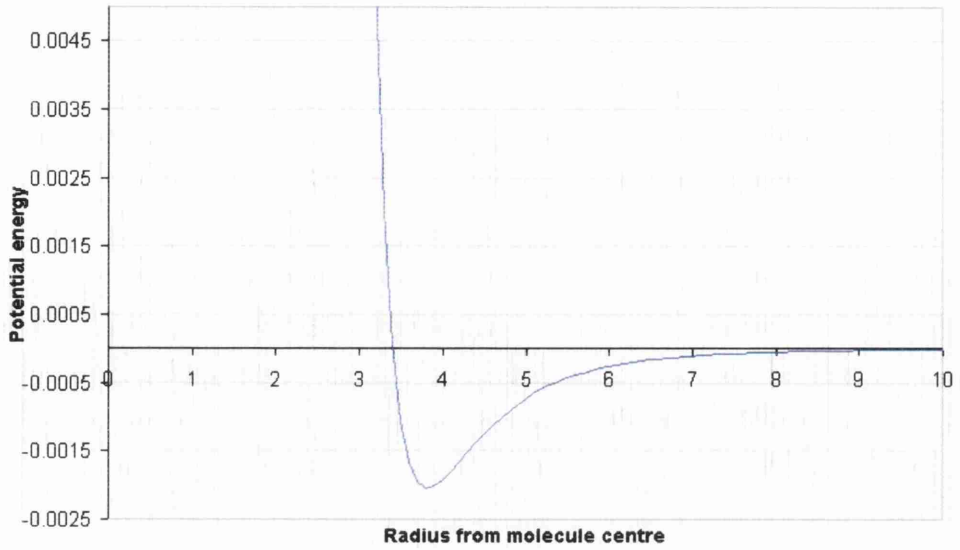


Figure 3.5: Lennard-Jones interaction potential for methane(CH4)

| | Well depth ($\epsilon/k_b$ (K)) | Collision diameter ($\sigma$ nm) |
|---|---|---|
| C | 28 | 0.34 |
| Ar | 124 | 0.342 |
| CH4 | 148 | 0.304 |
| Kr | 190 | 0.361 |
| Xe | 229 | 0.406 |

Table 3.1: Lennard-Jones potential parameters

and a repulsive part. This is described mathematically as:

$$U_{r_{ij}} = 4\epsilon \left( \left( \frac{\sigma}{r_{ij}} \right)^{12} - \left( \frac{\sigma}{r_{ij}} \right)^{6} \right) \tag{3.9}$$

where $U(r_{ij})$ is the potential energy between molecules $i$ and $j$, with $r_{ij}$ being the distance between them. Parameters $\sigma$ and $\epsilon$ represent the collision radius and well depth (strength of interaction) respectively. $\epsilon$ is commonly refered to in the form $\epsilon/k_b$.

Some common values for Lennard-Jones interactions are shown in Table 3.1

When these soft sphere interactions take place in simulations it is necessary to shorten the range of the potential to prevent overlapping in periodic systems and to reduce the computational load. The cut-off is usually performed at two and a half times the molecular diameter, but is dependant on the system

and is generally limited in periodic system to a maximum of half the distance between the two periodic boundaries.
The Lennard-Jones potential, despite its common use, should only be applied where there are no electrons available for bonding and there are only weak long range interactions. More complex materials such as metals and semiconductors require a more complicated many-body potential model rather than a pair-wise model such as the Lennard-Jones. Many bodied potentials are affected by local environment density, assigning weaker bonding where many molecules are present. Even in rare gasses, many body effects are present, however they are much less pronounced.

For systems containing multiple types of molecules, for example fluid mixtures, there are rules that combine the Lennard-Jones parameters of the two components, called the Lorenz-Barthelot mixing rules [65]. For the collision radius, the parameters are combined to give a single value for the evaluation of the Lennard-Jones potential between the two dis-similar molecules, for example the radius for molecules numbered 1 and 2 is given as,

$$\sigma_{1,2} = \frac{\sigma_1 + \sigma_2}{2} \tag{3.10}$$

which takes the average of the two values. For the well depth, they are combined as follows,

$$\epsilon_{1,2} = \sqrt{\epsilon_1 \times \epsilon_2} \tag{3.11}$$

For systems with many molecules, the searching through the flow domain for pairs of molecules, close enough to interact with non-negligible Lennard-Jones potentials, can take a significant amount of time to process. Efficient schemes for searching for, and keeping lists of, neighbouring molecules will now be presented.

### 3.3.2 Boundary conditions

In simulation of real systems, the molecules need to be contained in a controlled environment. Either geometric or computational constraints can limit the size of the simulation to a finite control volume, but molecules must be contained within the simulation cell and must have the ability for the system beyond the confines of the simulated volume to influence the system. The

method by which this is done must be carefully designed and applied.
In molecular simulations where fluid boundaries are used, periodic boundaries are frequently used.

### Periodic Boundary Conditions

Molecular simulation is currently only practical on a very small scale due to the computationally demanding particle based techniques. It is therefore necessary is some situations to cut down the size of the simulation region to decrease the run time, similar to the way finite element analyses take advantage of symmetry. Periodic boundary condition effectively surrounds the simulation cell with identical copies of the main cell as shown in Figure 3.6.

As a molecule passes over the boundary and out of the primary cell and

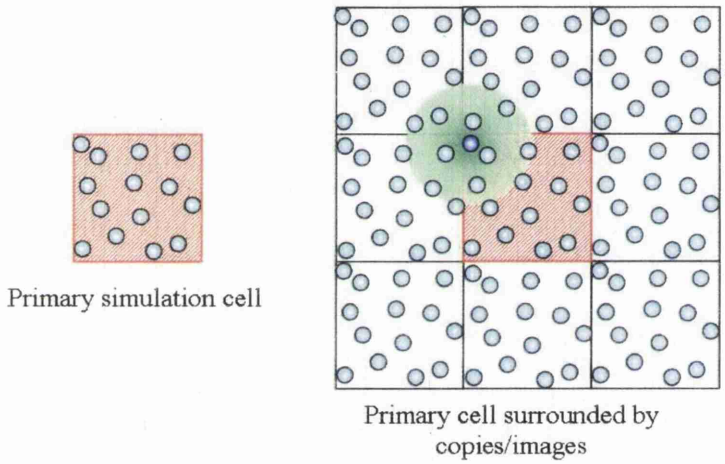


Figure 3.6: Periodic boundary conditions

into an adjoining image, at the same time an identical molecule with exactly the same properties passes in from the image on the opposite side into the primary cell. In the case of the soft sphere model, cross boundary interactions also need to be taken into account by finding the nearest image of an interacting particle. This is best illustrated by the one dimensional example in Figure 3.7 where it is shown that as the separation between two molecules becomes greater than $a/2$, the particle $i$ is nearest to the image of second particle, $j$.

At the boundaries of the main cell, the simulation sees and interacts with the opposite side of the same cell, effectively looping itself and creating the appearance of an infinite unconstrained simulation.

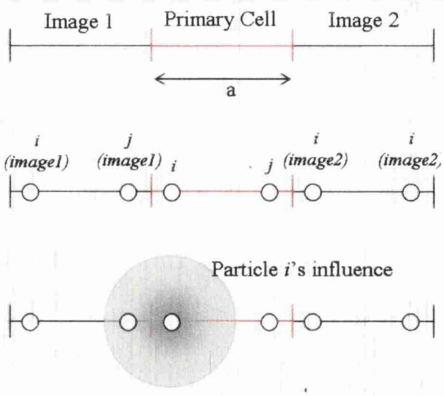


Figure 3.7: Soft sphere cross boundary interaction

The Periodic boundary conditions allow for the automatic conservation of flow properties. Mass is conserved perfectly as there is no molecule deletion or creation by the boundaries, the molecules simply pass through the boundary as if it were not there. Similarly, energy is conserved, and the boundary presents not obstacle to inter molecular interactions or molecule movement.
These periodic boundary conditions are for approximating a very large or infinite region of fluid with a relatively small simulation cell. There are also situations where it is necessary to confine a fluid to a region using solid walls or boundaries, and it is this situation that we will consider next.

### Wall boundaries

For a molecular simulation of fluid with solid boundaries, it makes sense to apply a solid molecular wall with a similar interaction model by simulating all the frozen solid molecules in that wall. Although this is the most numerically accurate approach, it is also the most computationally demanding. Even for the case of a single walled carbon nano tube, where there is only one layer of 'solid' molecules containing the flow, solid structures generally have a higher density and add a large number of particles to the simulation. There are several alternative strategies to save computation time, which we will now discuss.
Fortunately, there are several strategies available to model solid boundaries, while maintaining all the information about a molecular wall. To reduce the computational load of a molecular wall, the wall molecules can be completely frozen, removing all degrees of freedom from the wall. This allows the molec-

ular walls to retain their roughness/corrugation, but they loose the ability to absorb energy from the fluid [66] as the cost of reduced computation time. This also results in a stiffer wall interaction model as wall molecules cannot react to fluid molecule collisions, but significantly reduces the number of force interactions that need to be evaluated.
Over meso length and time scales, the collision rate with solid boundaries can be very high, which allow the molecular behaviour at boundaries to be applied as an approximation over many collisions. The main scheme for applying this is the diffuse boundary condition [67], which will be considered in the next Chapter

The above describes a molecular model for use at nano scales ($\approx 10^{-9}m$), however the scales of interest are between $10^{-6}m$ and $10^{-8}m$. Therefore this physics model must be able to provide information about the fluid, on these larger scales. Methods for up scaling the physics and information from these molecular simulations will now be discussed.

### 3.3.3 Bottom Up Meso Scale Methods

The main issue faced with Bottom up methods is the upscaling of information from the molecular model, and the removal of degrees of freedom from the system to save computational resources. The first approach considered is the serial approach, where a very small molecular simulation describes the physical relationships behind a large scale fluid system.
A serial approach is used when the scales are only weakly linked together. Parameters are calculated at the smallest scale and then the information is then fed into the next scale up where it is used to calculate a larger scale parameter, and so on until the large-scale analysis can be performed.
This approach is best described by an example. Clementi *et al.* [68] did a study of the tidal circulation in Buzzards Bay by starting with the quantum-mechanical simulation single water molecule. This information was then used to model the behaviour of a small cluster of molecules and then a database of interactions between the molecules was formed. The information contained in the database could then be used to describe an empirical potential to be used in a molecular dynamic simulation. The density and viscosity of water could then be calculated and fed into a continuum scale computational fluid

dynamic simulation to predict the tidal movement of the bay. This shows how an accurate solution can be derived by up-scaling information from molecular to kilometer scale. However, in the serial approach information only passes one way through the calculation and therefore it use is limited to situations such as the one described above where the scales are only weakly linked.

### Derived Scaling

Coupling techniques previously described, involve coupling several regions of different scales, now a method will be discussed that involves a single model that has a varying density in the same way that varying mesh densities are used in regular large scale FE simulations. This negates the need to couple models together so the system can be simulated as a whole.
The best way to understand this approach is to imagine the simulation in two layers, one containing molecular information and covering the whole system at a fine scale, and the other as an mesh, similar to FE, scaled from nodes corresponding to molecule sites close to region of interest up to large scales where elements contain many molecule, Figure 3.8.

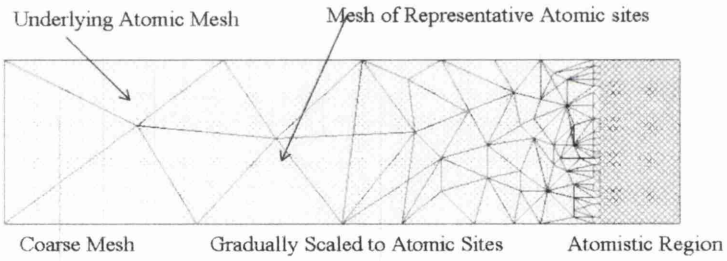


Figure 3.8: Constant Density molecular layer (Small dots) Overlaid with Equivalent FE Mesh

As the large-scale elements contain many molecules, there is a large amount of information that is unnecessary as in a region of low activity a lot of the data held by the parameters of each molecule is approximately the same. Therefore degrees of freedom need to be removed from the system to cut down on the processing of unnecessary information, and is done using the quasi-continuum method, which is described below. The cut-down molecular properties are then used to obtain the equations of motion by averaging molecules surrounding each node, resulting in the mean behavior represent-

ing an area of molecules. This is similar to a standard FE simulation but instead of the equations of motion being computed from a continuum model, the molecular model is used. As the size of the elements reduces, the number of molecules within each element reduces until the nodes of the mesh coincides with the sites of the molecules, where the equations of motion are derived from individual molecules and there is no longer a need to discard information. As can be seen, the less demanding element based simulation gradually breaks down into the more demanding molecular simulation as the scale is reduced, providing almost seamless coupling.

Further away from a region of interest there is less activity and the resolution of the solution can be reduced to cut down computation time. This is done by increasing the size of the elements in the mesh, removing degrees of freedom from the molecules, and averaging the properties to approximate the motion of the area. It was found that in some statistical models the Hamiltonian keeps its form as the degrees of freedom are removed, only the parameters change, so the parameters can be redefined as the scale of the mesh is changed by the use of an equation. The renormalization group equation [69] does just that and can update the Hamiltonian at any scale.

The method presented to reduce the number of degrees of freedom was created by Tadmor *et al.* [70] and later developed by Phillips and Coworkers at Brown [71–74] called the Quasicontinuum technique.

**Quasicontinuum Technique** In areas at a distance from the area of study, where the displacement fields contain no steep gradients, the energy of the molecules local to each other possess approximately similar values. It is this approximation that is the key to the Quasicontinuum method which aims to reduce the processing time of the mid to large-scale areas of the simulation. Assuming that this is true, the local neighborhood of molecules can be represented by the value of just one molecule. By doing this the number of degrees of freedom in the computation of the energy of the system can be dramatically reduced. The standard method for computing the system energy involves the summation of the energies of all molecules in the simulation, as below

$$E_{total} = \sum_{i=1}^{N} E_i \tag{3.12}$$

Where:

$$\begin{aligned} E_{total} &= \text{total energy} \\ E_i &= \text{energy of individual molecule } i \\ N &= \text{total number of molecules} \end{aligned}$$

However, by representing an area of molecules with a single node/particle can reduce the computational demand dramatically. This is applied by choosing an finite element mesh with nodes defined by a quadrature rule over the relevant area at summing the energies of the molecules at the quadrature defined sites multiplied by weights proportional to the volume of representation of each representative molecule and the number of molecules in that area. This reduced sum contains far fewer terms than the energy equation described above.

$$E_{total} = \sum_{\alpha=1}^{M} E_\alpha \tag{3.13}$$

Where:

$$\begin{aligned} E_{total} &= \text{total local energy} \\ E_\alpha &= \text{energy of representative molecule } \alpha \\ M &= \text{total number of local representative molecules} \end{aligned}$$

The molecules that are not included do not possess any properties of their own except their position vector. Only molecules local to the representative node contribute to the properties of the node, as shown in Figure 3.9.

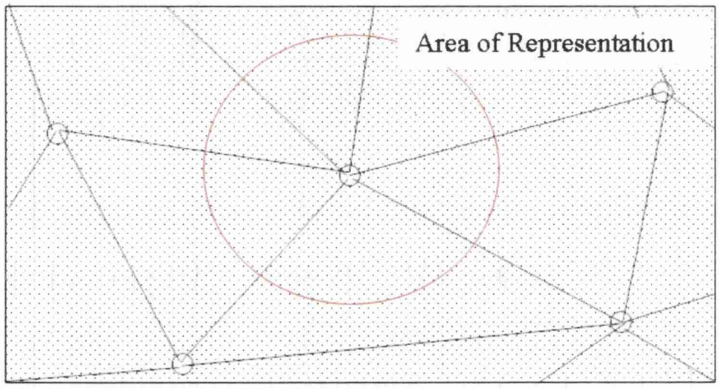


Figure 3.9: Lattice Structure of Molecules in Regions of Low Gradients

By assuming that the deformation gradient is also homogenous around the

representative node, the local deformation gradient can by defined, $F$. The deformed configuration has Bravais Lattice Vectors, $b$, that are obtained from those in the reference configuration $B$ as below.

$$Ba = Fba \tag{3.14}$$

Once the Bravais Lattice Vectors are found, the formation of the energy equation reduces to basic Lattice statics.
As the area of interest is approached, gradients increase causing the areas that can be assumed to have uniform energy get smaller and smaller until there cannot be any assumptions about the homogeneity of neighboring molecules. At this point the nodes of the mesh occupy all molecular sites. It is at this point that all quadrature weights become unity and every molecule is accounted for. The computational cost of applying this method is relatively high, however it stays constant throughout changing mesh sizes, however errors arise from the lack of continuity between cells. This becomes more dominant near the breakdown of the effective FE mesh where there are only a few molecules per cell and the position of the molecules becomes important. This leads to small added forces, which can be accounted for. This method is generally used for two or three-dimensional tests to model defective systems (cracks, dislocations and interfaces) and has recently been selected to study the effect of nano-indentation. [72].
So far, studies have been limited to solid problems as the lattice structure of a solid leads to an easily predictable deformation. This approach is difficult to apply directly to fluids as new laws for the removal of degrees of freedom will be needed.

### Approximating Methods

A wide range of methods are also available for up scaling molecular information from alternate applications. Molecular simulations rely on molecules being represented by data points with properties associated to them. Point approximating methods such as Smooth Particle Hydrodynamics (SPH) and Moving Least Squares (MLS), are capable of averaging data spread over a number of points. These methods show promise for the upscaling of information from molecular models.

**Smooth Particle Hydrodynamics (SPH)** SPH, first presented by Lucy [75], is a continuum particle method that solves continuum equations over a system of moving interpolation points [76, 77]. The property values at any point throughout the fluid relies on the properties of the surrounding points, and it is the method of sampling these properties that has most significance to this application. Instead of sampling the continuum properties, we seek to use this approach to extract the local bulk properties from the molecular motion at discrete nodes placed throughout the flow domain. The SPH method constructs average property values as a function of distance from each central point with the use of a weighting, or kernel, function.

**Moving Least Squares** The moving least squares approximation scheme relies on the construction of many least squares approximations applied over a large number of points [78]. This method is generally used for creating smooth surfaces over mesh structures in computer graphics. This method is generally applied as an approximation to all points in the system, taking each one in turn and constructing an approximation from its neighbours. The approximation in MLS is more advanced than the kernel averaging approach of SPH, where a polynomial function is fitted to the local property distribution.

This is similar to the approach taken by Liao and Yip [79], who used the underlying molecular information to fit a continuous pre-determined temperature function described over the flow field, to the molecular property distribution. Also, the Equivalent Continuum Mechanics (ECM) [80] method used the Meshless Local Petrov-Galerkin method to solve for the local displacement in a solid molecular lattice.

**Coarse Grained Molecular Dynamics** Coarse Grained MD (CGMD) [81] was developed to deal with dynamic and finite temperature systems. In the cases concerning crack propagation, hybrid models work well and allow transfer of strain fields and elastic waves from one region to another, with minimal back scattering. However finite element based methods start to break down as scales reach molecular dimensions. One of the basic principles behind finite element assumes that the energy of each element is evenly distributed, but when the elements only contain a few molecules, the energies are localised in the

nucleus (Kinetic energy) and in the covalent bonds between the molecules (Potential energy). CGMD provides an alternative to finite element that is slightly improved at large scales and greatly improves at small scales at the interface with molecular dynamic simulation. In situations such as crack propagation, or very small systems, high frequency elastic waves have more of an effect; CGMD provides improved methods to deal with these, however these waves are negligible for larger systems and systems with less strong sources. CGMD constructs the coarse-grained structure with statistical techniques evaluating the interpolation of the displacement field of the molecules and their equilibrium position, resulting in a weighted sum. This method acts as a replacement for the finite element method described before and shows significant improvement in the treatment of the elastic wave spectrum and small-scale analysis. The computational demand is higher than regular finite element techniques, so it is used mainly where high performance is required or where the interface region is close to an area of interest.

## 3.4 Summary

As has been shown in this and the previous chapters, the continuum equations are unable to account for the molecular scale effects that become important at meso scales. It is therefor necessary to include this molecular information in the simulation model. This chapter has presented and discussed two approaches by which to include these effects, the 'top down' and 'bottom up' approaches.

The top down approach uses molecular simulations only in regions where they are needed, as the final level of refinement in a mesh. This approach is useful when considering a large system possessing a few small areas where molecular scale detail is needed. However, several issues arise especially when considering fluids. To couple a molecular region to a continuum mesh requires the continuum analysis to be valid with only a small number of molecules in each element. This is at the extreme of, and possibly past, the limits of the continuum approximation. Also, problems occur at the boundary between the two regions in fluid systems. The chaotic molecular motion of fluid molecules does not allow for simple boundary treatment at fluid boundaries, as the surrounding continuum region will not allow the use of periodic boundaries.

The chaotic nature of meso scale fluid systems leads to a bottom up scheme is more suitable in most situations. Here, the physics of the system are governed by a molecular model, and information is upscaled and areas of low activity can be simplified. These methods are however, very computationally demanding for large scale systems but can present a very accurate solution. The way in which information is passed, and degrees of freedom are removed is critical to the success of this approach. Approximation methods such as least squares and SPH are well suited to this application as they provide a reliable and well tested method for approximating information over many points.
The method developed in the next chapter is designed specifically to tackle meso scale fluid systems.

# Chapter 4

# Meso Scale Model Based on First Principles

## 4.1 Introduction

The meso scale represents the range of scales in between the scales that can be defined by the continuum laws (typically $\gtrsim 10^{-6}m$) and molecular physics (typically $\lesssim 10^{-9}m$). The behaviour of fluid at these scales is neither fully described by the bulk continuum, or the molecular scale properties and physics. Continuum simulations are unable to model molecular scale effects, which presents a lower limit to the scale at which these approximations can be used. A molecular scale fluid model can predict the behaviour of fluid by considering thousands of molecular interactions, but provides no method of quantifying bulk effects, such as viscosity or temperature and velocity gradients throughout the flow field.

Continuum mechanics, however, can describe and quantify these bulk properties, but molecular scale effects are ignored. The onset of molecular behavior must understood to recognise the point at which the continuum approximations fail.

The molecular dynamics simulations are able to accurately predict the behaviour of the fluid, however in order to quantitatively describe the flow, the bulk characterising properties, such as pressure, temperature and velocity need to be extracted. Such properties arise from the molecular interactions intuatively modelled by the molecular simulation, but are not quantified locally

as at molecular scales they are not well defined and have little meaning. At meso scales, these have increased importance as the bulk effects are visible and need to be considered in engineering applications.

In this chapter a bottom up meso scale method is developed. A molecular model is implemented to control the physics of the fluid, along with tools and modifications to improve the efficiency when dealing with large numbers of molecules. Also, areas of low activity are simplified (such as solid boundaries) to further improve efficiency. This physics model then passes molecular information to the up scaling routines where it is used to characterise the bulk fluid effects in terms of useful engineering properties

## 4.2 Fluid Physics Model

To model meso scale fluid flows from first principles, the physics of the fluid behaviour must be considered at a scale smaller than the meso scale. For this, a molecular dynamics model is used to evaluate the system in terms of the molecular interactions. As it is intended for the model to work with dense as well as spares fluids, the molecules interact via a soft sphere model with the non-bonded Lennard-Jones 12-6 potential. The use of molecular dynamic simulations has been highlighted in Chapter 2.4 and will be used along with the diffuse boundary conditions. The molecular model must be capable of simulating large numbers of molecules to allow access to meso scale systems of reasonable density(computational demand of a molecular simulation is heavily dependant on the number of molecules in the system but also dependant on the number of neighbours possessed by each molecule, which is related to the fluid density).
To keep track of the neighbours of each molecule, an efficient book keeping scheme, the Verlet lists, is implemented to the molecular dynamics model.

### 4.2.1 Book keeping

#### Verlet Lists

The most common method for searching for, and storing possible interactions is known as the Verlet neighbour lists [82], and is described below.

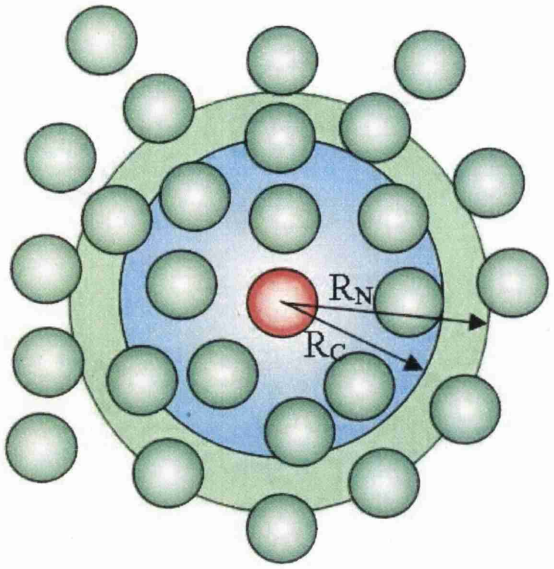


Figure 4.1: Interaction radius of cutoff potential $R_C$ and neighbour search $R_N$

This method works by using two arrays, one which stores the actual interactions (nlist), and another which acts as an index(npoint), referencing the start points for the neighbour lists of each individual molecule.
Once these arrays have been initialised, a full search is performed for every molecule, $i$, for all other molecules within $R_N$. The search is performed within a radius that is larger than the cut-off radius $R_C$ for the potential to include all particles that will interact with sphere $i$ over the next $n$ time steps (Figure 4.1). The difference between $R_N$ and $R_C$ is limited by the root-mean-square velocity of the simulation, with:

$$R_N - R_C < n\tilde{v}h \tag{4.1}$$

Where $R_C$ and $R_N$ are the cut off radius for the list and the potential respectively, $n$ is the number of time steps between list updates, $h$ is the time step length and $\tilde{v}$ is the root-mean-square velocity for the simulation. This limits the thickness of the region so that a molecule from outside the neighbour list cannot travel into a spheres interaction zone ($R_C$) without being included by an update of the list. This removes the need for the complete neighbour list to be repopulated at every time step, it is only updated periodically, saving a significant amount of computational time.
For any molecule in the system, $i$, the neighbour search is performed over all

molecules numbered $> i$. This prevents the same pairwise interactions being recorded twice, in an interacting pair, both will be in each others interaction zone.

This method works by using two arrays, one which stores the actual interac-

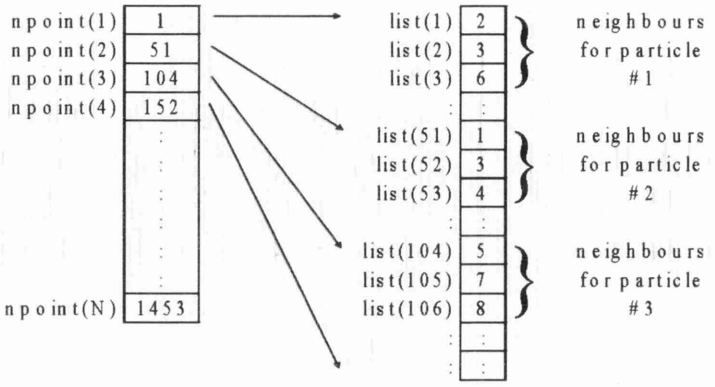


Figure 4.2: Verlet list book keeping scheme

tions (list), and another which acts as an index (npoint), referencing the start points for the neighbour lists of each individual molecule. For a system on $N$ particles, npoint contains $N$ entries. The value stored for each molecule refers to the entry number of npoint at which the neighbour list for that molecule starts. Therefore, the number of entries in npoint is much higher as, depending on density, each particle has around 50 neighbours which leads to an array of at least 15000 entries for a system of 300 particles. This is illustrated in Figure 4.2.

An alternative to the Verlet lists was proposed by Sun and Ebner [83] where arrays were used to achieve the same effect. This used no extra memory and performance scaled with the number of molecules in the system. However, the reference locality was broken in these lists, reducing the performance for large systems.

Once the neighbour lists have been updated, they are used to evaluate the net force exerted on each molecule by its neighbours.

### 4.2.2 Force interactions

The Lennard-Jones potential function is used for energy calculations and the force for each interaction is derived from the potential function as in Equation 4.2.

$$F_i = -\frac{\partial U(r_{ij})}{\partial r_{ij}} \tag{4.2}$$

Where $F$ is the force acting between the two molecules (positive for molecule $i$ and negative for molecule $j$, Newton's third law), and $U$ is the potential function. This represents the force acting along the line between the centres of the two molecules, and the resulting force is applied in opposite directions to both molecules using Newton's third law to save the same interaction being calculated again from the opposite direction. Applying the force of the collision to both molecules halves the number of collisions that need to be processes as each pair needs only to be evaluated once. This is done by only evaluating the entries in the list where $i > j$. The forces are converted to units of acceleration, the time step part of the simulation can proceed.

### 4.2.3 Time integration scheme

Given an initial resultant force for each molecule, the first step in the time progression loop is to predict the new positions of all the molecules at the new time. There are several methods [30] used to do this, and all are based on the simple finite difference algorithm.

**Verlet Algorithm** This is the most commonly used algorithm in molecular dynamic simulations, mainly because of its simplicity. The algorithm proceeds as follows:

1. Perform a Taylor-series expansion of $r(t)$ forward and backward in time:

$$r(t+\Delta t) = r(t)+\frac{\partial r}{\partial t}(t)\Delta t+\frac{1}{2!}\frac{\partial r^2}{\partial^2 t}(t)\Delta t^2+\frac{1}{3!}\frac{\partial r^3}{\partial^3 t}(t)\Delta t^3+O(\Delta t^4) \tag{4.3}$$

$$r(t-\Delta t) = r(t)-\frac{\partial r}{\partial t}(t)\Delta t+\frac{1}{2!}\frac{\partial r^2}{\partial^2 t}(t)\Delta t^2-\frac{1}{3!}\frac{\partial r^3}{\partial^3 t}(t)\Delta t^3+O(\Delta t^4) \tag{4.4}$$

2. Add these two expressions together:

$$r(t+\Delta t) = 2r(t)+r(t-\Delta t)+\frac{\partial r^2}{\partial^2 t}(t)\Delta t^2+O(\Delta t^4) \tag{4.5}$$

Equation 4.5 is the general form of the Verlet algorithm

It is easy to see that the truncation error varies with $\Delta t^4$ making the prediction accurate to the third order, despite the absence of any third order terms. However, there comes a problem when starting off the algorithm, the approximation for $t + \Delta t$ relies on the current and previous time steps, $t - \Delta t$ and . At t=0, it is common to use the backward Euler method to estimate a value for $r(-\Delta t)$.

**Gear's Predictor-corrector Algorithm** The predictor corrector algorithm devised by Gear [84, 85] is used to describe the progression of the molecules throughout the domain during the simulation time $t$, which is broken down into a finite number of short time steps. The time step is sufficiently small, so the forces and accelerations can be considered as constant. Forces and accelerations are updated once every time step. There are three basic steps in this algorithm, prediction, evaluation and correction.

- **Prediction** Position, velocity, acceleration, third, fourth and usually fifth derivatives are predicted at $t + \Delta t$ from current time $t$ using a simple Taylor series for each molecule in the time step:

$$r_i(t+\Delta t) = r_i(t)\dot{r}_i(t)\Delta t + \ddot{r}_i(t)\frac{(\Delta t)^2}{2!} + r_i^{iii}(t)\frac{(\Delta t)^3}{3!} + r_i^{iv}(t)\frac{(\Delta t)^4}{4!} + r_i^{v}(t)\frac{(\Delta t)^5}{5!} \tag{4.6}$$

$$\dot{r}_i(t+\Delta t) = \dot{r}_i(t) + \ddot{r}_i(t)\Delta t + r_i^{iii}(t)\frac{(\Delta t)^2}{2!} + r_i^{iv}(t)\frac{(\Delta t)^3}{3!} + r_i^{v}(t)\frac{(\Delta t)^4}{4!} \tag{4.7}$$

$$\ddot{r}_i(t+\Delta t) = \ddot{r}_i(t) + r_i^{iii}(t)\Delta t + r_i^{iv}(t)\frac{(\Delta t)^2}{2!} + r_i^{v}(t)\frac{(\Delta t)^3}{3!} \tag{4.8}$$

$$r_i^{iii}(t+\Delta t) = r_i^{iii}(t) + r_i^{iv}(t)\Delta t + r_i^{v}(t)\frac{(\Delta t)^2}{2!} \tag{4.9}$$

$$r_i^{iv}(t+\Delta t) = r_i^{iv}(t) + r_i^{v}(t)\Delta t \tag{4.10}$$

$$r_i^{v}(t+\Delta t) = r_i^{v}(t) \tag{4.11}$$

- **Evaluation** The force evaluation at time $t$ yields an net force on each particle, which is converted to acceleration ($F = ma$) and compared with the predicted acceleration from the previous step, resulting in an error signal.

$$F_i = \sum_{i \neq j}^{N} -\frac{\partial U(r_{ij})}{\partial r_{ij}} \hat{r_{ij}} \tag{4.12}$$

Where $\hat{r_{ij}}$ is the unit vector between the centres of spheres $i$ and $j$. this force is then converted to an acceleration by dividing by the mass of the particle and subtracting from it, the predicted value for acceleration, $\ddot{r}_i(t + \Delta t)$ , giving $\Delta\ddot{r}_i$

- **Correction** The error signal $\Delta\ddot{r}_i$ from the difference between the accelerations is multiplied by a stability factor and used to adjust the positions. The stability factor set depending on the time step to maximise the stability of the algorithm.

$$\Delta\ddot{R}_i = \frac{\Delta\ddot{r}_i(\Delta t)^2}{2!} \tag{4.13}$$

$$r_i = r_i^p + \alpha_o \Delta\ddot{R} \tag{4.14}$$

$$\dot{r}_i = \dot{r}_i{}^p \Delta t + \alpha_1 \Delta\ddot{R} \tag{4.15}$$

$$\frac{\ddot{r}_i(\Delta t)^2}{2!} = \frac{\ddot{r}_i{}^p(\Delta t)^2}{2!} + \alpha_2 \Delta\ddot{R} \tag{4.16}$$

$$\frac{r_i^{iii}(\Delta t)^3}{3!} = \frac{r_i^{iiip}(\Delta t)^3}{3!} + \alpha_3 \Delta\ddot{R} \tag{4.17}$$

$$\frac{r_i^{iv}(\Delta t)^4}{4!} = \frac{r_i^{ivp}(\Delta t)^4}{4!} + \alpha_4 \Delta\ddot{R} \tag{4.18}$$

$$\frac{r_i^{v}(\Delta t)^5}{5!} = \frac{r_i^{vp}(\Delta t)^5}{5!} + \alpha_5 \Delta\ddot{R} \tag{4.19}$$

The corrected positions are then fed back into the Taylor series approximation for the next time step, and the simulation can proceed.

Values for stability factors, $\alpha_i$ depend on the order of the Taylor series expansion [8] and are shown in Table 4.1

These values can be derived from the studying the resulting stability matrices

| Order | 3rd | 4th | 5th |
|---|---|---|---|
| $a_0$ | $\frac{1}{6}$ | $\frac{19}{120}$ | $\frac{3}{16}$ |
| $a_1$ | $\frac{5}{6}$ | $\frac{3}{4}$ | $\frac{251}{360}$ |
| $a_2$ | 1 | 1 | 1 |
| $a_3$ | $\frac{1}{3}$ | $\frac{1}{2}$ | $\frac{11}{18}$ |
| $a_4$ | | $\frac{1}{12}$ | $\frac{1}{6}$ |
| $a_5$ | | | $\frac{1}{60}$ |

Table 4.1: Coefficients of the 5th order verlet algorithm

the accuracy of the prediction relies of the order, $k$, of the expansion, due to truncation error, $O(\Delta t^{k-1})$.
The main advantage of this method is its versatility. This method takes a single step forward in time, but can be modified to become a multi step method by combining it with the Verlet algorithm. The algorithm can be extended by adding terms to the Taylor series or using the stability factor to maintain stability for a larger or smaller time step.

**Velocity Verlet** The velocity verlet algorithm is similar to the verlet algorithm, but is performed over two half time steps. The algorithm proceeds as follows

1. Evolve velocities by half the total time step: $\delta t/2$

$$v_i(t + \delta t/2) = v_i(t) + a_i(t)\delta t/2 \tag{4.20}$$

2. Use these projected half time step velocity values to evolve positions a full time step, $\delta t$.

$$r_i(t + \delta t) = r_i(t) + v_i(t)\delta t + a_i(t)\delta t^2/2 \tag{4.21}$$

   becomes

$$r_i(t + \delta t) = r_i(t) + v_i(t + \delta t/2)\delta t \tag{4.22}$$

3. Update the intermolecular forces, and convert using Newtons law, $F = ma$, to achieve updated accelerations for all the molecules

4. Complete the velocity time step

$$v_i(t + \delta t) = v_i(t + \delta t/2) + a_i(t + \delta t/2)\delta t/2 \tag{4.23}$$

The velocity verlet algorithm is the most compatible time integration method with thermostats and temperature controls, and is implemented into the model as described above. This method also requires less storage than the predictor-corrector algorithm as only the position, velocity and acceleration vectors need to be stored between time steps, reducing the computational resources required. It is also simple, and easily integrated with a wide variety of thermostating methods.

**Time step** The selection of the optimal time step is crucial in molecular dynamics simulations. A large time step will progress the simulation time with minimal CPU time, however a time step which is too large can have two effects:

- Large time steps - The integration scheme assumes that the forces on each molecule are constant over the length of the time step, if the step is too large the deviation from this assumption causes errors in the calculation and conservation of energy.
- Very large time steps - Molecules may move large distances between sucessive steps and when close to other molecules may jump from a low interaction to an extremely high interaction forces where the molecules overlap. This can cause un-physically high forces and instability in the system. This behaviour often results in a complete breakdown of the molecular behaviour and energies which tend to infinity.

The optimal time step will conserve energy, and provide the greatest leap forward for the simulation time for each step. To examine this effect, the results of a simple investigation are presented. The system contains 114 molecules in a $2nm$ wide periodic cube and the effect on average energy with a range of time steps is evaluated.

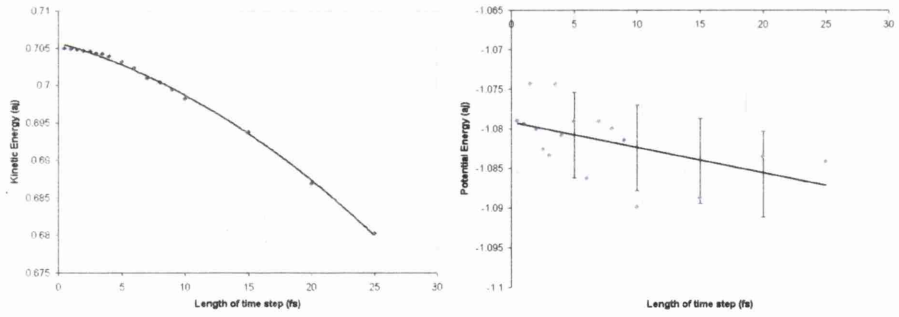


Figure 4.3: Graphs showing the effect of increasing the time step from $0.5fs$ to $25fs$ on kinetic energy (left) and potential energy (right)

Figure 4.3 shows a plots for kinetic and potential energy against a range of lengths of time step, varying from $0.5fs$ to $25fs$. It was found that increasing the time step beyond $25fs$ causes massive instabilities in the system and energy levels become extremely unphysical. The kinetic energy of the system is shown to drop by larger and larger amounts as the time step increases.

The potential energy shows an slightly increasing trend (In terms of negative values) but noise of 0.5% about the line of best fit.
As the time step approaches zero, the kinetic energy approaches a value of $0.7057aj$, and the potential energy approaches approximately $-1.0792aj$. To obtain the best and most stable results, the systems energy should be as close as possible to these values. A time step of $2fs$ can be seen maintain energy levels to within 0.02% for kinetic energy and $\pm 0.5\%$ for potential energy, whilst still progressing the simulation at an acceptable rate. A time step of $2fs$ is used in all models presented in this thesis.

### 4.2.4 Boundary Conditions

Having achieved an efficient molecular physics model, the boundary conditions surrounding the fluid should also be efficient and be appropriate to the scale of the system of interest. This is done with the implementation of the diffuse boundary conditions.

#### Diffuse boundary conditions.

The diffuse boundary condition replaces a dynamic/static molecular wall with a smooth planar boundary with appropriate hydrodynamic conditions to replicate the scattering occurring from the corrugation, or roughness, of the molecular wall [67]. This effect is shown if Figure 4.4, where the figure on the left shows a single molecules approaching a molecular wall, and depending on whether it hits a wall molecule on its side or on top, it rebounds in a different direction. The figure on the right, shows the effect of the diffuse boundary

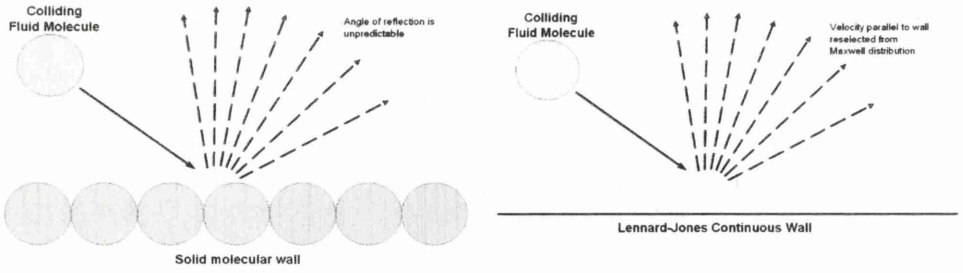


Figure 4.4: The diffuse boundary conditions

conditions, where the same effect of the molecular scattering is replicated over many molecular collisions.

The scattering is performed by selecting a proportion of molecules, and re-selecting their component of velocity parallel to the wall from the Maxwell-Boltzmann distribution for the set temperature of the wall. The Maxwell-Boltzmann distribution for velocity is different from the speed distribution (Equation 2.50), and defined as

$$g(v) = \sqrt{\frac{m}{2\pi k_b T}} e^{-\frac{mv^2}{2k_b T}} \tag{4.24}$$

which is shown in Figure 4.5

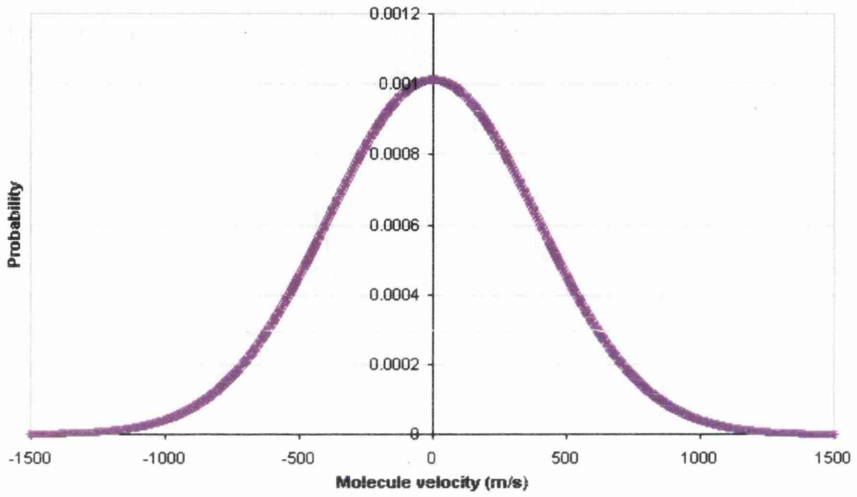


Figure 4.5: Velocity distribution molecules in fluid system for a single component of velocity

The proportion of molecules selected for this 'thermalisation' is set by the *tangential momentum accommodation coefficient*, $f$, for the solid.

**Tangential Momentum Accommodation Coefficient, $f$** The tangential momentum coefficient is the proportion of molecules that go through the thermalisation process in the diffuse boundaries. Its value can range from 0 to 1, to represent the degree of corrugation of the solid. Different degrees of corrugation occur from the following cases:

- $f = 0$
  This is the extreme case, where none of the colliding molecules are thermalised by the solid. The colliding molecules maintain 100% of their

momentum parallel to the wall and are only affected by the intermolecular interaction potential perpendicular to the wall.
In this case the walls are perfectly smooth and there is no thermal exchange between the two.

- $f = x$
  In the case of $f = x$, the proportion of colliding molecules, $x$, have their velocities parallel to the wall re-selected from the Maxwell-Boltzmann distribution. This effectively removes $(x \times 100)\%$ from the momentum of the fluid close to the wall (as the average of the Maxwell-Boltzmann distribution is zero), thereby creating a drag force between the fluid and wall.
  The Maxwell-Boltzmann distribution is a function of wall temperature, and the thermalised molecules, enable the addition or removal of thermal energy from the fluid. This can be used as a method of thermostating the system or applying a temperature gradient or boundary condition to the flow.
  The tangential momentum coefficient, therefore acts to vary the exchange that occurs between the fluid and wall in terms of thermal and bulk kinetic energy.
  The re-selection of the velocities also achieves molecular scattering of colliding molecules, similar to the effect of a fully molecular wall, but averaged over a large number of collisions.

- $f = 1$
  This is the extreme case of perfect stick between the fluid and the wall. In this case, 100% of the colliding molecules undergo the thermalising process, removing all of the linear momentum of the fluid at the wall (as the average of the velocities applied will be zero). This represents the condition of no slip between the fluid and boundary, and the condition that the fluid and wall will be at the same temperature at the boundary. This is not to be confused with the no-slip condition used in continuum mechanics, as this extreme case is unlikely and results from strong interaction forces in a molecularly sparse solid, whereas the continuum no-slip condition occurs from an approximation of scale, as well as frictional effects.

Arya *et al.* [67] demonstrated that the tangential momentum accommodation coefficient was dependant on two dimensionless variables, the reduced roughness and the reduced energy. The reduced roughness

$$\frac{\sigma_{fw}}{L} \tag{4.25}$$

is the ratio of the fluid-wall Lennard-Jones interaction radius, $\sigma_{fw}$, and the lattice spacing, $L$. $L$ is the diagonal spacing between solid molecule sites, shown in Figure 4.6. The reduced energy, is defined as the ratio of the Lennard-

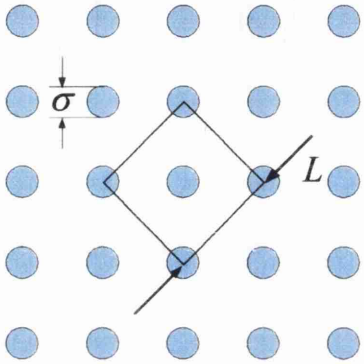


Figure 4.6: Example of a solid lattice displaying the lattice spacing parameter $L$, and wall molecule diameter $\sigma$

Jones well depth, $\epsilon_{fw}$ to the thermal energy.

$$\frac{\epsilon_{fw}}{k_b T} \tag{4.26}$$

They also found that $f$ was dependant on the bulk velocity of the fluid, but this only has an effect at large velocities.
By studying a fully molecular boundary, Arya *et al.* [67] were able to plot values for a wide range of $f$, as shown in Figure 4.7

Values for $f$ are also confirmed by the work by Sokhan [66] who performed similar investigations for the tangential momentum accommodation coefficient for the flow between parallel plates. Values for carbon nanotubes have been studied in depth by Cooper *et al.* [86] and Bhatia *et al.* [87].

**Implementation** Because of the separate treatment of the parallel and perpendicular components of the colliding molecule, the diffuse boundaries require a more complex implementation than an interacting molecular wall.

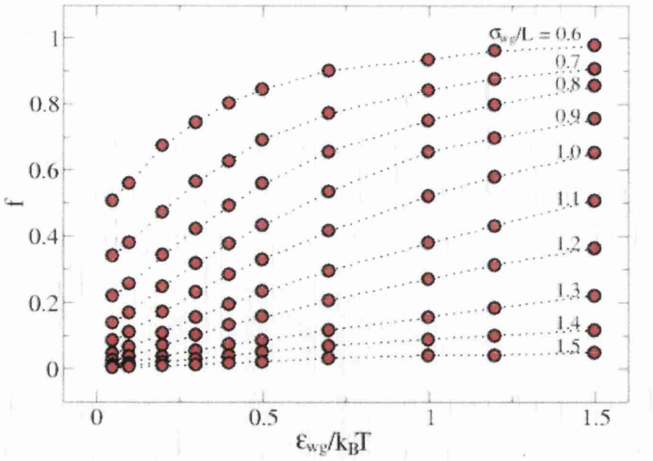


Figure 4.7: Tangential momentum accommodation coefficient, $f$, plotted for values of reduced roughness and reduced energy [67]

Because of the soft sphere nature of the simulation, there are no instantaneous collisions, only molecules that are interacting with the wall. It is therefore critical to clarify the definition and criteria a molecule near a boundary must satisfy if it is to be considered as colliding. To be accepted as a colliding molecule, a molecule must be:

- Within the repulsive zone of the walls interaction potential
- Experience a change of direction perpendicular to the wall

The first criteria is tested by calculating the perpendicular distance, $d$, between the molecule and the wall, as illustrated in Figure 4.8. The section of boundary

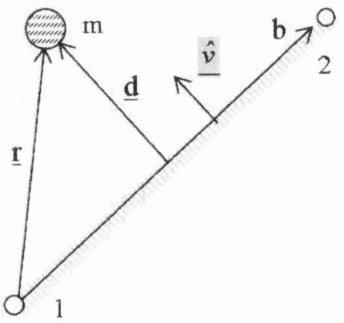


Figure 4.8: Calculating distance, $d$ between molecule and wall, from position vector, $r$, boundary vector, $b$. $d$ has unit vector $v$.

is defined by the line between two points, stored in the boundary vector $b$.

$$b = \begin{bmatrix} x_{b2} - x_{b1} \\ y_{b2} - y_{b1} \end{bmatrix} \tag{4.27}$$

and the position vector $r$ is defines the distance between the molecule ($m$) and the start of the boundary, at point 1.

$$r = \begin{bmatrix} x_{b1} - x_m \\ y_{b1} - y_m \end{bmatrix} \tag{4.28}$$

The unit vector, $\hat{v}$, normal to the boundary is the found,

$$\hat{v} = \frac{\begin{bmatrix} y_{b2} - y_{b1} \\ -(x_{b2} - x_{b1}) \end{bmatrix}}{\left| \begin{matrix} y_{b2} - y_{b1} \\ -(x_{b2} - x_{b1}) \end{matrix} \right|} \tag{4.29}$$

To find distance $d$, the dot product of the position vector and the unit vector $\hat{v}$ is taken,

$$\alpha = |\hat{v} \cdot r| = \frac{|(x_{b2} - x_{b1})(y_{b1} - y_m) - (x_{b1} - x_m)(y_{b2} - y_{b1})|}{\sqrt{(x_{b2} - x_{b1})^2 + (y_{b2} - y_{b1})^2}} \tag{4.30}$$

which can be simplified to,

$$\alpha = \frac{(x_m(y_1 - y_2) + y_m(x_{b2} - x_{b1}) + x_{b2}y_{b1} + x_{b1}y_{b2})}{\sqrt{(x_{b2} - x_{b1})^2 + (y_{b2} - y_{b1})^2}} \tag{4.31}$$

$d$ can then be calculated by multiplying $\alpha$ by the direction $\hat{v}$ and the magnitude of $r$

$$d = \alpha |r| \hat{v} \tag{4.32}$$

Distance $d$ can then be used to calculate the strength of the interaction between the molecule and wall, which in turn can be used to detect the first criteria for a colliding molecule, as described above,as well as calculating the repulsive force.

The second criteria is evaluated in a similar way. By looking at the dot product of velocity and the unit vector perpendicular to the boundary, and monitoring its change between time steps, the point at which the molecule

stops moving toward the boundary and starts moving away can be identified. At this point, the sign of the dot product changes sign, as shown in Figure 4.9 If a molecule is considered to collide with boundary, by satisfying the criteria

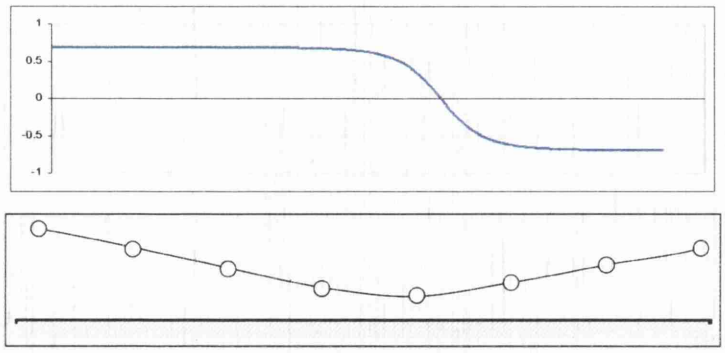


Figure 4.9: Variation of dot product with molecular distance from wall

described above, it is then given a random number to be compared against the tangential momentum accommodation coefficient, $f$. If this test is successful and the molecule is accepted for thermalisation by the wall, the parallel component of velocity is found, again by taking the dot product, but parallel to the boundary. This velocity is then randomly picked from the Maxwell-Boltzmann distribution (Equation 4.24) for the temperature of the wall.
This boundary method provides a good approximation for solid boundaries right down to the molecular scale [88], and as the scale of the simulation increases, and the number of collisions in the length and time scale of the system increases, the accuracy of the approximation also increases.

### 4.2.5 Modified Boundary Potential

As these diffuse boundaries are modelled as smooth planes, a standard Lennard-Jones interaction at the boundary does not take into account the depth of the solid. If the solid is more than one layer of molecules thick, the fluid may experience a stronger attractive force as the long range attractive part of the potential of other solid layers reaches into the fluid domain. Figure 4.10 shows this effect, the smooth boundary is positioned at $x = 0$ and the effect of two layers within the solid are shown. The resulting potential shows a much stronger attractive component. This must be taken into account by the interaction potential between the solid and fluid, and can be done so by modifying

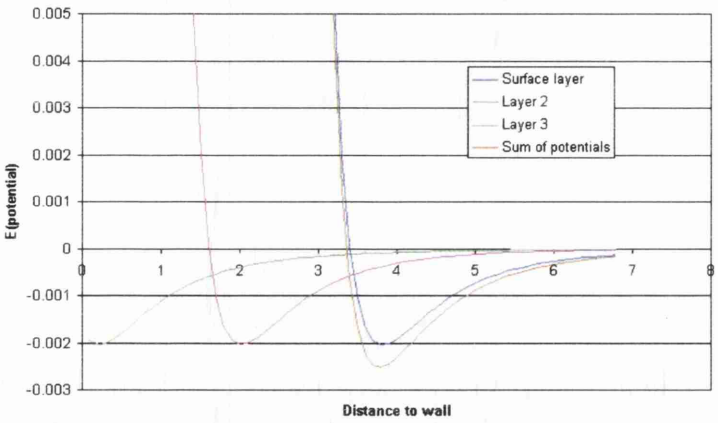


Figure 4.10: Total Lennard-Jones potential for three molecular layers

the parameters, $\sigma$ and $\epsilon$ for the solid and fluid of interest.

This section has developed a molecular fluid model capable of efficient simulation of systems containing large numbers of molecules. However, this model handles the motion of individual molecules. The information from this model describes, but fails to characterise, the bulk fluid effects present in meso scale fluid systems. The characterisation of theses bulk effects and the description of the fluid in terms of its bulk properties is critical to engineering applications. The next section implements a method for extracting such information from the molecular system using the ensemble properties described in Section 2.2.1

## 4.3 Extracting local Bulk Properties

The data possessed within the molecular flow model, is chaotic and adjacent molecules can possess very different properties, that average out over a large number of molecules at an approximately stable value. To allow the examination of bulk properties and their distribution throughout the flow domain, ensemble properties are assembled from local averages at discrete points through the flow field. Each point is assigned a sub-domain from which to draw its information. The number of molecules within each sub-domain can vary significantly for a large number to only a few. The approximating method must therefore be able to deal with these potential problems. The bin averaging method presents a crude approximation, that has no refinement or weight-

ing parameter, which gives noisy local averages even with a large amount of data, making it impractical for property distributions over short simulation runs (time is critical, especially for simulations of large numbers of molecules, within the meso scale). The Smooth Particle Hydrodynamics (SPH) method, improves the approximation by applying a weighting (or kernel) function to the approximation. The least Squares approximation uses the strength of the SPH method to fit a predetermined polynomial to the underlying property distribution. This is the most demanding of the three methods (and requires a small matrix inversion), but provides good opportunity for high sampling resolution in time and space.

### 4.3.1 Approximation Method

The up-scaling of information needs to be done in such a way that no important information is lost or altered. During this process some information is lost, as the point of up-scaling is to remove unnecessary detail and degrees of freedom. Therefore, the information must be included into the assembly of the bulk properties. There are several well known interpolating schemes available, such as moving least squares and smooth particle hydrodynamics that will be discussed along with the simple bin averaging scheme. The methods below aim to construct local ensemble averages of molecular properties at points placed throughout the domain, that together can be used to study the distribution of bulk properties over the whole domain.
The most simple method of assembling bulk property distributions is the bin averaging scheme.

### 4.3.2 Bin Averaging

The simplest way of averaging and upscaling molecular properties is the bin averaging scheme. This is where the molecular domain is divided into discrete cells, and all the molecules in each cell are averaged to construct the ensemble properties for that cell (Figure 4.11). The bin averaging scheme has significant drawbacks. The resulting distributions can have significant variations, as adjacent molecules could be in different cells, and two molecules on opposite sides of the same bin could have completely different properties but contribute equal weighting to the average. The result of which is that the resulting distribution is rough and contains a substantial amount of noise, and in order to

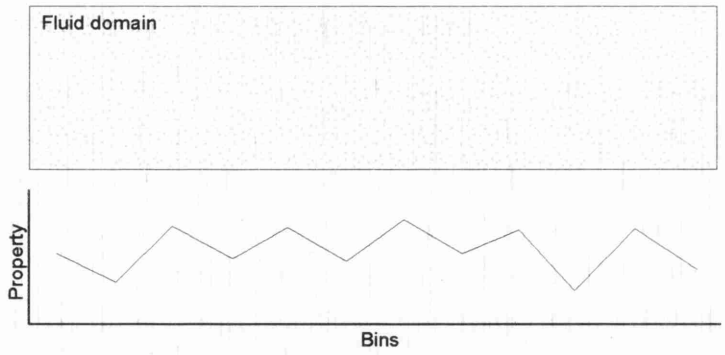


Figure 4.11: Bin averaging scheme

be able to obtain smooth property distributions throughout the flow field, a large sample time is necessary. This reduces the time resolution of the samples that can be taken, and can increase the overall time of the system to get a stable steady result.

The bin averaging is however, easy to implement and is still widely used to investigate steady systems [66]. The drawbacks of this method lead to the search for a more refined approach that will allow for better time resolution and shorter sample times with less statistical noise.

### 4.3.3 Smooth Particle Hydrodynamics (SPH)

SPH, first presented by Lucy [75], is a continuum particle method that solves continuum equations over a system of moving interpolation points [76, 77]. The property values at any point throughout the fluid relies on the properties of the surrounding points, and it is the method of sampling these properties that has most significance to this application. Instead of sampling the continuum properties, we seek to use this approach to extract the local bulk properties from the molecular motion at discrete nodes placed throughout the flow domain.

The sampling is done similar to the molecular dynamics searching, where the molecules around each node are evaluated, but the properties of each node are given a weighting as a function of their proximity to the node. This way the molecules closest to the node contribute more than the molecules further away, allowing the node to best represent the property value at that exact point in the flow field. The resulting distribution is much smoother than the bin averaging method, but is completely reliant on the strength of the weighting, or

kernel function.

### Approximation

The approximation is constructed using an integral for the function based on the delta function.

$$f(x) = \int_{\Omega} f(x')\delta(x - x')dx' \tag{4.33}$$

$$\delta(x - x') = \left\{ \begin{array}{ll} 1 & x = x' \\ 0 & x \neq x' \end{array} \right\} \tag{4.34}$$

This equation is exact as the function value is calculated at $x$, integrated over its volume. The delta function however, is no use when approximating many molecules so a weighting function is used instead. This replacement causes the function to become representative, and therefore approximate.

$$f(x) \approx \int_{\Omega} f(x')w(x - x', h)dx' \tag{4.35}$$

Where $w(x - x', h)$ is the kernel weight function with $h$ being the smoothing length, also known as to radius of the zone of influence. The kernel function is of critical importance to SPH as there is no assumption made about the distribution of data with which to form an approximation, it is solely the strength of the kernel that governs the accuracy. The integral is converted to a summation of a set of molecules to be used in a simulation, with the approximation of property $f(x)$ denoted by the addition of angled brackets $\langle f(x) \rangle$

$$\langle f(x) \rangle = \sum_{j=1}^{N} f(x')w(x - x', h)\Delta V \tag{4.36}$$

This sums the weighted contribution for all the particles, $j = 1, 2, 3, \cdots, N$ within the smoothing length, or the zone of influence of the approximated point to achieve the approximate value at point $i$.

The derivative of a function, and hence the flux of a property, can also be represented by the SPH approximation, by substituting $f(x)$ with $\nabla \cdot f(x)$ in the above equation.

$$\langle \nabla \cdot f(x) \rangle = \int_{\Omega} \left[ \nabla \cdot f(x') \right] w(x - x', h)dx' \tag{4.37}$$

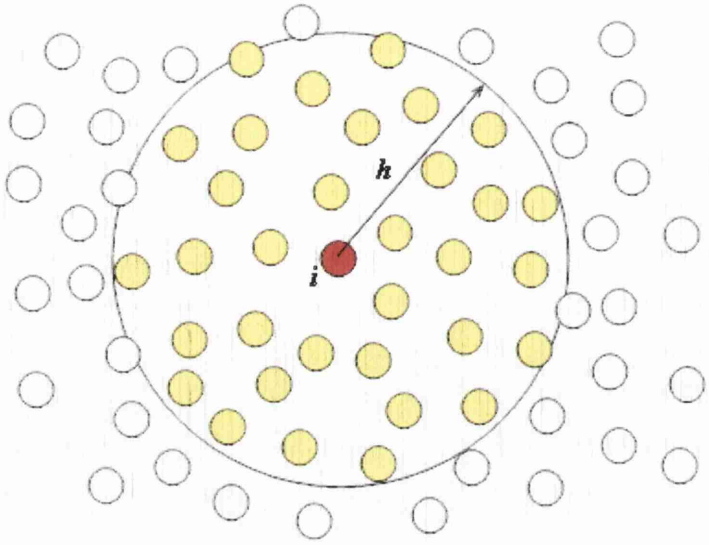


Figure 4.12: Smoothing Length, h

### Errors

As the approximation relies mainly on the strength of the kernel, to perform an error analysis is expanded in a Taylor series within the integral form.

$$\langle f(x)\rangle = \int_{\Omega} \left[f(x) + f'(x)(x-x') + r((x-x')^2)\right] w(x-x',h)dx' \tag{4.38}$$

$$\langle f(x)\rangle = f(x)\int_{\Omega} w(x-x',h)dx' + f'(x)\int_{\Omega}(x'-x)w(x-x',h)dx' + r(h^2) \tag{4.39}$$

Where r is the residual and the first integral, $f(x)\int_{\Omega} w(x-x',h)dx'$ , can be simplified from the continuity conditions of the weighting functions discussed previously, where the integral of the kernel is equal to 1

$$\int_{\Omega} w(x-x',h)dx' = 1 \tag{4.40}$$

The kernel is also an even function, so

$$\int_{\Omega}(x'-x)w(x-x',h)dx' = 0 \tag{4.41}$$

This reduces the error function down to

$$\langle f(x) \rangle = f(x) + r(h^2) \tag{4.42}$$

So the error of the SPH kernel approximation of a function is of the order $h^2$.

The Smooth Particle Hydrodynamics (SPH) method, adds a weighting (or kernel) function to the approximation, however as the SPH approximation is only based on the kernel, it is best suited to stable property distributions, where there is little noise and values change slowly and steadily throughout the sub-domain.

### 4.3.4 Moving Least Squares

#### Method

The moving least squares approximation scheme relies on the construction of many least squares approximations applied over a large number of points [78]. This method is generally used for creating smooth surfaces over mesh structures in computer graphics. This method is generally applied as an approximation to all points in the system, taking each one in turn and constructing an approximation from its neighbours. This is best described in one dimension, Figure 4.13. In the whole domain there are nodes distributed with positions,

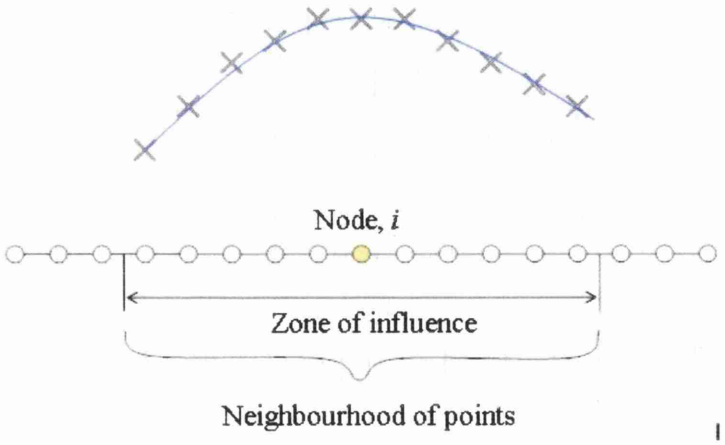


Figure 4.13: Least squares neighbourhood approximation

$x$, so we start by selecting an arbitrary node, $i$. This node is then assigned

a 'zone of influence' and all neighbouring particles contribute to the local approximation of the function. The distance from the central node, $i$, determines the strength of the influence a neighbour has on the approximation so that nodes closer to $i$ have more influence than a node close to the limit of the zone.

These approximations are performed on every node, so that the end result is a system of particles with associated functions describing the approximation at each node. The combination of all of the local approximations leads to a global approximation over the whole simulation domain.

The moving least squares method applies a least squares approximation of the neighbourhood, at points throughout the domain to construct a global approximation, Figure 4.14. In the molecular up scaling framework, the molecular properties are averaged at points defined by a coarse fixed grid over the domain, at each point the ensemble bulk properties are constructed as follows: A set of $N$ molecules within a system, with individual position $x_i$, $y_i$ and $z_i$

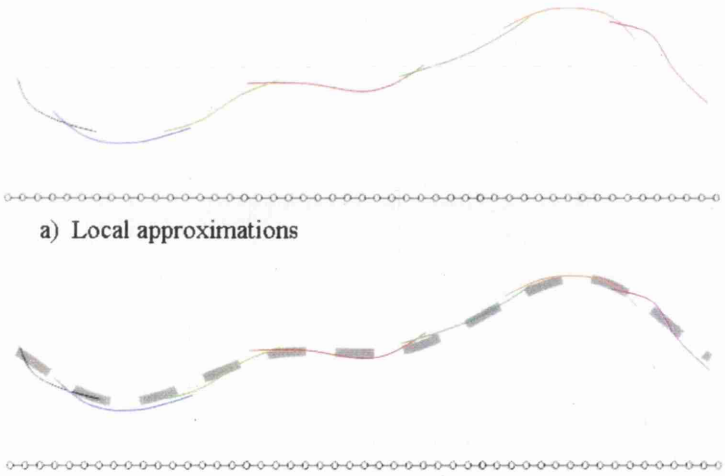


Figure 4.14: MLS local to global approximation

have associated parameter value $u_i$ for $i = 1$ to $N$. The calculation will be illustrated using two dimensions for the propose of simplicity and readability.

So for a system of n neighbouring points with positions $x_i$, and $y_i$, $(i = 1, 2, 3, \cdots, n)$ and the parameters are stores as

$$u^T = \left\{ \begin{array}{cccc} u_1 & u_2 & \cdots & u_i \end{array} \right\} \tag{4.43}$$

The local approximation at the node $(x,\ y)$ of $U$, $U^h$, is assumed to take the form of a polynomial over the local sub-domain. For this example, the approximation will use a quadratic basis function.

$$U^h = a_0 + a_1 x + a_2 y + a_3 x^2 + a_4 xy + a_5 y^2 \tag{4.44}$$

which can be written in matrix form as:

$$U^h = P^T a \tag{4.45}$$

where P contains basis function (which is in this case quadratic) and a contains the coefficients

$$P^T = \left\{ \begin{array}{cccccc} 1 & x & y & x^2 & xy & y^2 \end{array} \right\} \tag{4.46}$$

$$a = \left\{ \begin{array}{cccccc} a_0 & a_1 & a_2 & a_3 & a_4 & a_5 \end{array} \right\} \tag{4.47}$$

The coefficients must be found in order to complete the approximation, which is done by considering the function describing the error in the approximation at each molecule:

$$error = [U^h(x,y) - U_i] \tag{4.48}$$

over molecules $i = 1, 2, 3, \cdots, N$

Substituting equation 6.3 and summing over $N$ local molecules using a sum weighted as a function of the molecules distance from the central node:

$$J = \sum_{i=1}^{N} w(x - x_i, y - yi)[U^h(x,y) - U_i] \tag{4.49}$$

Minimisation of the weighted error function, 6.6, leads to:

$$(wP^T P)a = (wP^T)u \tag{4.50}$$

$$Aa = Bu \tag{4.51}$$

where:

$$A = \left\{ \begin{array}{c} w(x-x_1, y-y1) \\ w(x-x_2, y-y2) \\ \vdots \\ w(x-x_i, y-yi) \end{array} \right\} \left[ \begin{array}{cccccc} 1 & x & y & x^2 & xy & y^2 \\ x & x^2 & xy & x^3 & x^2y & xy^2 \\ y & xy & y^2 & x^2y & xy^2 & y^3 \\ x^2 & x^3 & x^2y & x^4 & x^3y & x^2y^2 \\ xy & x^2y & xy^2 & x^3y & x^2y^2 & xy^3 \\ y^2 & xy^2 & y^3 & x^2y^2 & xy^3 & y^4 \end{array} \right] \tag{4.52}$$

$$B = \left\{ \begin{array}{c} w(x-x_1, y-y1) \\ w(x-x_2, y-y2) \\ \vdots \\ w(x-x_i, y-yi) \end{array} \right\} \left[ \begin{array}{cccccc} 1 & x & y & x^2 & xy & y^2 \end{array} \right] \tag{4.53}$$

$$U^T = \left[ \begin{array}{cccc} u_1 & u_2 & \cdots & u_i \end{array} \right] \tag{4.54}$$

$$a = \left\{ \begin{array}{cccccc} a_0 & a_1 & a_2 & a_3 & a_4 & a_5 \end{array} \right\} \tag{4.55}$$

so the a coefficients can be found by solving:

$$a = A^{-1}uB \tag{4.56}$$

Once the coefficients have been calculated, they can then be used in the original approximation for the local parameter values, Equation 4.44, to yield the approximated value of the bulk property $U$ at the node at ($x$, $y$)

### Basis Functions

The basis or approximating function used in the approximation depends on two conditions, the dimensionality of the system and the order of the approximation required. Basis functions are constructed using a form of Pascal's triangle as shown below.

The triangle is shown in three dimensions with the first two levels shown. A linear basis function is constructed by summing all the components in the linear level and above.

$$P(x, y, z) = 1 + x + y + z \tag{4.57}$$

The quadratic basis function is constructed in the same way, by summing

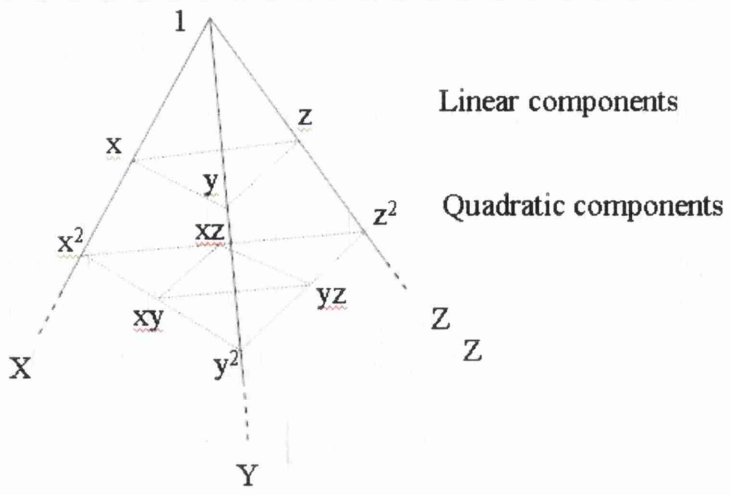


Figure 4.15: Basis function construction

all components in and above the quadratic level.

$$P(x, y, z) = 1 + x + y + z + x^2 + y^2 + z^2 + xy + yz + xz \tag{4.58}$$

These are the full basis functions for three dimensional systems, so for systems with fewer dimensions simple set the coordinates that are not needed to zero and the basis reduces, for example to two dimensions.

$$\text{for } z = 0 \tag{4.59}$$

$$P = 1 + x + y + x^2 + xy + y^2 \tag{4.60}$$

Higher order basis functions can provide improved accuracy, however as the order increases the number of terms in the basis function substantially. Figure 4.16 demonstrates the difference between linear and quadratic approximations for a sample data set. Comparing the above examples of three dimensional basis functions above for linear and quadratic, shows an extra 6 terms in the quadratic form. This may not appear as a great increase, but this increases the size of the $A$ matrix from a 4x4 to a 10x10 which can add a significant amount of time to a simulation, especially when a large number of nodes are being solved. For this reason, cubic basis functions are rarely used as the $A$ matrix is almost double the size of the quadratic version. A balance must be reached between accuracy and practicality.

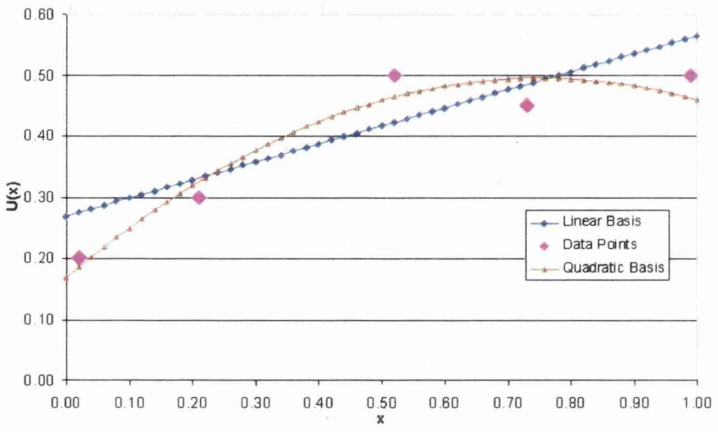


Figure 4.16: The difference between linear and quadratic basis functions for a one dimensional example with 5 sample points (approximated around centre point)

### Solving Equations

In order to determine the coefficients for the local approximation, Equation 4.44, we must find the solution of Equation 4.56. The equation is basically the matrix form of a set of simultaneous equations, so the analytical solution is fairly trivial and easy to solve by hand for one or two calculations by simply inverting the A matrix. However, to be used in a simulation this solution to this equation must be found many times for every time step, a task that cannot be done by hand. There are many methods for solving such sets of equations, but LU decomposition is used in this case because it provides an efficient solution, without the need to inverting large matrices.

**LU decomposition** In order to solve a system of equations of the form:

$$Ax = B \tag{4.61}$$

where $A$ is an $N$x$N$ matrix, $B$ is a vextor of size $N$, and $X$ is the vector of $N$ unknowns. LU decomposition starts by decomposing matrix $A$ into two diagonal matrices, one upper and one lower as follows, for an $N = 3$ example:

$$A = LU \tag{4.62}$$

$$\begin{bmatrix} A_{1,1} & A_{1,2} & A_{1,3} \\ A_{2,1} & A_{2,2} & A_{2,3} \\ A_{3,1} & A_{3,2} & A_{3,3} \end{bmatrix} = \begin{bmatrix} L_{1,1} & & \\ L_{2,1} & L_{2,2} & \\ L_{3,1} & L_{3,2} & L_{3,3} \end{bmatrix} \begin{bmatrix} U_{1,1} & U_{1,2} & U_{1,3} \\ & U_{2,2} & U_{2,3} \\ & & U_{3,3} \end{bmatrix} \tag{4.63}$$

so that

$$\begin{bmatrix} A_{1,1} & A_{1,2} & A_{1,3} \\ A_{2,1} & A_{2,2} & A_{2,3} \\ A_{3,1} & A_{3,2} & A_{3,3} \end{bmatrix} = \begin{bmatrix} L_{1,1}U_{1,1} & L_{1,1}U_{1,2} & U_{,}U_{,} \\ L_{2,1}U_{1,1} & L_{2,2}U_{1,2} + L_{2,2}U_{2,2} & U_{2,1}U_{1,3} + L_{2,2}U_{2,3} \\ L_{3,1}U_{1,2} & L_{3,2}U_{1,2} + L_{3,2}U_{2,2} & L_{3,1}U_{1,3} + L_{3,2}U_{2,3} + L_{3,3}U_{2,3} \end{bmatrix} \tag{4.64}$$

This gives $N$x$N$ equations for $N$x$N + N$ unknowns as the decomposition is not unique, but can be solved by Crout's method as follows:

$$Ax = LUx = L(Ux) = B \tag{4.65}$$

$$B = Ly; \qquad y = Ux \tag{4.66}$$

Now solve for y using back substitution

$$y = \frac{1}{L_{i,i}} \left( b_i \sum_{j=1}^{i-1} L_{i,j} y_j \right); i = 1, 2, 3, \cdots, N \tag{4.67}$$

use the result of y to solve for x using forward substitution

$$x = \frac{1}{U_{i,i}} \left( y_i \sum_{j=i+1}^{N} U_{i,j} x_j \right); i = 1, 2, 3, \cdots, N \tag{4.68}$$

Which results in the values of the original unknowns, $x$.

LU decompositions however, are still unable to solve for matrices with singularities (where the determinant is zero).

### 4.3.5 Weight Functions

The error function used to find the coefficients for the approximating function is calculated at each point and added as a weighted sum. The weighting function determines how important it is to get the error at that point to a minimum so that points closer to the central point are approximated with a higher accuracy than those further away. There are five criteria that all weighting functions must satisfy:

1. Must be $> 0$ within the sub-domain of centre particle. Particles within the subdomain of the central point are allowed to influence the local approximation.

2. Must be $= 0$ outside the sub-domain of centre particle. Particles outside the sub-domain are not allowed to contribute to the local approximation.

3. Integral over sub-domain must be equal to one. This is known as the 'consistency condition' which is a condition that states that the weighting function is sufficient to interpolate the minimum requirement (constant function) exactly, for example:

$$f(x) = c \qquad c = constant \tag{4.69}$$

approximated as:

$$\langle f(x) \rangle = f(x) = c \tag{4.70}$$

so,

$$\langle f(x) \rangle = \int_{\Omega} f(x) w(x) dx = c \tag{4.71}$$

which becomes,

$$c \int_{\Omega} w(x) dx = c \tag{4.72}$$

So for this to be true, $\int_{\Omega} w(x) dx$ must be equal to one.
When this condition is satisfied, the approximation is able to integrate, at least, the minimum of a constant function exactly.

4. Must decrease as distance from centre increases The particles within the sub-domain that are closer to centre point are given a higher weighting in the approximation.

5. Must approach 'Dirac's delta function' as the radius of the sub-domain,$r \rightarrow 0$.
The delta function, accredited to Paul Dirac, is a function which has the value of infinity at $x = 0$ , and zero everywhere else. It is simple to see that as the radius of the weight function decreases, the zone of influence shrinks around the central point where it is a maximum, and zero elsewhere.

These conditions describe a weighting function that will give the best approximation close to the central point. The fifth condition is not always necessary as it is difficult to find a function that fits the other four criteria and not the fifth, but is included for completeness. An additional condition usually added is that the function is positive over all the sub-domain; however there are exceptions to this rule such as the weight functions used in Point Interpolation Methods (PIM). There are three basic weighting functions in general use, the quadratic spline, Gaussian and exponential, all are a function of the radius from the central node, $i$.

In one, two and three dimensions:

$$r = x - x_i \text{ for one dimension} \tag{4.73}$$

$$r = \sqrt{(x - x_i) + (y - y_i)} \text{ for two dimensions} \tag{4.74}$$

$$r = \sqrt{(x - x_i) + (y - y_i) + (z - z_i)} \text{ for three dimensions} \tag{4.75}$$

and the weighting functions are:
Quadratic spline:

$$w(r) = 1 - 6r^2 + 8r^3 - 3r^4 \tag{4.76}$$

Gaussian:

$$w(r) = \exp^{-(2.5r^2)} \tag{4.77}$$

Exponential:

$$w(r) = \frac{1}{100^r} \tag{4.78}$$

The choice of weighting function has a substantial influence on the local approximation generated by the MLS method as will be shown in later chapters. The profiles of the weighting functions is shown in Figure 4.17

### 4.3.6 Grid Structure Implementation

The least squares approximations are performed at nodes placed within the flow field. The three dimensional molecular domain is overlaid with a grid of nodes, in either one, two, or three dimensions, depending on the problem and the distributions of interest or expected.

Figure 4.18 shows a representation of a molecular region overlaid by a two

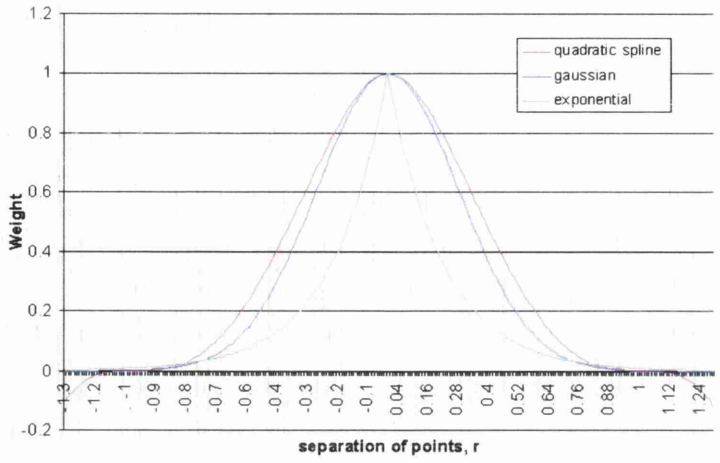


Figure 4.17: The three most common weighting functions: Quadratic spline, Gaussian and Exponential

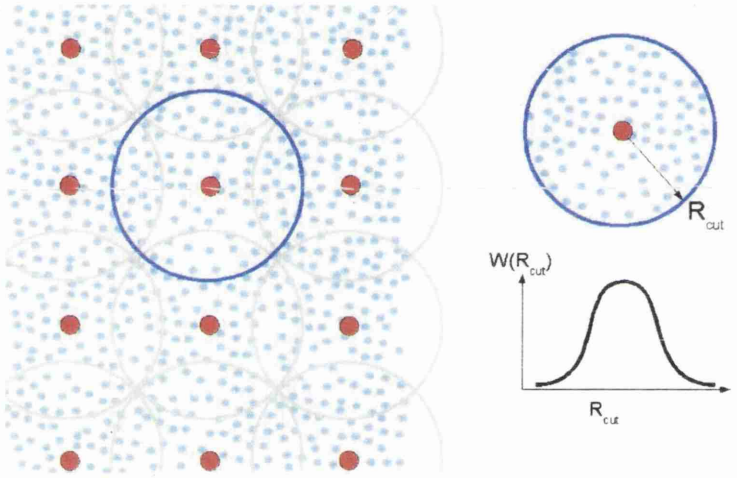


Figure 4.18: Net of approximating nodes placed over the molecular flow region. Molecules within each nodes sub-domain contribute to the property average at that node with weighting $W(r_{cut})$, according to their proximity, $R_{cut}$

dimensional net of nodes, each having a zone of influence. Each molecule within the zone of a node, contributes to the approximation at that node, and is weighted as a function of is distance.

The molecular parameters are collected from the molecules at intervals during the simulation. Ensembles for density, pressure, temperature, are stored in separate $A$ matrix and $B$ (of the least squares approximation described above) vector for each node. As described in Section 4.3.4, the matrices are used to

form the vector of coefficients of the fitted polynomial basis function,

$$A = (wP^T P); \quad B = (wP^T) \tag{4.79}$$

$$Aa = Bu \tag{4.80}$$

where $P$ is the basis function (a function of position of molecule, relative to node) and $w$ is the weighting function. For convenience, the $B$ vector is combined with the vector of property values, $u$, which is a function of phase space (position and momentum of molecule) position of each molecule within the sub-domain.

The sampling of the properties in no way influences the dynamics of the molecules in the molecular system, they are used purely to extract information from the molecular model. It is however important to consider the way in which the sampling is done in order to present the best data for the averages without losing information.It is also important to keep the number of sampling points to a minimum.

### 4.3.7 Sampling

When ensemble averages are constructed it is important to make the distinction between samples and ensembles. In this method, a sample is taken as an instantaneous snapshot of the local data at each node. Ensembles are generated using the data collected over a number of these samples over a period of simulation time. Molecular data collected in different ensembles can construct the different bulk fluid properties at these local points. A number of ensemble averages can be taken over the duration of the simulation to capture time dependant effects, as well as providing a measure of the approach to equilibrium state.

Each individual sample is combined into the $A$ matrix and $B$ vector, and a number of samples are used to make an ensemble average at the node, providing an approximate value for the parameter, over time as well as space in the simulation (Figure 4.19). The length of simulation time between samples, and length of time over which the approximations are computed is key to stability and accuracy in the ensemble averages.

The objective of the sampling is to provide the ensemble with data about the bulk state of the fluid, but information is not required about the behaviour of

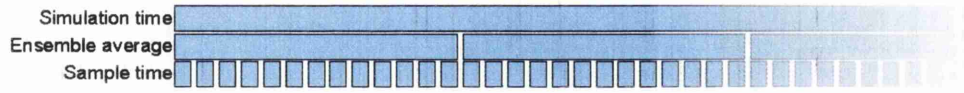


Figure 4.19: Highlighting the differences between samples collected to makeup the ensemble averages, accumulated at points throughout the simulation time.

individual molecules. To ensure that it is the bulk behaviour and not individual molecular behaviour that is being fed into the ensemble, the information is expressed in terms of the local phase space. Phase space is a function of the position and momentum of all molecules in the system. For a local bulk fluid property, there is a region that contains all of the available phase space positions for the current state and time. By sampling as many points in the phase space available to the local molecules, the best description of the state of the fluid at that point can be found. If samples are taken too often, only a narrow portion of phase space can be sample. Whereas if there is time for the molecules to interact and move within the domain the next sample may contain different data about the same available phase space volume. If the sample time is too long, the sampling becomes inefficient and reduces the amount of useful data that is collected during a simulation.
Similarly, if the ensemble averages of the samples are taken over a short period of time, there is insufficient sample data is available to represent the available phase space to provide a stable ensemble average. If the averaging time is too long, then an unnecessary amount of information is contributed to the approximation and the time resolution is unnecessarily decreased.
In the next chapter, the effect of changing the sample and ensemble times is investigated, and its effect on the resulting bulk properties that are extracted.

These two sections have shown the implementation of a method designed to simulate meso scale fluid systems from a bottom up approach. The developed method relies on a molecular scale fluid model and bulk properties are extracted from the underlying molecular motion. The next section examines the operation of the molecular model in more detail.

## 4.4 Verification of Proposed Meso Scale Model

The information in the above section has discussed how fluid can be modelled via the consideration of physics on a molecular scale. This section will provide an example of a molecular dynamic simulation to demonstrate the operation of the developed model.

For this, the example considered will be a cubic volume of methane molecules suspended away from any boundaries to allow the use of periodic boundary conditions in all three dimensions (Figure 4.20).

The 512 methane molecules (CH4) used in this example interact via using

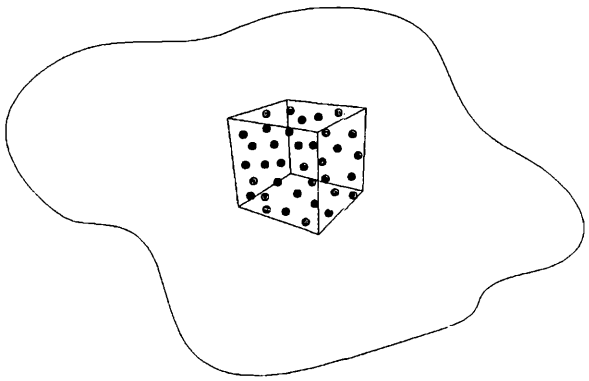

Figure 4.20: Cubic control volume considered away from any physical boundaries

the soft sphere Lennard-Jones 6-12 potential and moved using Newtons law via the verlet algorithm as described above. Although this is a simple steady state system, this example can demonstrate the application of molecular dynamic simulations.

To start of the simulation, the number of molecules and their properties are input into the initialisation stage of the simulation. This allows a lattice of molecules to be created to fill the domain with the given number, to generate the required density. The set temperature is then used to apply random velocities to the molecules according to the Boltzmann distribution.

The next part of the simulation is to equilibrate, or settle, the molecules, as the initial lattice is not a stable maintainable state, but a lattice makes for easy initial placement. During the breakout of this lattice, there is also large variations in molecular properties.

Figure 4.21 displays what happens when the molecules in the lattice are relaxed. Here, potential (PE), kinetic (KE), and total energy (E total) are

plotted from $t = 0$ to $t = 1ps$. During the equilibration period, the kinetic energy (and hence the temperature) is kept constant, this is because while the molecules are settling down, they can be exposed to unphysical and high interaction forces which can cause the energy of the system to become out of control. For this, simple velocity scaling is used.
Velocity scaling is a crude method of temperature control in molecular systems, where the kinetic energy of the molecules calculated using

$$E_{Ke,t} = \frac{1}{2}mv^2 \tag{4.81}$$

and compared to the kinetic energy of the initial temperature,

$$E_{Ke,t=0} = \frac{3}{2}Nk_bT \tag{4.82}$$

The scaling factor is then

$$\alpha = \frac{E_{Ke,t}}{E_{Ke,t=0}} \tag{4.83}$$

Which is then used to scale all the velocities of all the molecules in the system using

$$v_i = v_i\alpha \tag{4.84}$$

to maintain global kinetic energy at each time step.
This is a crude and unphysical approach to temperature control and only suitable for steady state simulations to achieve equilibrium. For more complex simulation, such as those examined later, require a more refined approach to temperature control.
Consequently, the only variation in energy comes from the potential energy component in the simulation. The plot of energies shown in Figure 4.21 is for the initial breakout of the lattice and three parts a, b, and c are identified.

- **a:** The initial lattice, the potential energy value computed from the initial positions of molecules
- **b:** Molecules move with initial velocity, and slack across periodic boundaries is taken up. The peak in potential energy occurs from the momentum of particles crossing empty spaces.
- **c:** Potential energy begins to stabilise, molecules are constantly moving, colliding and exchanging momentum but global potential energy is con-

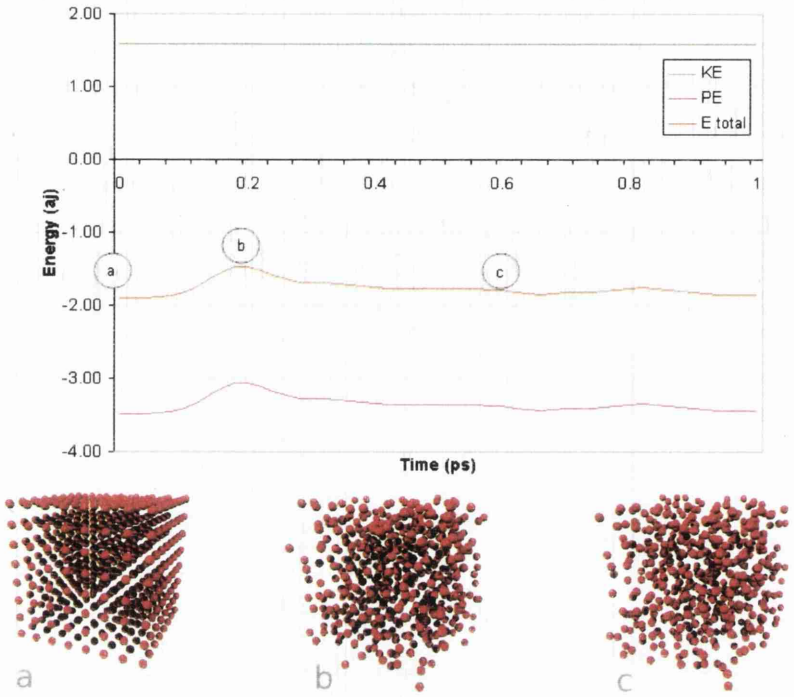


Figure 4.21: Top: Kinetic, potential and total energy for initial stages of equilibration. Bottom: Distribution of molecules at stages throughout equilibration process, a. initial lattice. b. peak in potential energy. c. stabilisation of randomised system

served. Fluctuations occur from molecules changing state, but system is in equilibrium state.

Equilibrium state can also be monitored using the order parameter described previously, tending from one at point a, to zero at point c.

To check the thermodynamic state of the fluid, the velocity distribution in each of the three dimensions can be compared to the Boltzmann distribution, as shown in Figure 4.22. If the distributions match, then a stable thermodynamics state could be present, and when combined with the other equilibrium tests, can identify when the whole system is stable. Figure 4.22 shows the instantaneous distribution of speeds of the molecules within the system and is shown against the exact distribution with 15% error bars.

Once this equilibrium state has been reached, the production stage can start, which collects all the useful properties of the simulation. At the start of the production stage, the velocity scaling is removed, effectively freeing the simulation of any constraints. At this point the global ensemble averages can start

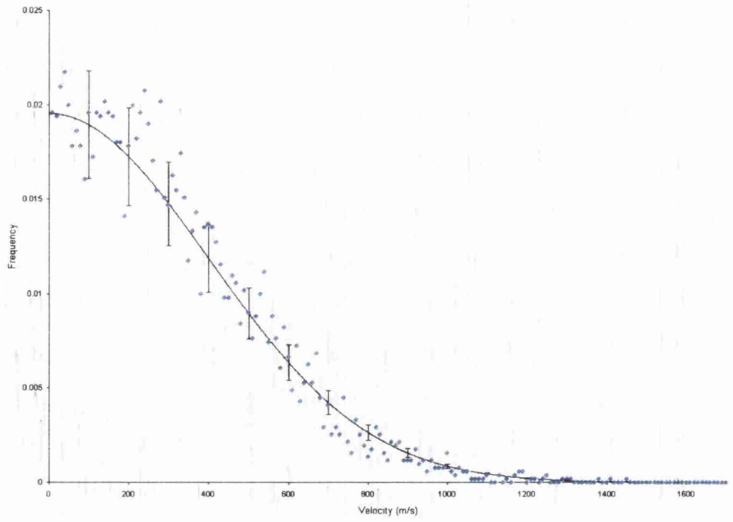


Figure 4.22: Distribution of velocities in molecular simulation compared to Boltzmann distribution, shown with 15% error bars

to take data from the molecules in the system.

On the left of Figure 4.23 is a plot of the equilibrium stage, similar to Figure

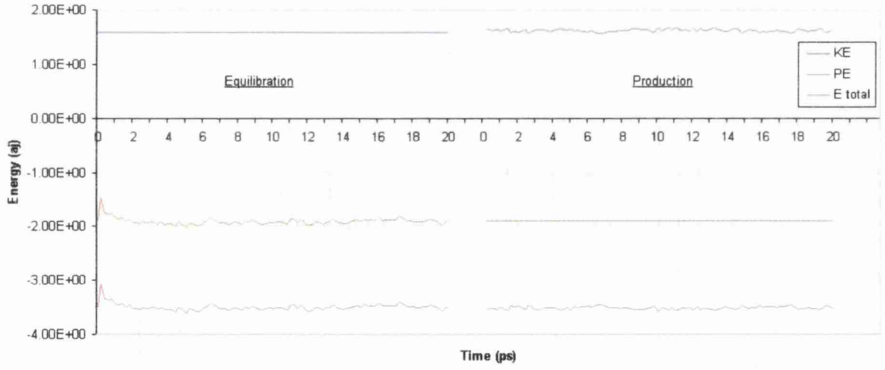


Figure 4.23: Potential (PE), kinetic (KE), and total energy during the equilibration and production stages of the simulation

4.21, but the time has been extended to $20ps$. Here, the initial peaks are present as the lattice structure breaks down, but then the potential energy remains approximately constant. On the right, is the production run that follows the equilibration stage. In this case the production run has also been performed over $20ps$ but the velocity scaling is removed. With the kinetic energy allowed to change, the constant exchange between potential and kinetic energy can be observed. In the equilibration stage, the fluctuations of

the potential energy were directly translated onto the total energy because the kinetic energy was being continually rescaled. Now the kinetic energy has been released, the molecules exchange their kinetic and potential energy in perfectly elastic collisions, such that the net energy in the system remains constant.

It is during this period that the ensemble properties may be taken over the desired simulation time, as this is the period where the system is in steady state.

Our simulations so far have been using a control volume of 512 molecules. Figure 4.24 shows a plot of the variation in the potential energy per molecule

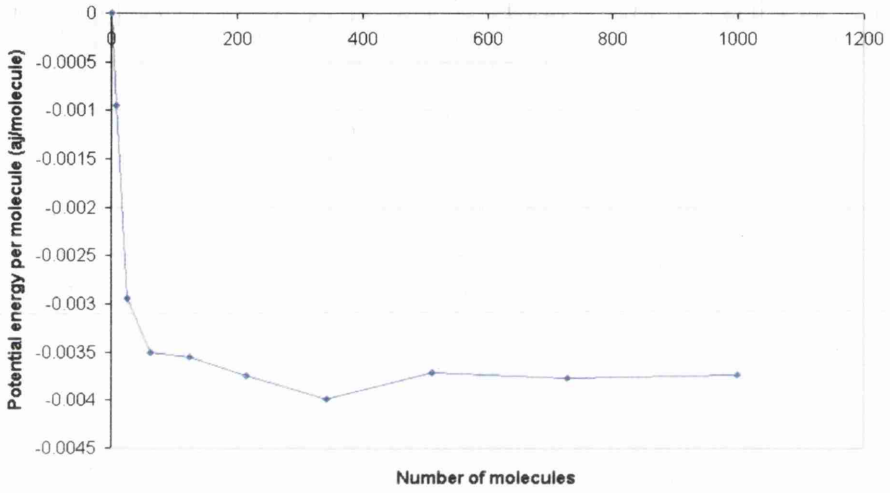


Figure 4.24: Average potential energy per molecules verses number of molecules in periodic cell

with respect to number molecules in the simulation. All simulations have the same density, and the volume per molecule remains constant, but the average potential energy gathered in the simulation differs significantly. There is a clear region where there are enough molecules to correctly predict the potential energy of the simulation, where the energy per molecule is approximately constant. Also from this graph, it is clear that increasing the system size from 512 molecules to 1000, would not have a significant effect on the results, and present a much higher demand on the computational resources.

If this potential energy is to be accepted as correct, there needs to be a benchmark with which to test the results for the simulation. This can be done by assembling an ensemble average for the pressure using a form of the virial equation of state summed over all the interactions and molecules. This equa-

tion of state allows the calculation of global pressure from the kinetic and potential energy in the system. The simulation of the above system yielded a global pressure of

$$P_{sim} = 44.28MPa \tag{4.85}$$

which can be compared the pressure obtained from an analytical equation of state, in this case the Lennard-Jones equation of state, which yields

$$P_{lj} = 44.53MPa \tag{4.86}$$

This gives the difference in pressure between the simulation result and the analytical pressure to be 0.58%, which gives confidence to the accuracy of the simulation model.

## 4.5 Summary

This chapter has developed an implementation of molecular simulation specific to meso scale fluid systems. The molecular model is capable of handling very large numbers of molecules using processing power and memory requirements efficiently. This is further improved by the implementation of the diffuse boundary conditions, which allow the computational resources to concentrate on the highly dynamic part of the simulation, the fluid.

The bulk property averaging scheme allows the fluid properties and fluid effects displayed by the bulk of the fluid to be characterised as distributions within the flow field. The implementation of this method is in the form of a versatile node based structure. Property interrogation nodes can be placed throughout the domain wherever needed, sample and ensemble times can be tuned to suit the current application. These parameters are covered in more depth in the case studies in the next chapter.

This new meso scale method provides a new insight into meso scale fluid systems.

# Chapter 5

# Enhancements to the Meso Scale Model

## 5.1 Introduction

This chapter focuses on the further development of the meso scale method presented in the previous chapter. The development starts by extending the method to handle flowing fluids. When a fluid flows through a pipe or channel, the interaction between the fluid and solid molecules causes the molecules close to the wall to slow down, as has been discussed in the viscous fluid discussion in Chapter 2. This, combined with the internal collisions of fluid molecules causes a boundary layer to form. Capturing this boundary layer in the form of a velocity profile can tell us a great deal about the fluid behaviour, as will be seen in Chapter 6. This section discusses the generation and capture of fluid flow behaviour in molecular systems. The first issue to be discussed is the method of driving molecules to generate a flow.

This extended method is then explored and tested in a number of case studies. The first case studies focus on the parameters of the bulk property extraction scheme, examining the sample and ensemble length, radius of sub-domain, and weighting function. These studies are performed on a fluid at rest and do not employ the thermal control element of the method.
The second section of case studies look at the collected bulk properties as distributions throughout the domain. A temperature gradient through a fluid

confined between two parallel plates is considered on a fluid at rest. In this example thermal energy is propagated by the thermal motion of the molecules in the fluid. A study of a fluid flowing between parallel plates is also considered. This example employs both the thermostat and flow driving elements of the model, and is compared with results published in literature.

## 5.2 Driving Forces

In order to generate a flow, there must be a driving force to push the molecules between one point and the next. A flow can be generated in a number of ways, varying in their complexity and computational demand. In the following section, methods for generating fluid/molecular flows will be presented and discussed, focusing on their application to meso scale systems.
The first method is the most demanding computationally, but presents the simplest concept. It relies on three components, a high pressure reservoir, a low pressure reservoir, and a test section that connects them, as shown in Figure 5.1.

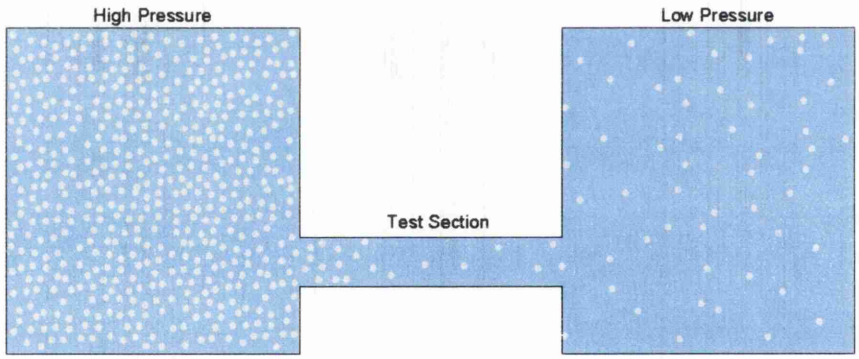


Figure 5.1: Schematic of molecules driven through test section by maintaining two reservoirs at different pressures. Low pressure reservoir is usually maintained at a vacuum

The high pressure reservoir is maintained at a constant high pressure, by recycling the molecules that exit the test section into the low pressures reservoir. This has the effect of keeping the low pressure reservoir at a vacuum, but the high pressure reservoir must be sufficiently large to smooth out the effect of molecules being inserted, which can lead to anomalies and discontinuities if

they are inserted too close to the entrance of the test section, or overlapping another molecule.

This approach to flow generation needs a very large number of molecules, most of which are not within the test section and contribute little to the results of the simulation. This method does however, allow pressure driven flows to be directly modelled in a controlled and stable environment. However, in order to model the flow of fluid or molecules through a meso scale test section, the number of molecules needed would be prohibitively large.

Two similar, but reduced approaches were developed by Liao and Yip [79] and Sun and Ebner [83]. The first, by Liao and Yip is known as the reflecting particle method [79]. This method removes the large reservoir, and uses an extended part of the test section, with periodic boundary conditions at each end, to form a smaller reservoir in line with the flow. The high and low pressures are generated by using a selective membrane at some point along the flow, that allows molecules to pass freely across in one direction, but in the other direction a proportion of the molecules are reflected back.

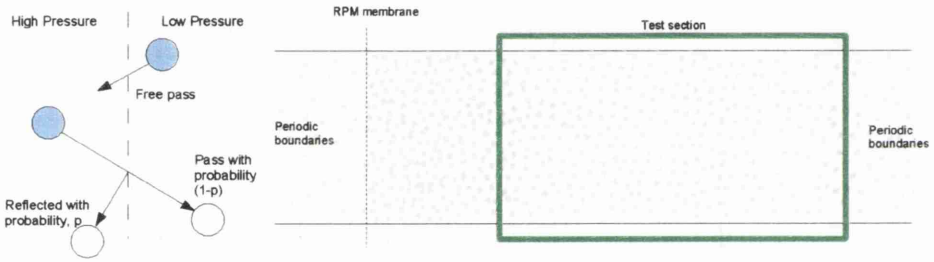


Figure 5.2: Left: The reflecting particle method, molecules may pass freely in one direction, but are reflected with probability $p$ when exiting the 'high pressure' region. Right: The RPM membrane used to investigate channel flow. The test section must be clear of the membrane

Figure 5.2 demonstrates the application of the membrane to model pressure driven flow along a test section. The pressure difference can be controlled by altering the probability of reflection of the membrane.

The second approach is by Sun and Ebner [83] where the high and low pressure regions are created by replacing the periodic boundary conditions with a source region and a sink region. The sink is maintained at a vacuum by removing from the system, all molecules which enter this region. The source

region, at the opposite end of the cell, is a small volume with a moveable boundary at the end. This boundary acts as a piston, reducing the volume of the source region and pushing the molecules into the volume considered by the simulation. Once the boundary has travelled a short distance, the density of the system is measured and the boundary resets to its original position and the void created, fills with enough molecules of the same density. Molecules are added with velocities as described by the Maxwell velocity distribution at the temperature of the wall. This approach maintains a pressure gradient between the source and sink regions, causing a flow of molecules. The number of molecules injected and the volume swept by the boundary is very small to minimise oscillations occurring as the new particles breakout of the regular lattice used to initially position the particles. Sun and Ebner applied this successfully in two-dimensions to study compressible flow [83], and has the potential to be applied in three-dimensions.

By using these methods of applying a pressure gradient to drive the flow of molecules, force is transmitted in a very natural way, through the interactions of the particles. This is useful in modelling the reaction of a fluid to pressure gradients, as the pressure and density vary continuously along the length of the test section between the source and sink regions. However, this is not useful for considering steady, fully developed flows, which model the flow in channels with no density variation along their length (infinitely long test section). These systems require a different approach.

To model fully developed flows, Sokhan *et al.* [66] modelled a driven flow between parallel plates by applying a uniform acceleration, in the required direction of flow, uniformly to all molecules in the system. The application of an acceleration in way is similar to a gravitational effect pulling the molecules along the test section, although the acceleration is typically much larger. This however, creates the problem that by applying an external force to the molecules, adds energy to the closed system. As this external work is being done on the system in order to approximate the effect a constant pressure gradient (effectively applied over an infinitely long section), the energy added to the molecules must be removed. The energy is removed by the application of a thermostat.

The simplest form of thermostat, velocity scaling, has been described in Section 4.4, but is far too crude for this application as temperature must be

controlled throughout the duration of the simulation, even during the production phase.

## 5.3 Thermostats

The aim of a thermostat is to maintain a control on the temperature, and hence kinetic energy, globally within the system. However, the way in which this is done is critical as controlling/altering the energy of molecules within the system affects the dynamic behaviour of the whole system. Control must be maintained without having an effect on the system behaviour. If energy is being added to the system in the form of an acceleration to model the effect of a pressure gradient acting in one direction, it should have the effect of influencing the proportions of energy within the system, but not change its global value.

### 5.3.1 Gaussian Thermostat

The Gaussian thermostat aims to control the temperature of the system by using Gauss's principle of least constraint [89]. The principle of least constraint states that the constrained trajectories actually followed, should deviate as little as possible from the trajectories of unconstrained equations of motion. In the motion of the molecules in the system, the equation of motion is simple Newton's law,

$$F = ma \tag{5.1}$$

which we wish to constrain to a constant global temperature, leading to the formation of a constraint function which constrains the system temperature to the set temperature, as,

$$g(r, v, t) = \frac{1}{2}\sum_{i=1}^{N} mv^2 - \frac{3}{2}Nk_bT = 0 \tag{5.2}$$

which is the difference between the system temperature and the temperature set by value $T$. Differentiating once with respect to time gives the equation for the constraint plane

$$\sum_{i=1}^{N} m_i v_i \cdot a_i = 0 \tag{5.3}$$

Assuming that the unconstrained equations of motion lead the simulation away from the constraint surface, the equations of motion are corrected by considering the function of the square of the curvature [90], $C$,

$$C = \frac{1}{2}\sum_{i=1}^{N} m_i \left(a_i - \frac{F_i}{m_i}\right)^2 \tag{5.4}$$

The physical accelerations in the system correspond to the minimum value of $C$, so for an unconstrained system $C = 0$ and the system evolves under newtons equations.
This leads to the constrained equation of motion:

$$a_i m_i = F_i - \lambda v_i m_i \tag{5.5}$$

where $\lambda$ is the friction factor applied to the molecules as scaling by their momentum, and defined as,

$$\lambda = \frac{\sum_{i=1}^{N} F_i \cdot v_i}{\sum_{i=1}^{N} m_i v_i^2} \tag{5.6}$$

Equations 5.5 and 5.6 are known and implemented together as the *Gaussian isokinetic equations of motion.* It is important to note that the scaling/friction factor is different to that used in the velocity scaling approach, and friction/scaling is applied as a function of the individual molecules momentum.

### 5.3.2 Nosé Hoover

The Nosé Hoover thermostat [91,92] is a method of temperature control that is based on the inclusion of an extra parameter in Nosé Hoover dynamics coordinate space [93]. This means the inclusion of thermostat parameter, $\xi$. The second derivative of which is simply a function of the kinetic energy of the system and the temperature,

$$\ddot{\xi} = \frac{1}{Q}\left[\sum_{i=1}^{N} m_i v_i^2 - N_f k_b T\right] \tag{5.7}$$

Where $N_f$ is the number of degrees of freedom of the system. This equation for $\ddot{\xi}$ is the difference between the actual and set temperature of the system,

which is multiplied by the reciprocal of a weighting function, $Q$, and can be defined as

$$Q = N_f k_b T \tau^2 \tag{5.8}$$

where $\tau^2$ is the characteristic time scale of the motions of real particles [94]. This weighting function controls the application of the thermostat, and can be adjusted for particular applications. A low weighting function can cause high frequency oscillations in $\dot{\xi}$, where as a high value can over constrain the system.

The Nosé Hoover thermostat is used in this method because of its level of control can be tuned to the specific system of interest using the mass parameter, allowing the thermostat to work effectively whilst applying the minimum of constraint on the system. It is however more complex to implement in to the equation of motion, the implementation will be considered next.

### Implementation in the Proposed Meso Scale Model

The thermostat parameter therefore has its own equation of motion, and can be included in the velocity verlet equations of motion of the molecules. The equations of motion for the complete system proceed through simulation time as follows:

1. Thermostat parameters, and mass $Q$, are computed:

$$\ddot{\xi}(t) = \frac{1}{Q}\left[\sum_{i=1}^{N} m_i v_i(t)^2 - N_f k_b T\right]$$

$$\dot{\xi}(t + \delta t/2) = \dot{\xi}(t) + \ddot{\xi}(t)\delta t/2$$

$$\xi(t + \delta t) = \xi(t) + \dot{\xi}(t + \delta t/2)\delta t$$

2. Molecular velocities and positions are updated, including the corrections from the thermostat parameter, using the velocity verlet algorithm

$$v_i(t + \delta t/2) = v_i(t) + [a_i(t) - v_i(t)\dot{\xi}(t + \delta t/2)]\delta t/2$$

$$r_i(t + \delta t) = r_i(t) + v_i(t + \delta t/2)\delta t$$

3. Molecular forces are updated using interaction and boundary forces, $F = ma$

4. Complete time step for velocity of molecules and thermostat parameter:

$$v_i(t+\delta t) = v_i(t+\delta t/2) + [a_i(t+\delta t) - v_i(t+\delta t)\dot{\xi}(t+\delta t)]\delta t/2$$

$$\dot{\xi}(t+\delta t) = \dot{\xi}(t+\delta t/2) + \left[\sum_{i=1}^{N} m_i v_i(t+\delta t)^2 - N_f k_b T\right] \frac{\delta t}{2Q}$$

This coupled equation is then solved using the iterative Newton-Raphson method.

These thermostats allow for the control of molecular systems, whilst presenting the minimum effect on the dynamics of the system. This allows for molecules to be driven by a pressure gradient, modelled by an acceleration applied to the molecules. However, with such a complex system operating, there needs to be careful benchmark tests made to make sure of the accuracy of the simulated molecules.

## 5.4 Case Studies

To explore that capabilities of the developed approach, a number of case studies are presented. These are split into two sections, a study of the parameters of the bulk property collection scheme and the examination of temperature and flow driven systems. The initial simulations are performed with the thermostat disabled, and temperature control is not necessary, but the simulation of a driven flow has the thermostat feature enabled.

### 5.4.1 Sampling

To study the parameters for the extraction of the ensemble averages, a molecular scale system is used to provide the most challenging for this bulk method. The reason for this is two fold, to reduce the computational load of the simulations to allow many simulations to be performed in a reasonable amount of time, and secondly, with only a few molecules the least squared approximating nodes are starved for data, providing an excellent test for the performance of this approach at its weakest point, systems with low numbers of molecules.

To test the operation and sensitivity of these parameters, a simple molecular dynamics simulation is used as a demonstration, and is setup in a similar way to the simulation presented in Section 4.4. For this application, the limits of the system set to a $15 \times 15 \times 8.3nm$, containing 5104 methane molecules interacting with a Lennard-Jones 12-6 potential. Periodic boundary conditions are applied in all three dimensions. The fluid is permanently at rest, with motion occurring only from internal thermal diffusion for the system temperature of $300K$. Within the molecular flow field a one dimensional line of nodes was inserted along the $y$ direction, at $0.5nm$ intervals (shown in Figure 5.3).

As mentioned, the simulated fluid is at rest, so by recording the bulk velocity

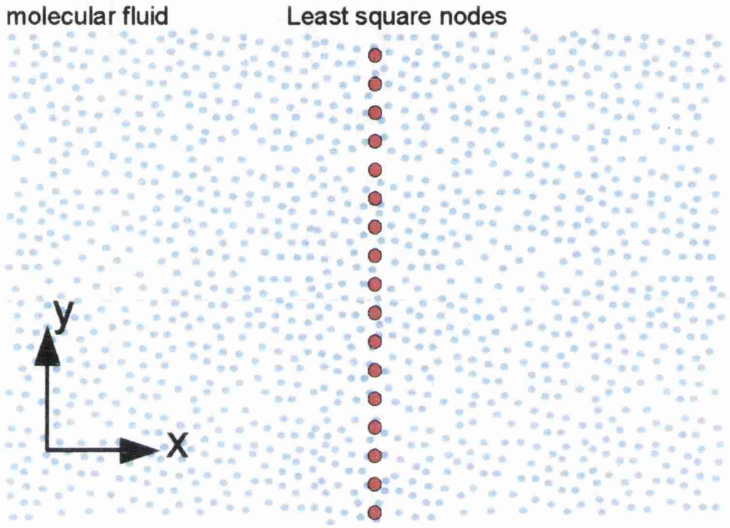


Figure 5.3: Simulation of a periodic molecular system, modelling fluid at rest, molecular properties are averaged by an array of one dimensional nodes placed across the field.

of the fluid in the $x$ direction, the molecular velocities occurring by thermal diffusion should cancel out to yield and ensemble average of zero velocity at each of the nodes.

With this knowledge, this system can be used to explore the effect of the parameters used to gather the least square approximations of the molecular behaviour. Investigations into the optimal number of time steps between samples, number of samples used in each ensemble average and the radius of the weighting function for each node, are presented below. A study of the effect of the different weighting functions is also presented.

### Case Study 1 - Length of Time Between Samples

This investigation looks into the effect of coherence between samples, and will identify if the molecules local to each node have had sufficient time to change their individual points in phase space so that the maximum number of available configurations in phase space is covered by each ensemble. The investigation proceeds as follows. The number of samples for each ensemble average taken at each of the nodes is kept constant at 20. The length of simulation time that elapses between each sample is taken is varied between 25 and 400 time steps. The simulation time step is $2.0ps$, which relates to gaps between samples of $50ps$ and $800ps$, respectively.
5104 molecules are placed in a lattice $15nm$ by $15nm$ by $83nm$, which is equilibrated to a stable point at rest at a temperature of 300K, and periodic boundary conditions in all three dimensions. Temperature controls are removed, and the molecules are left to maintain an equilibrium state. No external forces are applied to the molecules, and only molecular motion/diffusion for the system temperature is present. The local velocity is monitored at 29 nodes arranged in a one dimensional array as shown in Figure 5.3, with each node having a cutoff radius of $1.0nm$. All simulations are performed from exactly the same starting point, with identical molecular data at the beginning of the production phase

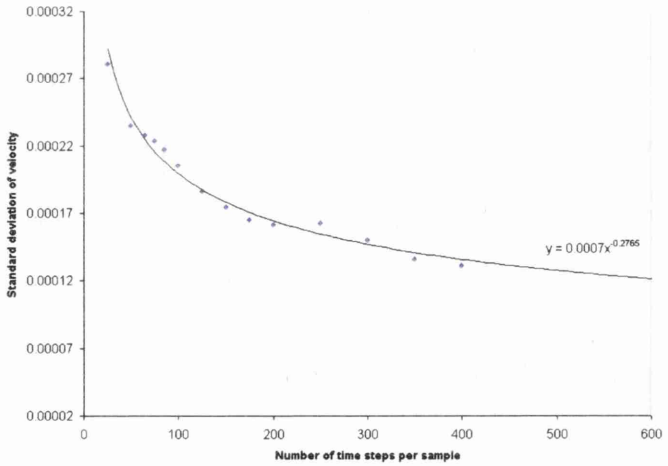


Figure 5.4: A graph demonstrating the relationship between the interval between samples are taken, and the standard deviation of the resulting one dimensional velocity distribution. The equation of the best fit line is also shown

The fluid is at rest, so the bulk velocity of the fluid is zero. However, the molecules of the fluid are constantly moving throughout the fluid diffusing with thermal motion. Poor phase space sampling will yield a non-zero value of velocity at the nodes, and lead to larger variation in the ensemble values at the nodes. A good sample of a wider portion of phase space will lead for the thermal motion of the molecules to cancel out, giving consistent values at the nodes, all of which should approach zero.
Figure 5.4 shows a plot of the average standard deviation (averaged over all nodes) of the values of velocity, plotted against the number of time steps between each sample. It is necessary at this point to remember that the same number of samples are taken for each case so that every ensemble taken contains the same amount of data. The results show an exponential decrease in the standard deviation of the nodal values as the time between samples increases. This leads to the conclusion that samples taken at more than 200 time step intervals (400ps) gives a good result, but the larger the time between samples the less variation there will be in the results. Increasing the sample interval to 400 time steps reduces the variation 18% but the ensemble time increases by 200%. The line of best fit is asymptotic to zero variation, indicating that the sample length could be extended indefinitely whilst still reducing the variation in the results. However, in practice the an acceptable variation must therefore be accepted to allow for an acceptable resolution in time. For these cases, the variation is considered acceptable at 200 time steps or greater.

Figure 5.5 shows a plot of the average value of velocity (averaged over all nodes) plotted against the interval between samples. This shows the accuracy of the ensemble increasing as the time between samples increases, achieving an average velocity closer to the zero velocity specified. However, the data presented contains a significant level of noise making a relationship difficult to determine, but the average velocity shows a definite trend to zero as the sample time increases, giving a very close approximation for sample times greater than 250 time steps.

Both of these graphs demonstrate the same result. The more time molecules are allowed in order to change state before being re-sampled, the better the interrogation of the available phase space performed by each of the local ap-

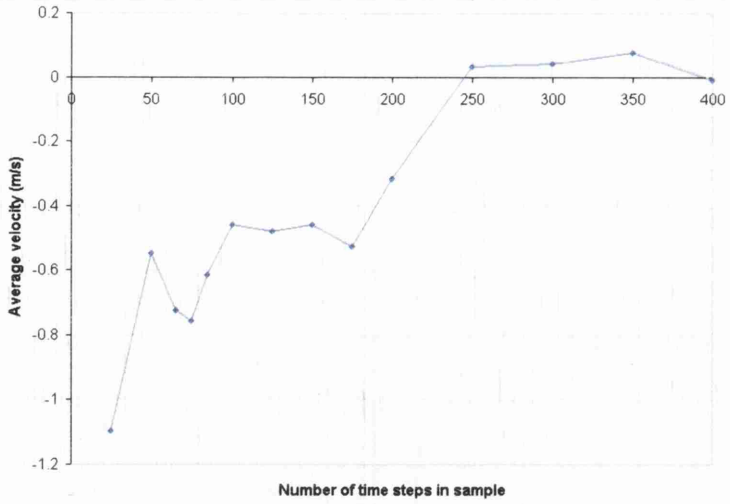


Figure 5.5: Graph showing the average value of velocity plotted against the number of time steps between samples

proximations. In both cases, the improvement is exponential, although the average velocity data is noisy. However, a longer time between samples reduces the resolution of the ensembles in terms of simulation time. This must be considered when long sample times are used. A way of increasing the time between samples is to take fewer samples per ensemble, which will be discussed in detail in the next case study:

### Case Study 2 - Number of Samples per Ensemble

By performing a similar study, the effect of the number of samples collected per ensemble average can be investigated. Simulations were setup as described above, with the samples taken at regular intervals of 75 time steps, but the ensembles were constructed of between 2 and 40 samples.

Figure 5.6 shows a plot of the average standard deviation of the collected ensemble velocity over all the nodes, against the number of samples collected per ensemble average. The graph shows a similar relationship to sample timing study, with a slightly lower gradient where, as the number of samples increases in each ensemble, the variation in the results of this steady state system reduces to give more stable values. As the number of sample points increases, more points throughout the available phase space are sampled, leads to a better representation of the local ensemble by the approximation.

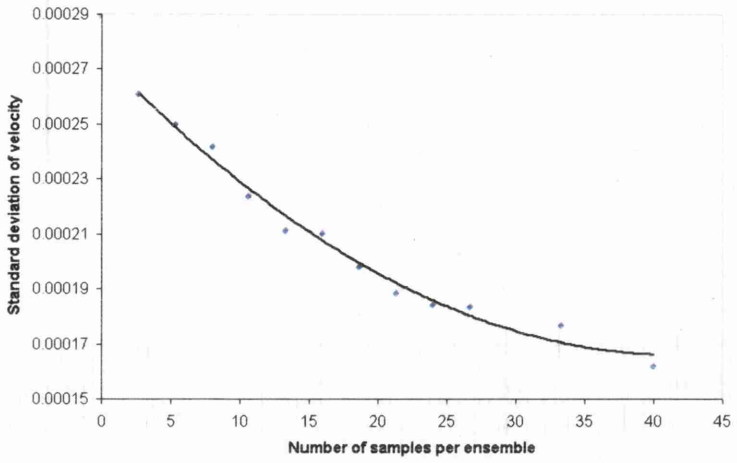


Figure 5.6: Graph standard deviation of velocity plotted against the number of samples per ensemble

### Case Study 3 - Time Between Samples verses Number of Samples Per Ensemble

The above study suggest that increasing the time between successive samples of the molecular data should be as long as possible in order to sample the widest available area of phase space. Similarly, to obtain bulk properties with the least amount of noise, there must be the maximum number of samples taken for each ensemble average, to sample as many different points in phase space as possible. However, in a realistic simulation example, there is a limit to the amount of simulation time that can be allowed between the ensemble averages being taken. This could be a limit on an ensemble taken for a steady system over a long period of time or short intervals for a dynamic system, where greater resolution in terms of time is required. In these cases, there is a maximum time over which an ensemble can be taken. This means that within one ensemble a balance must be made between the number of samples used in each ensemble, and the time between each sample taken.

To test the sensitivity of this tradeoff, the same example of fluid methane at rest, as described above, was used. The total ensemble time is limited to $20,000$ time steps, and the sample interval is varied between 100 and 1000 time steps to correspond to 200 and 20 samples per ensemble, respectively. Figure 5.7 shows a plot of the standard deviation of the ensemble velocity, averaged over three ensembles taken for the varying time between samples. In

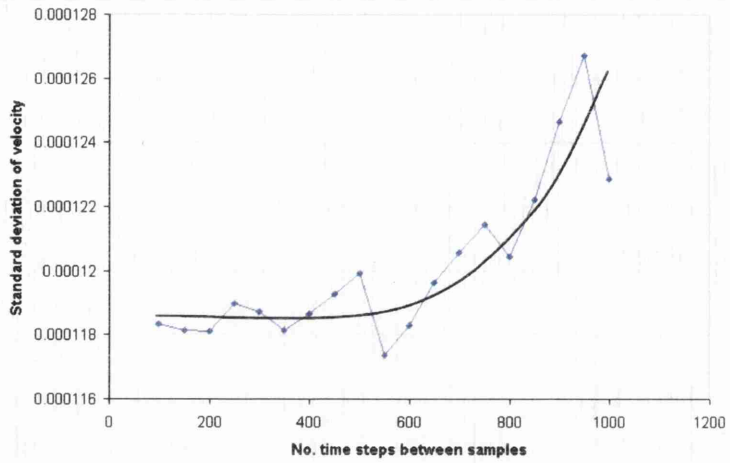


Figure 5.7: Plot to demonstrate the effect of trading off the length of time between samples against the number of samples per ensemble, for a fixed ensemble length of 20,000 time steps

the previous results, it has been shown that the best and most stable results are obtained by leaving long periods between taking each sample, and taking a large number of samples. However, for simulations with a finite time frame, there is a limit on this behaviour. As the length between samples increases, the number of samples that can be taken in the ensemble reduces, this causes the variation in the results to increase as the time between samples increases. The results shown in Figure 5.7 are dominated by the variation caused by the reduced number of samples in the ensemble, and the variation expected to be caused by the short sample times does not have an observable effect in the sampled region.

From these results, it can be concluded that the largest acceptable time between samples between is approximately 400 time steps, for this case. To generalise this, 400 time steps represents 2% of each ensemble time, allowing for 50 samples to be taken in each ensemble. Although the variation in the solution maintains a similar value for lower times between samples, the highest available values should be used to achieve the best representation of phase space, saving on the computational time involved with processing a higher number of samples.

### Case Study 4 - Radius of Weighting Function

The radius of the weighting function governs the area or volume over which the approximation is constructed at each node. This parameter is critical, as a smaller radius gives better resolution in space, at the cost of fewer molecules within each sample. Simulations were performed as above for the same sample times and number of samples per ensemble, and in this case only the radius associated to the nodes was altered. To give a idea of scale, the 29 nodes are spaced at $0.5nm$ intervals across the $15nm$ width of the simulation. The radius at each node is changed from $0.2nm$ up to $2nm$. Figure 5.8 gives an

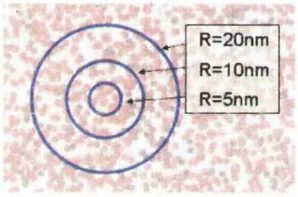


Figure 5.8: Two dimensional example of the radius of weighting function compared to the number of molecules present, for the example simulation

approximate idea of scale, showing the radius in two dimensions. Figure 5.9

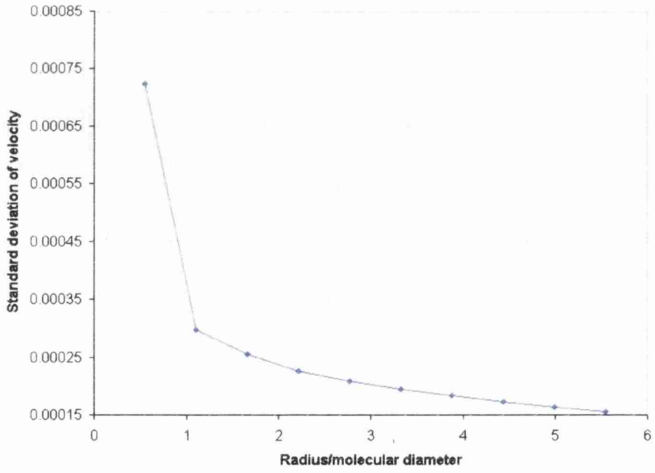


Figure 5.9: Standard deviation of velocity collected at the nodes, plotted against the ratio of node radius to molecular diameter

shows a plot of the standard deviation of the velocity obtained at each of the ensembles, against the ratio of the node's radius to the diameter of the underlying molecules (for methane $\sigma = 0.381nm$). This shows an increasing

accuracy as the radius is increased, with an abnormally large value for standard deviation at $R/\sigma = 0.5$. This is due to the radius being so small that only a single molecule can fit in the nodes 'zone' making the node very sensitive to the properties of an individual molecule.

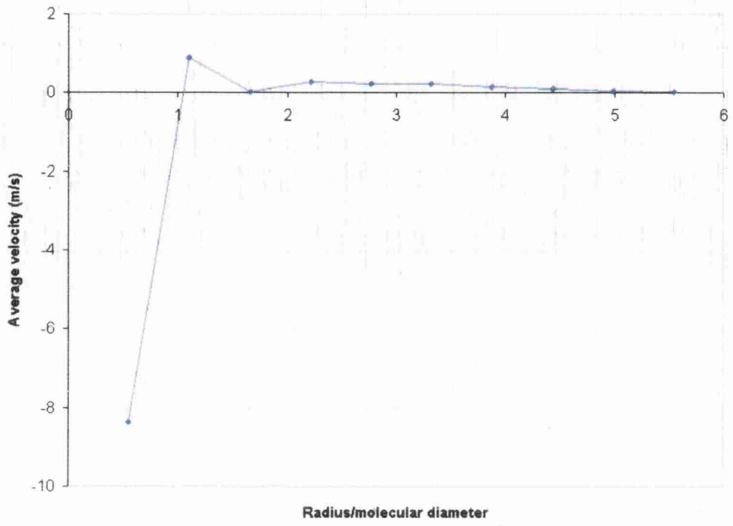


Figure 5.10: Average ensemble velocity plotted against ratio of node radius to molecular diameter

This is can also be highlighted in the plot of the average velocity, shown in Figure 5.10. Which reinforces the fact that one of the nodes has sampled a molecule with a speed that is on the higher side as given by the Maxwell-Boltzmann distribution. This has had a dramatic effect on the value of one of the nodes.

These results highlight that the radius of a node must be large enough to capture as many molecules as possible, but be small enough to be able to capture any variations that may be present in the distribution of the property, leading to a compromise between resolution, stability and statistical error.

### Case Study 5 - Weighting Function

The weighting function plays a very important part in the property extraction, being the basis on which molecules are allowed to contribute to a nodes ensemble average. By again performing the same test simulation, the effect of the different weighting function highlighted in Section 4.3.5, (quadratic,

exponential and Gaussian weighting functions) can be tested.

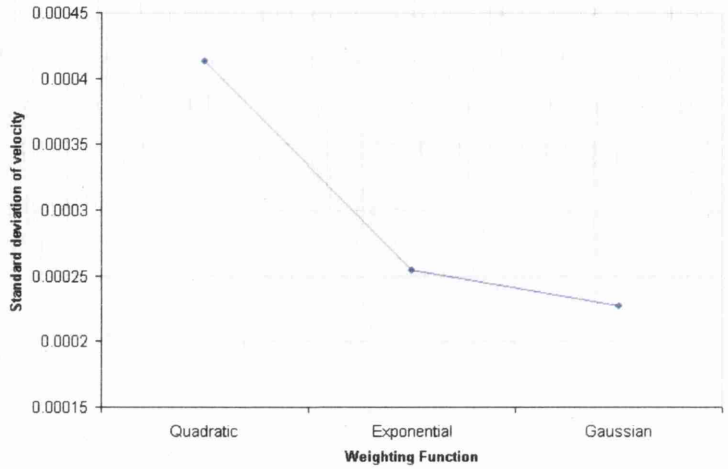


Figure 5.11: Values of standard deviation for each of the weighting functions

Figure 5.11 shows the values of the average ensemble standard deviation for the three weighting functions tested. From this, the Gaussian weighting function comes out on top, providing the most stable result, closely followed by the exponential function. In this application, the quadratic weighting function gives the most variation.

From these studies, we can conclude that in order for to obtain good stable results for the bulk properties collected at the least squares nodes, each sample must probe the available local phase space as comprehensively as possible. To do this, the ensembles must be constructed from as many samples as possible, and the samples must be taken with long intervals between them to allow the molecules to select a new phase space position. For this, a sample interval between 100 and 400 time steps should be used. However, these two parameters must be selected with any the resolution of the distribution of properties with respect to time in mind. Similarly, for the nodal radius a larger radius will provide better phase space sampling but reduces the resolution in terms of simulation space.
The parameters for the bulk property collection must therefore be carefully chosen for the system of interest, especially for systems that include gradients, and properties dependant on position and time within the simulation.

### 5.4.2 Gradient Study

In the previous section, the local averages have been extracted and evaluated for stable systems with approximately uniform properties throughout. This was used to study the effect of the parameters of the bulk ensemble approximations, against a known value. In this section, systems involving properties that vary a in space as well as time. These provide more of a challenge, as spatial and temporal resolution of the nodes must be seriously considered and traded off against the stability and accuracy of the ensemble averages collected at the nodes.

Two distributed bulk properties will be considered. Firstly the distribution of temperature, which will be studied in a fluid at rest, contained between two parallel plates at different temperatures. The nodes will then monitor the distribution of temperature throughout the field, as the thermal energy propagates through the fluid via the molecular collisions. Secondly, velocity distributions will be studied within a flowing fluid field. As will be shown, the study of velocity distributions requires special treatment, as extra controls on the system are needed, which will be presented and validated against existing fully molecular simulations.

#### Case Study 6 - Temperature gradient

As an initial test of this method, the molecular simulation was performed on a fluid at rest. The fluid is trapped between two parallel plates of different temperatures as shown in Figure 5.12. The plates are separated by $7.1nm$, with the left hand wall having a temperature of $300K$ and the right hand wall having a temperature of $250K$. The fluid methane in the middle interacts with the wall via the diffuse boundary conditions. The tangential momentum accomodation coefficient was chosen to be $f = 0.81$, to simulate a sparse solid lattice of carbon molecules. A large value of $f$ was used to achieve a large amount of variation of the temperature withing the simulation domain to examine the ability of the bulk property extraction component to capture details of a relatively high gradient property.

The fluid molecules were equilibrated from their initial lattice and temperature of $275K$ and settled to an equilibrium state. The temperature of the molecules were observed using 36 nodes placed at $0.2nm$ intervals within the

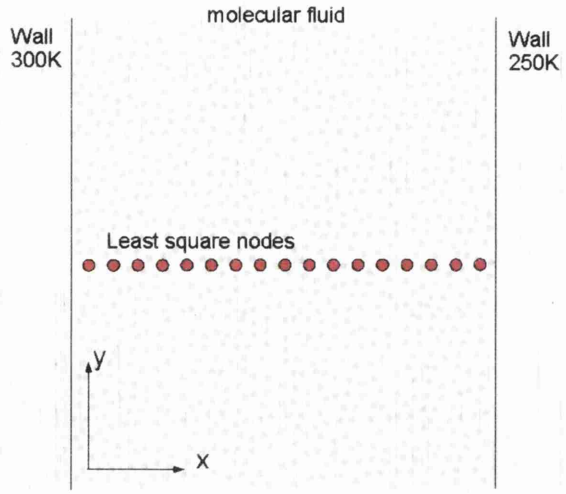


Figure 5.12: Schematic of fluid with temperature gradient. Wall on left is maintained at 300K, and the wall on the right at 250K. An array of one dimensional least squared nodes crosses the fluid between them to collect local values for temperature.

domain. The radius of interaction was set to $0.4nm$, and ensembles were taken over $50,000$ time steps ($2.fs$ time steps)

The molecules were free to interact with each other with the only temperature control being applied by the boundary walls. The resulting velocity profiles for the steady state result are shown in Figure 5.13. From this graph, the temperature gradient extracted from the molecular model can be clearly seen between the average ensemble temperature collected near the left hand wall, and the value at the right hand wall. In the centre of the fluid section, the temperature gradient is almost linear, however the gradient gets steeper in a relatively wide region close to the walls. This is due to the slip and jump at the boundary, where a discontinuity is allowed. Error bars are shown at 0.5% indicating the variation between profiles extracted.

This simple example highlights how the least squares nodes can be implemented and used to interrogate a molecular domain, providing distributions of useful engineering properties. The next step is to move this method onto a more challenging system that can aid in the validation of the molecular mechanics model.

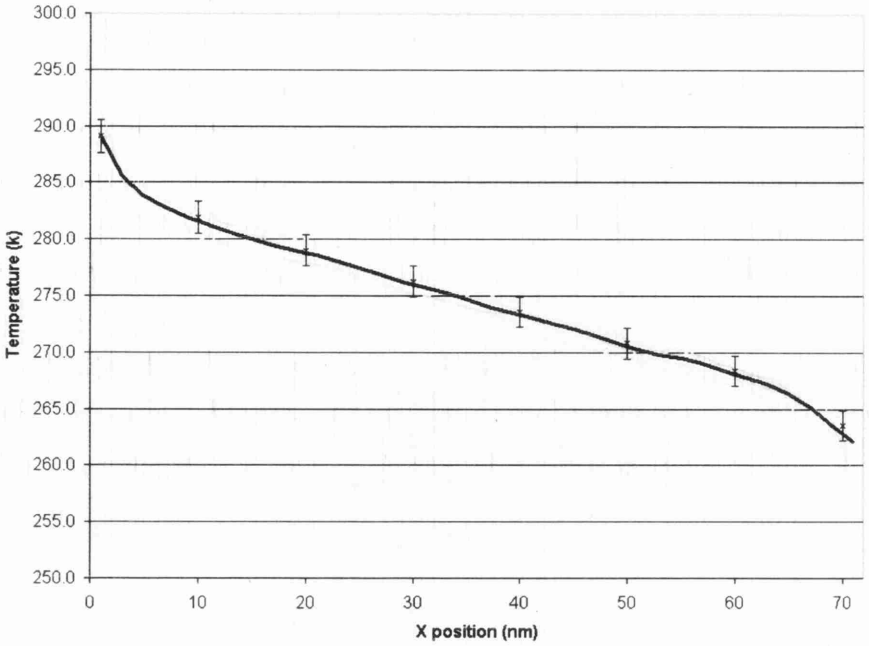


Figure 5.13: Temperature gradient for methane between two parallel plates at $x = 0$, maintained at 300K, and at $x = 7.1nm$ maintained at 250K. The black line shows the average temperature profile shown with a 0.5% variation.

### Case Study 7 - Velocity

This method allows the molecular model to simulate engineering systems at meso scale dimensions with large numbers of molecules. However, the accuracy of this model with its simplifications for boundary conditions and pressure gradients needs validation with existing work to ensure the model is still accurate. The performance of a molecular simulation can be tested in a number of ways, and in this section validation results are presented to give an idea of the accuracy of the method. There is almost no experimental data available for meso scale systems, and computational restrictions limit comparisons on the continuum scales, so tests are performed at high end molecular scales where information on simulations is readily available. This also allows the testing of the molecular model separately from the approximating (least squares) components.

The molecular dynamics model was tested against the molecular simulations performed by Sokhan *et al.* [66], whose simulations were performed using model based on the DL_POLY [95] package. The system considers fully de-

veloped poiseuille flow of methane through a graphite slit pore (Figure 5.14).

The system is simplified to methane molecules flowing between two par-

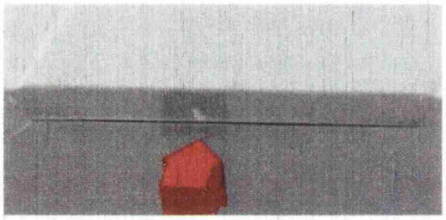

Figure 5.14: Cross section of an artificially created slit pore

allel plates of graphite, which contain the molecules in the $y$ direction, and periodic boundary conditions in the $x$ and $z$ directions. The system dimensions are shown if Figure 5.15, with the graphite plates being separated by $7.1nm$ and the length of the simulating cell in $x$ and $z$ directions are $7.875nm$ and $8.368nm$ in the $z$ direction. Into this volume was put 5104 methane molecules, corresponding to a reduced density of $\rho' = 0.61$, and interacting via a Lennard-Jones potential with collision radius $\sigma = 0.381nm$ and well depth $\epsilon/k_b = 148.1K$.

The graphene plates were modelled in Sokhan's simulation using two fully

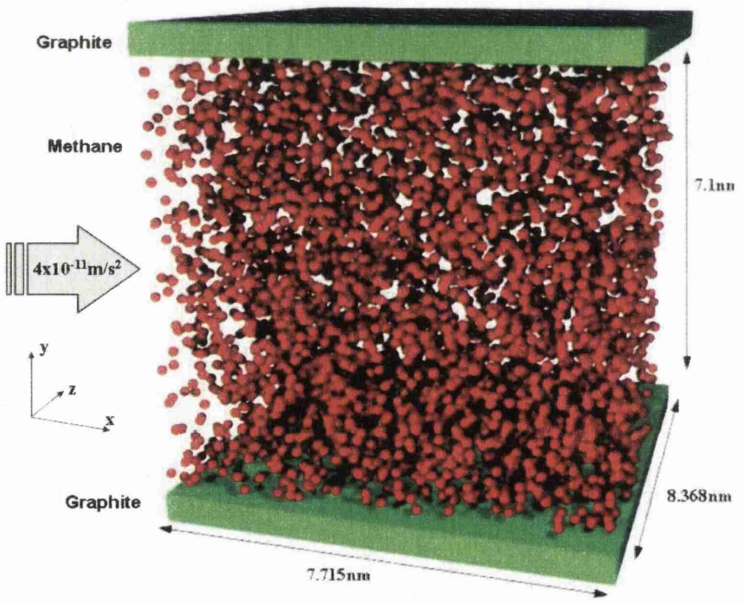


Figure 5.15: Cross section of an artificially created slit pore

molecular solid lattices of carbon atoms ($\sigma = 0.34nm$, and $\epsilon = 28K$). The

wall used in this simulation was modelled with diffuse boundary conditions, with a tangential momentum accommodation coefficient of 0.029, which was derived for this system in the same paper by Sokhan *et al.* [66], and confirmed by the work of Arya *et al.* [67] for methane on graphite.
Typically, the solid-fluid interaction parameters are computed using the Lorentz-Berthelot combining rule which between the carbon and methane molecules, leads to parameters $\sigma = 0.3605$ and $\epsilon/k_b = 64.39K$. However, the work presented by Sokhan *et al.* shows results for different strengths of interaction between the wall and fluid molecules, so a stronger potential of $\epsilon/k_b = 148.1K$ was used to simulate a higher degree of wetting.

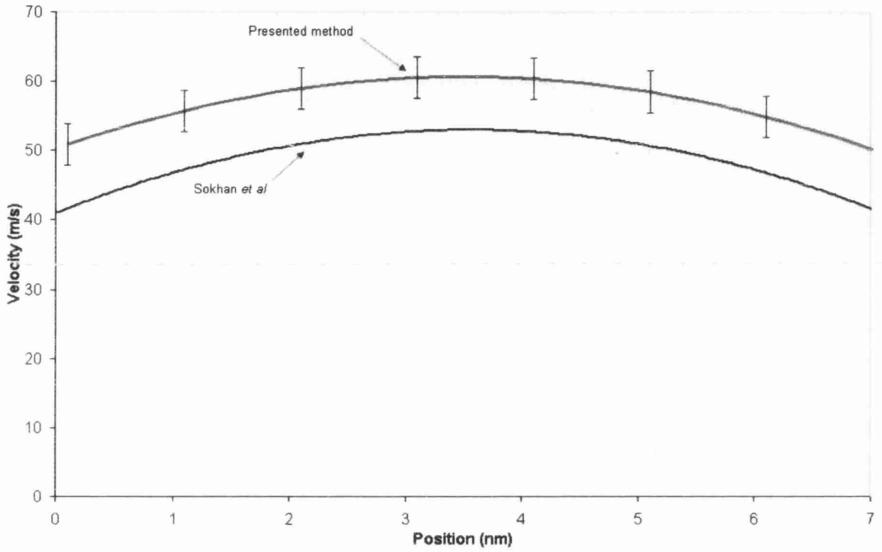


Figure 5.16: Comparison between the presented model and results published by Sokhan *et al.* [66]. Error bars are shown at $\pm 3m/s$

The fluid molecules are driven down the channel by applying a uniform acceleration to all molecules of $4 \times 10^{-11} m/s$. In Sokhan's simulations with flexible walls, the energy added via this acceleration could be removed and adsorbed by the wall molecules. However, in the case of the rigid molecular walls, and the diffuse boundaries used in our model, a Gaussian thermostat was used to perform the same task.

The resulting velocity profiles are shown for comparison in Figure 5.16. The results from Sokhan were taken over a $1ns$ period, whereas the results

obtained by the presented method were constructed within a $0.1ns$ long ensemble. The variation displayed by successive profiles extracted by the presented method is less than $\pm 3m/s$ or 5% of the average velocity, the variation of Sokhan's comparison is not known. The two velocity profiles show very similar curvature, however the results of Sokhan *et al* display a slightly lower average velocity than the results of the presented method. The similarity between the profile shapes means that the fluid molecules propagate the fluid energy in the same way, however the differences in the average velocity appear to be caused by differences in the boundary conditions applied. As an additional check extra validation tests were performed to test the system conformity to the thermal distributions.

The molecular dynamics of the fluid molecules was checked against the

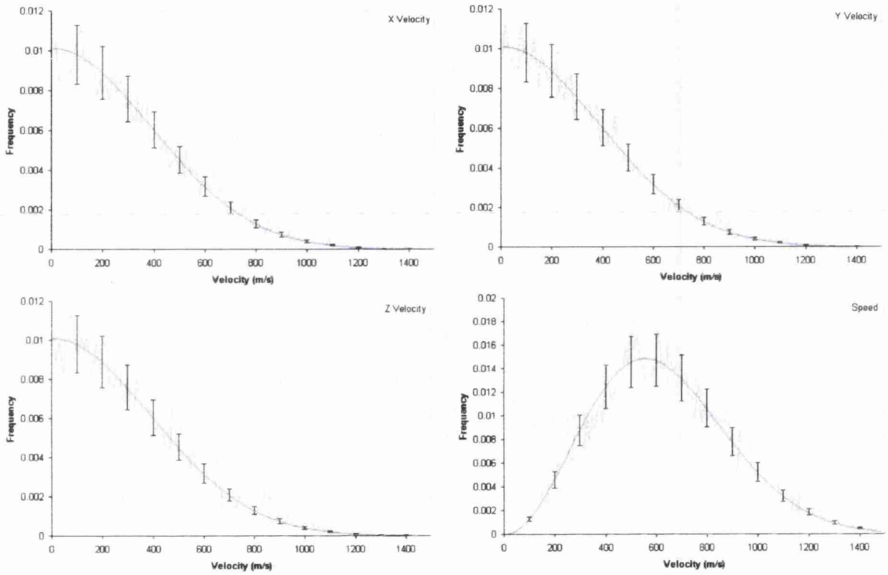


Figure 5.17: Distribution of $X$, $Y$, and $Z$ components of velocity, and distribution of resultant speed compared to distributions for temperature of 300K with 15% error bars

Maxwell-Boltzmann velocity distribution in each of the three dimensions, as well as the total speed distribution.

Figure 5.17 shows the distributions from a short snapshot of the steady state simulation above, along with the exact versions of the distributions. All distributions show good agreement with the profile of the exact versions within 15%, demonstrating that the molecules of the fluid are conforming to the correct thermodynamic state and that the thermostat is not having ad-

verse effects on the velocity distributions.

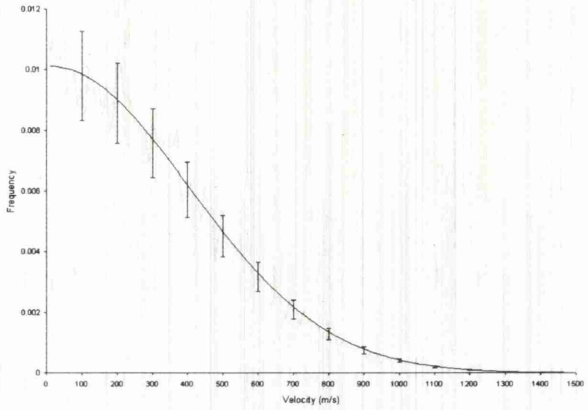


Figure 5.18: Velocity distribution of molecules thermalised by boundary, shown against velocity distribution for 300K with 15% variation

The velocity distribution for the velocities assigned to the thermalised molecules at the boundary were also tested, to ensure the thermalisation was being performed correctly. This is shown in Figure 5.18 and shows the same level of variation as the bulk temperature distributions within the fluid.

These results provide confidence in the developed meso scale molecular model. The simplifications applied to allow larger molecular systems to be accessed have not had an adverse effect on the mechanics, as shown by this molecular scale example compared to existing molecular simulation data from a well established and developed code.

## 5.5 Summary

In this chapter the method developed in the previous chapter has been extended to enable the simulation of flowing fluid systems. The generations of a flow has been implemented in the form of applying a representative acceleration to all molecules in the system. This addition of energy is balanced by a thermostatting system designed to remove thermal energy from the simulation without effecting the dynamics of the molecules.
A number of case studies have been presented to look at the behaviour of the bulk property extraction scheme. These highlighted the importance of sam-

ple length and the size of the ensemble and their effect on the stability and resolution of the solution. Also highlighted was the tradeoff between sample and ensemble time for simulations within a restricted time frame.

Case studies involving property gradients were also considered. The temperature gradient simulation example highlights the thermal control that can be imparted on the fluid by the boundaries. This also highlighted the methods ability to capture bulk property distributions with high accuracy and resolution. The velocity profile case study results demonstrated good agreement with both published results and thermal distributions.

# Chapter 6

# Modelling Fluid Regimes at Nano/Meso Scales

## 6.1 Introduction

In this chapter, the application of the developed method and how it may be used to extract useful data and properties from a fluid system dominated by molecular physics is discussed. To highlight its application, the bulk property extraction method is used to investigate flow regimes present in nano scale channel flows.

In the first section, flow regimes and the characterisation of fluid flow in a continuum framework are discussed as a background to existing knowledge of fluid behaviour. Fluid flow from the molecular scale exists as a flow of molecules, however in meso scale systems the behaviour of both bulk and molecular flow becomes important. The second section presents a molecular fluid model for flow in a slit pore, $15nm$ high. The method developed in Chapters 4 and 5 is used to analyse the fluid at different flow rates by purely considering the bulk velocity distribution of the fluid. From this information the flow at high and low flow rates is compared allowing for the different flow behaviour to be analysed. To begin, continuum flow regimes will be discussed.

## 6.2 Flow Regimes

Fluid can flow in two basic forms, which were investigated by experiment, by Reynolds (1842-1912) in the early 1880's [11]. These experiments highlighted the two different flows present in fluid systems, which will now be considered with the same approach as this experiment.

Figure 6.5 shows the setup of Reynolds experiments. A large tank of water

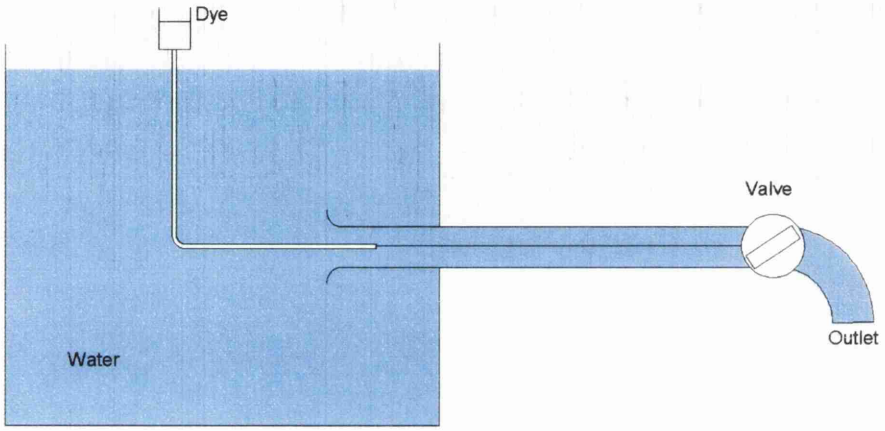


Figure 6.1: Apparatus used by Reynolds to study flow regimes

has a long thin transparent tube, through which the water must pass to exit via the valve. The water is driven down the tube by the pressure difference between the pressure at the inlet to the tube in the tank and pressure of the outlet. The flow rate of the water along the tube can then controlled by opening and closing the valve.

Dye is released into the centre of the flow along the tube via a thinner tube ending just inside the entrance. The dye is allowed to flow along the tube at the same speed as the water, and is used to visualise the internal behaviour of the fluid.

By altering the flow rate of water passing down the transparent tube, Reynolds was able to study the way in which water flows through channels and tubes at varying speeds.

If the valve is only partly open, restricting the flow in the tube to only a small velocity, the thin stream of dye remains in the centre of the flow and is almost completely undisturbed (Figure 6.2). This is the observable result, at continuum scales, of the infinite molecular interchange occurring within the

fluid, as has been discussed in Chapter 2. If multiple dye streams were em-

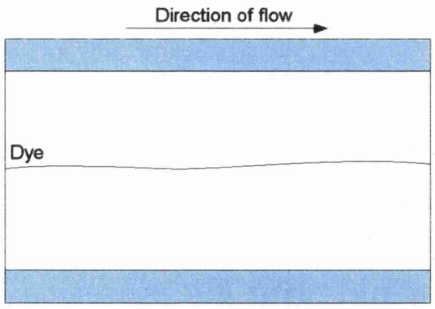


Figure 6.2: Parallel motion of a filament of dye within a laminar flow.

ployed at different places across the tubes section, none would be disurbed, although those close to the boundary would move with a slower velocity. This gives the effect of the fluid being composed of layers of fluid moving parallel to each other, which is commonly refered to as *laminar* flow.
As the valve is opened further, the velocity of the fluid in the tube increases, and at some point the stream of dye begins to oscillate. If the valve were to be opened further, the comes a point at which the stream begins to diffuse at a distance away from the inlet. Further opening the valve gives rise to a point at which a sudden breakdown of the dye stream at a distance from the inlet occurs, where the dye mixes almost completely with the water. Reynolds noticed that these disturbances only occurred at high flow speeds, at a distance away from the inlet, and that the mixing commenced suddenly.

The mixing of flow that occurs at these high flow rates is known as the

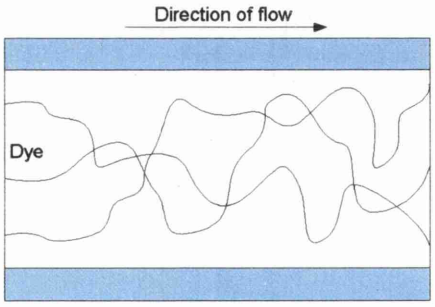


Figure 6.3: Chaotic mixing of filaments of dye within a turbulent flow.

*turbulent* flow regime. At this point, the fluid cannot be described in terms of fluid layers particles of fluid (in terms of the continuum description of a fluid particle) a constant velocity along the channel, but mix throughout the

width of the tube. The fluid particles in this flow regime have components of velocity not just in the direction of flow, and their paths criss-cross over each other in a seemingly unpredictable and chaotic way (Figure 6.3). In turbulent flow, the motion is irregular and conforms to no pattern in terms of frequency or formation of eddies, as the mixing occurs on a wide range of scales. However, there still remains a bulk average flow of fluid towards the outlet which the fluid particles follow, but they do not follow as pure a trajectory as fluid particles in a laminar flow.

Gotthilf Ludwig Hagen [96] a German physicist and hydraulic engineer, was the first to notice that the transition occurred in a tube at a specific velocity. He also noted that this velocity was dependant on the temperature of the fluid flowing through the tube, directly related to which is the viscosity. However, Hagen was unable to derive a general law to describe this behaviour. Further experiments performed using the above apparatus by Reynolds [11], who noticed the inverse relationship between the transition velocity and the diameter of the tube. This lead to the construction of the Reynolds number,

$$Re = \frac{\rho u l}{\mu} \tag{6.1}$$

which is a function of density $\rho$, viscosity $\mu$, velocity $u$, and characteristic dimension $l$ (in this case the tube diameter). The relationship that Reynolds came up with, a measure with which to judge the transition to turbulence, but also take advantage of the similarity of flows.
Reynolds noticed that large scale flows, showed similar behaviour to that of flows of the same geometry, but on a smaller scale with a higher viscosity. This similarity of flows, is used extensively in experimental investigations, and similar flows can be considered similar if they possess the same Reynolds number.

The smooth, predictable nature of laminar flow allow it to be easily analysed mathematically. However, the complex and chaotic behaviour of turbulent flows does not allow for easy prediction. Turbulent flows are individual, and the exact dynamics of a turbulent flow is unrepeatable and it is affected by dynamics on many scales. However, the behaviour of the fluid on small scales can be represented by statistical methods to provide an approximation of the multi-scale mixing and eddy effects.

There are three basic models used for turbulent flow simulation on the continuum scale, DNS, LES and RANS. DNS (Direct Numerical simulation) presents the fullest simulation model turbulence that can be very accurate, but is also very computationally expensive. RANS (Reynolds Averaged Navier-Stokes) is the most simple, where turbulent terms are approximated as a function of Reynolds number. LES (Large Eddy Simulation, and Very Larger Eddy Simulation) presents a balance between the two, where the eddies on the scale of the simulation are evaluated fully, and smaller scale eddies are approximated using a diffuse term.

### 6.2.1 Laminar Flow

Laminar flow, can be described as fluid flowing in adjacent parallel layers, or laminae. Layers of fluid that flow over each other, imposing shear or drag forces on adjacent layers. Also the streamline followed by continuum fluid particles do not cross, but follow smooth predictable paths. This is the description commonly used for laminar flow at continuum scales. This description however, is not valid at molecular scales as fluid layers and continuum particles cannot be described through the chaotic thermal motion of the molecules. It is therefore necessary to identify other distinguishing features to determine weather a flow is laminar in a molecular system.
For laminar, low speed flows, both Hagen and Poiseuille (1799-1869) found, through experimentation, a linear relationship between the head loss in a length of pipe, and the flow rate of fluid. This head loss is the result of a linear relationship between the friction force experienced by the fluid from the wall imposing a velocity gradient on the flow. Here, the shear force between fluid layers results in a velocity gradient across the channel or pipe. This is quantified by the Hagen-Poiseuille equation for the flow rate $Q$, in a cylindrical pipe of radius $R$,

$$Q = -\frac{\pi}{4\mu}\left(\frac{dp}{dx}\right)\int_0^R \left(R^2 r - r^3\right) dr \tag{6.2}$$

Which simplifies to,

$$Q = -\frac{\pi R^4}{8\mu}\left(\frac{dp}{dx}\right) \tag{6.3}$$

The velocity at any radius of the pipe can also be calculated as,

$$u(r) = -\frac{1}{4\mu}\left(\frac{dp}{dx}\right)\left(R^2 - r^2\right) \tag{6.4}$$

Velocity profiles of flows can be extracted from molecular simulations using

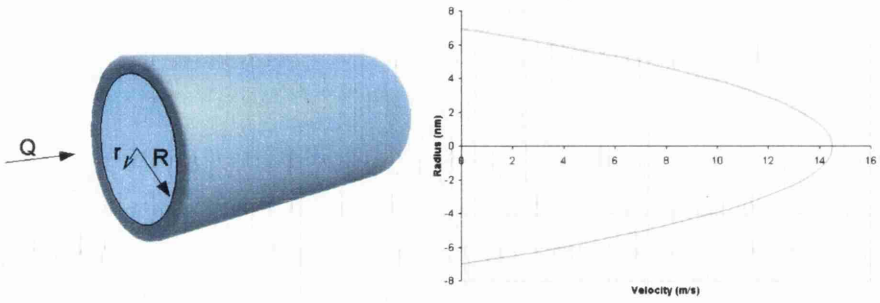


Figure 6.4: Velocity profile for laminar flow in a cylindrical pipe of radius $R$, as described by Hagen and Poiseuille

the methods described in Chapter 5, and compared with those computed from the above equations. These equations however, do not account for the slip between the solid and fluid at molecular scales [46]. On the continuum scale, it is assumed that there is no slip at the boundary and the fact that slip is present may have an effect on the linear relationship between flow rate and pressure head. The velocity distribution of the flow in a channel or pipe, extracted from a molecular simulation, contains information about both the conformity to the laminar profile described by Hagen and Poiseuille and the flow rate in the tube. This information can be used to identify laminar behaviour through the chaotic molecular motion.

### 6.2.2 Turbulent Flow

Turbulent flow occurs at high speeds, where the inertial terms of the Reynolds number dominate the viscous terms. In a turbulent flow regime, there is a high level of chaotic mixing and diffusion. From a continuum view point, the paths followed by fluid particles are erratic and cross continuously as the flow is mixed up. On a molecular scale, the dynamics of the molecules does not appear to significantly change, as the chaotic random motion is present in both laminar and turbulent flows.

Experimental tests were performed by Henri Darcy(1803-1858) in 1857 [97]

on turbulent flow in long pipes of different sizes, which resulted in the Darcy law for head loss in turbulent pipes. Due to the chaotic unpredictable nature, almost all models for turbulence contain some form of experimental results, as pure numerical analysis is not currently possible.
To identify a turbulent flow, observations of chaotic behaviour is not sufficient at molecular scales, as it is present in laminar flow as well in the form of thermal motion. However, the mixing within turbulent flows occurs on a wider range of scales which has the effect of increasing the energy losses internally within the fluid, where energy is dissipated away from the direction of flow. As a result, this increased instability in the fluid can be noted by observing the relationship between pressure loss and flow rate. The relationship should be similar to the laminar relationship, but with a lower gradient as the energy needed to drive the flow is higher. The increased energy perpendicular to the direction of flow should also increase the mixing of the fluid, leading to a different velocity profile that is more uniform across the centre of the channel.

This section has introduced continuum scale behaviour of fluid in the form of two flow regimes, laminar and turbulent flow. These regimes can be easily observed, tested and simulated on at continuum scales. However, as these simulation methods break down as the meso scale is approached, little is known about the behaviour of molecular flows. In the next section, the method derived in Chapter 5 is used to extract information from a molecular simulation over a range of flow rates, to allow the behaviour of the flow to be analysed at different speeds.

## 6.3 Fluid Flow Characterisation from Molecular Simulation

In this section, a molecular simulation is used to model the physics of a fluid passing through a slit pore of height $15nm$. Least square nodes are used to extract the bulk velocity distribution to provide information about the behaviour of the fluid at these scales. The slit pore is approximated by two parallel plates with diffuse boundary conditions in the $y$ direction, and periodic boundary conditions in the $x$ and $z$ directions.
In the following case, the velocity profile of the flow is extracted to measure

the fluid response to increasing pressure gradients. The velocity gradient contains information about the flow rate of fluid along the channel which, for traditional laminar flows, should increase linearly with the increasing pressure gradient. However, at molecular scales, there is a definite amount of slip between the fluid and the boundary. This will affect the velocity gradient by raising the mean velocity in the channel, as the frictional effect of the wall is reduced. The shape of the velocity gradient should maintain its Poiseuille profile approximately, allowing for molecular variation, but with a non zero velocity at the boundary, and shown in the validation tests in Chapter 5.
The system used in the tests is designed to replicate the flow of methane confined within a graphite slit pore. A two dimensional schematic of the simulated three dimensional system is shown in Figure 6.5. The pore walls are modelled as two single layers of carbon molecules in a graphite lattice, interacting via a Lennard-Jones potential. The Lennard-Jones parameters for methane were a collision diameter of $\sigma = 0.381nm$, a well depth of $\epsilon/k_b = 148.1K$, and with a molecular mass of $16.043amu$. The Lorentz-Berthelot mixing rules were used for the collision diameter, giving $\sigma = 0.3605nm$ for the carbon-methane interaction. The well depth used, was $\epsilon/k_b = 148.1K$ equal to the methane-methane well depth, similar to the methane wall used by Miyahara [41, 66], but the tangential momentum accomodation coefficient of the diffuse boundary was derived from the parameters of the carbon lattice, $f = 0.025$ [66]. The boundaries are fixed and possess no momentum, and therefore need no mass parameter.

The pore walls are 15nm apart, and infinite dimensions parallel to the pore are replicated using periodic boundary conditions in the $x$ and $z$ directions, with lengths $15nm$ and $8.5nm$ respectively.
Simulations were performed using a range of pressure gradients, simulated by applying a uniform acceleration to all fluid molecules. All tests were performed with the temperature at the wall maintained at $300K$ and as the boundaries are solid and cannot remove sufficient energy from the system, the fluid temperature was maintained at $300K$ using a Nosé Hoover thermostat. The driving acceleration applied to the fluid was varied from $2 \times 10^{11} m/s^2$ to $1 \times 10^{12} m/s^2$, to test response of the fluid over a wide range of flow rates.
The fluid response was measured using a one dimensional array of nodes placed across the domain in the $y$ direction, at $0.5nm$ intervals. Samples of the $x$

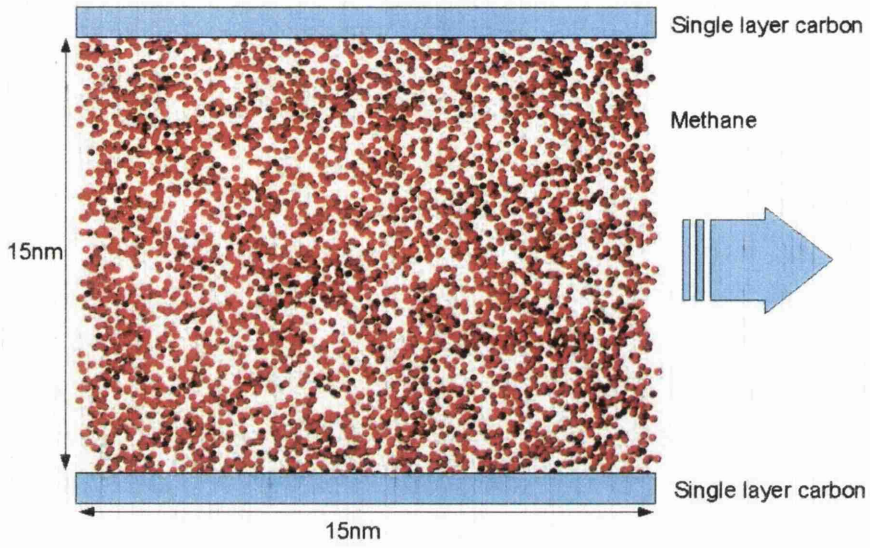


Figure 6.5: System to test flow regimes between parallel plates

component of velocity (along the channel) of the molecules were taken every 200 time steps, and ensemble averages were computed every 2000 time steps. By taking ensemble averages at these relatively short intervals, the progress of the simulation can be monitored using the velocity profile to check that a stable solution is reached for each run.

### 6.3.1 Characteristics of Low Speed Molecular Flow

For the above model of a slit pore, the driving force along the pore was ranged from $2 \times 10^{11} m/s^2$ to $1 \times 10^{12} m/s^2$. The resulting velocity profiles computed from the ensemble averages were recorded, and the average velocity of the flow in each case was found. Figure 6.6 shows a plot of the resulting stable average velocity against the driving force applied to the flow.

The average velocity is plotted in Figure 6.6, as it is proportional to the flow rate of the fluid in the channel, against the driving force applied to the flow. The graph shows a linear relationship between average velocity and driving force, which passes through point (0,0). A degree of deviation is present from the linear line due to the short time over which the ensemble averages were taken but a clear relationship is present.
In the chaotic molecular structure of a fluid, the molecules are continually

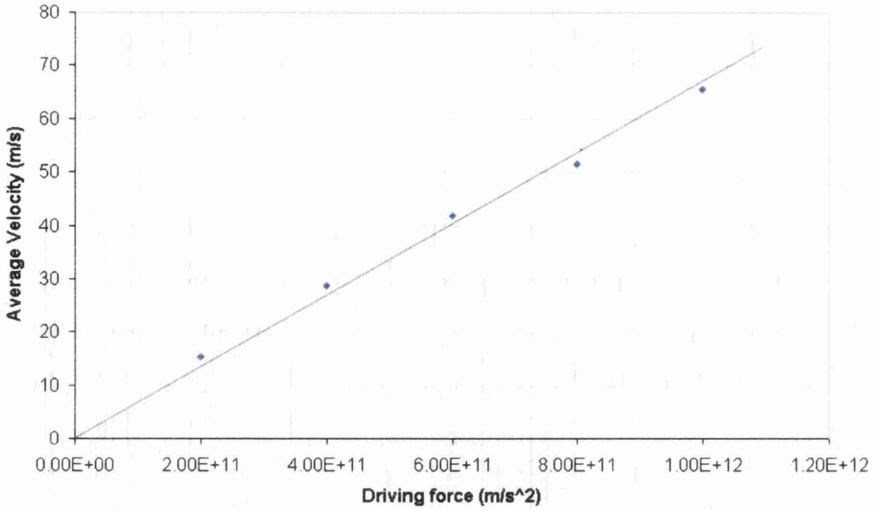


Figure 6.6: Average velocity in channel plotted against driving force (simulating pressure gradient) for low speed flows.

moving with their own thermal velocity, conforming to the Boltzmann distribution. A useful comparison to draw, is between the average of the thermal motion of the molecules and the average 'bulk' velocity of the flow. The average speed of a molecule in on direction can be computed from the Boltzmann equation as,

$$v_{average} = \sqrt{\frac{Tk_b}{m}} \tag{6.5}$$

For a system temperature of 300K, the average velocity due to thermal motion becomes [8],

$$v_{average} = 394.34m/s \tag{6.6}$$

The lowest driving force tested in this system gives an average bulk velocity of $15m/s$, corresponding to a total of 3.8% of the average thermal velocity of molecules. Similarly, for the largest velocity of $65.5m/s$ corresponds to 16.6%, both of which are very small compared to the magnitude of the motion of the molecules.

### 6.3.2 Characteristics of High Speed Molecular Flow

By extending the range of driving forces applied the bulk velocity extracted captured a change in the behaviour of the flowing molecules. Figure 6.7 shows

a plot of the average velocity of the flow against the driving force for values up to $\frac{F}{m} = 5.0 \times 10^{13} m/s^2$. On the left hand side of the graph, the same data as the graph shown in Figure 6.6 is displayed. However, for larger driving forces, a change in the behaviour can be seen beyond this region.

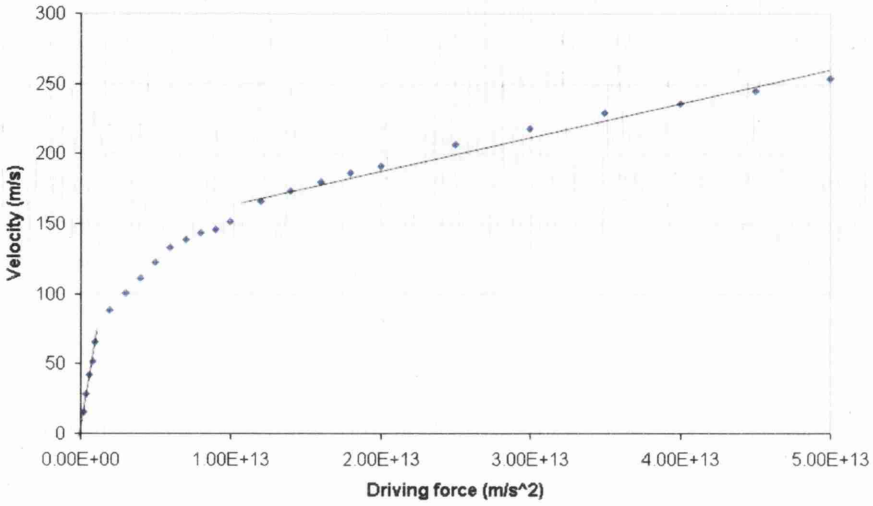


Figure 6.7: Average velocity in channel plotted against driving force (simulating pressure gradient)

Beyond the linear, slow speed flow region (far left of graph), the same increase in driving force causes less of an increase in the average velocity. The fluid response reduces further until another approximately stable relationship is displayed for driving forces of between $1.2 \times 10^{13} m/s^2$ to $5 \times 10^{13} m/s^2$. This high speed flow regime is present over a range of velocities from $190 m/s$ to $254 m/s$, which to compared with the average thermal velocity of the molecules is 48.2% and 64.4% respectively. The low gradient of the graph in the high flow rate region of the graph indicated that a higher proportion of the energy given to the fluid by the driving force is diffused away from the direction of motion.

The range of driving forces tested was stopped at $5 \times 10^{13} m/s^2$ because it was found that at higher values the thermostat interfered with the dynamics of the simulation. At values of $6 \times 10^{13} m/s^2$, the molecular motion becomes unstable causing clusters of molecules to form. This is due to the system becoming over constrained and molecules settle into a quasi equilibrium state in which they change energy states a little as possible, however they still maintain the global

velocity distributions.

The results shown in Figure 6.7 demonstrate that the behaviour of different flow regimes can be captured and identified from a molecular simulation, where the high flow regime displays much higher losses than low flow rate regime. The low speed flow can be likened to a laminar flow, where losses are low meaning that the exchange between layers parallel to the direction of flow should be minimal. In the high flow case, losses are higher and higher level of interaction and exchange is expected perpendicular to the flow direction. This can be examined by comparing further data extracted during the simulations.

### 6.3.3 Comparisons and Data Analysis

To further aid in the characterisation of these two regions, comparisons can be drawn between their behaviour. The presented method for obtaining the bulk properties has been used above to extract velocity profiles of the flow to plot the average velocity of the flow against the applied driving force. From these results, two regions have been identified one which displays significantly higher losses than the other. Further analysis of these regions can be performed by comparing the velocity profiles extracted from simulations performed in each of the regimes. Figure 6.8 shows the velocity profiles extracted for driving forces of $2 \times 10^{12} m/s^2$ and $4 \times 10^{13} m/s^2$, corresponding to flows within the low and high flow rate regimes respectively. The velocity profiles were extracted using 29 nodes placed at $0.5nm$ intervals across the channel, sampling at 75 time step intervals ($2.0fs$ time step), and each ensemble was measured over $0.4ps$.

The extracted profiles are shown if Figure 6.8. The profile extracted from the simulation with a low flow rate (bottom), displays a profile that is much more curved than the high flow rate profile. Accounting for the slip between the wall and the boundary, the profile is similar in shape to the analytical Poiseuille profile for describing laminar flow in pipes and channels. The profile is caused by the smooth propagation of energy throughout the system, where a molecule diffusing across the channel experiences many low energy collisions, altering its thermodynamic state as it passes each point. Both pro-

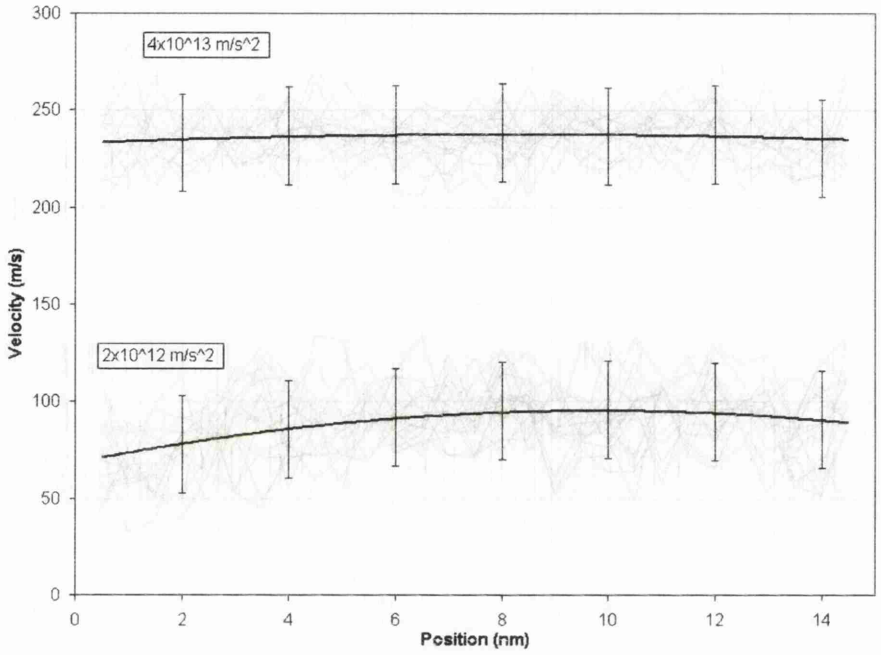


Figure 6.8: Velocity profiles extracted from molecular simulations for driving forces of $2. \times 10^{12} m/s^2$ and $4. \times 10^{13} m/s^2$. Flows at the two speeds show a variation of $\pm 25 m/s$

files show the same degree of variation, $\pm 25 m/s$. The variation is dependant on the thermal motion of the underlying molecules and therefore the same for high and low speed flows.
The High flow profile on the other hand, displays a markedly different shape. For this flow regime, the molecules possess more energy and display a significantly flatter velocity profile, showing that there is less difference in kinetic energy at neighbouring points through the simulation. This is in agreement with the continuum description of a turbulent flow with a flatter profile, as there is a higher degree of energy transfer between adjacent layers of fluid (mixing of energy), causing this velocity profile to form. This highlights the difference in the propagation of energy within the system, however, this does not tell about the propagation of mass within the channel.

An examination of the diffusion of mass within the system was performed using the following tests. The same simulation as above was setup and equilibrated to steady state for driving forces of $2. \times 10^{12} m/s^2$ and $4. \times 10^{13} m/s^2$ corresponding to the same low and high flow rates between parallel plates used

above. All the molecules falling within a vertical band between $x = 3.0nm$ and $x = 5.0nm$ were selected and tagged at the start of the production stage. The simulation then proceeded for a short $282fs$ period, to allow the molecules to diffuse from their original positions, but not reach the periodic boundaries (for clarity). After this short time period the final distributions of the molecules can be plotted to determine the spread achieved as a result of diffusion.
Figure 6.9 shows the initial and final plots for the low and high flow rates, for only the molecules tagged at the start of the simulation, all other molecules have been removed from the images.

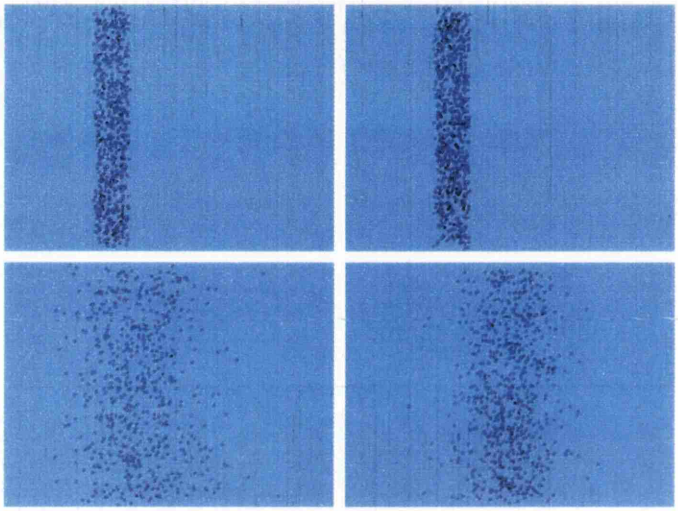

Figure 6.9: Initial and final distributions of molecules in centre of channel after $282fs$ (Flow is from left to right). **Left:** Low flow rate **Right:** High flow rate

From the images, it is clear that the molecules in the high flow rate stream have moved further than those in the low flow rate stream. It is also noticeable that the high flow molecules have not dispersed as much as those in the low flow. This is confirmed by looking at a histogram plot of the distribution of the molecules, as shown in Figure 6.10.

In this Figure, the frequency has been normalised for the number of molecules in each band, as the low and high flow examples contained a slightly different number of molecules. These results highlight that there is a substantial difference between the distributions of the two regimes. The standard deviation of the low flow rate simulation is 0.0443, whereas the high flow value is sub-

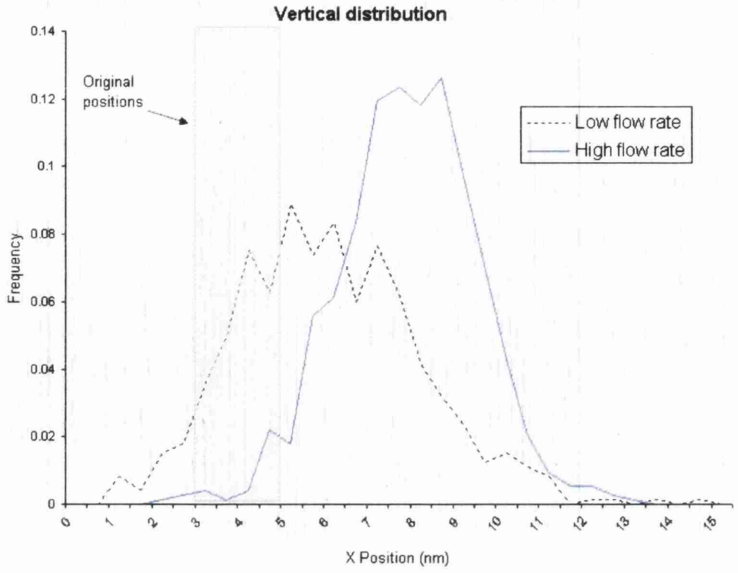


Figure 6.10: Graph comparing the distributions of the molecules in low and high flow rate simulations after $282fs$ of simulation time.

stantially lower, at 0.0302.

The same test performed with a horizontal band, between $y = 6.0nm$ and $y = 9.0nm$ allows the examination of the way in which the molecules diffuse vertically, perpendicular to the solid boundaries. Figure 6.11 shows the initial and final plots. In these figures, the distribution of molecules in the low and high flow rate in the $y$ direction is visibly the same in both cases. Figure 6.12 shows a histogram of the data collected, along with the initial position of the band. The graph shows that the majority of molecules have diffused in different directions in the low and high cases, however the distributions of the molecules after the short time is almost identical. The low flow rate gives a standard deviation of 0.0320 and the high flow gives a value of 0.0304

These results give an indication over a small time frame, the diffusion of mass within the molecular system in the $x$ (streamwise) and $y$ (perpendicular to pore walls) directions. In the $x$ direction, the molecules within the high speed flow diffuse less than those travelling in the lower speed flow. However, there is little change in the diffusion of the molecules in the $y$ direction due to the interaction with the solid boundaries. The molecules in the high flow case, have a bulk motion that is a greater proportion when compared to the ther-

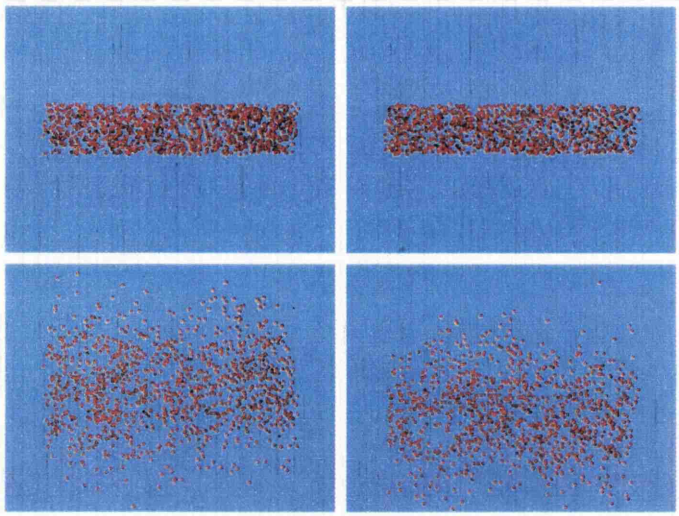

Figure 6.11: Initial and final distributions of molecules in centre of channel after $282fs$. (Flow is from left to right). **Left:** Low flow rate **Right:** High flow rate

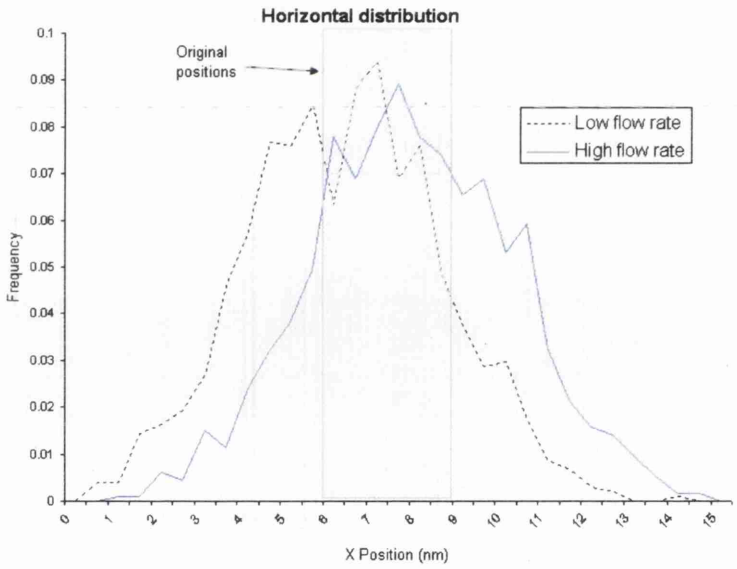


Figure 6.12: Graph comparing the distributions of the molecules in low and high flow rate simulations after $282fs$ of simulation time.

mal motion of the molecules which has the effect of ordering the molecules. Also, the increased energy being diffused perpendicular to the direction of motion has the effect of containing the molecules by the increased strength of the neighbour interactions (due to the increased energy perpendicular to the direction of flow). In the low flow case, the molecules have a much smaller

component of bulk velocity, and have more freedom to drift within the fluid domain.

The result is that as the speed of the flow increases, energy is distributed internally within the fluid. This is shown in Figure 6.7, where the energy lost identifies two regimes where a change of behaviour can be identified. Beyond this point, it can be shown in the comparison between the two velocity profiles in Figure 6.8 that for high flow rates the energy is diffused over a wider area across the channel, however the mass diffuses less. This is due to the increased molecular exchange between regions of fluid in terms of molecular interactions.

However, in the high flow case energy appears to be distributed in directions perpendicular to the direction of flow, showing turbulent behaviour. In a continuum framework, this would be accompanied by an increase in temperature across the channel. But in this case, the thermal constraints imposed by the thermostat fix the average temperature of the channel. This over constraining of the system could be a factor in the behaviour that has been extracted from the molecular dynamics. This is an area of meso scale simulation that needs more investigation and comparison with experiments for extra clarification and maybe the development of a new meso scale energy constraint system.

## 6.4 Summary

In this chapter, it has been shown how bulk behaviour can be extracted from the simulation of the internal molecular interaction, and how this information can be used to investigate fluid flow systems. This chapter has concentrated specifically on the extraction of bulk velocity of a fluid in a slit pore, but the same principles can be implemented for pressure, density, and temperature distributions, either independently or investigated together, depending of the dynamics of the system of interest.
In the slit pore case study, the velocity profiles were extracted as ensembles of average velocity at nodal sites placed at regular intervals across the channel. The spacing of the nodes, together with the radius of influence associated with each node allows for spatial resolution and clearly displays the curved velocity profile in the low flow rate case. In all the extracted profiles, a degree of sta-

tistical variation is present, and profiles are approximated as averages. This is due to the short ensemble time allotted between ensemble profiles being taken to provide good temporal resolution and allow the approach to steady state to be monitored.

Using this approach, a change in behaviour could be captured, highlighting the possibility of two flow regimes present. This combined with analysis of the diffusion showed a reduction in the mass diffusion, but an increase in the diffusion of energy within the fluid, which together with the consideration of the system energy constraints goes to account for the high losses in the high flow system. This example has highlighted how this method may be employed to extract useful data from a molecular physics dominated system, and allow the analysis and characterisation of a fluid system in terms of useful engineering properties and behaviour. Also highlighted, is the energy constraint issues with the use of the current thermostat systems.

# Chapter 7

# Performance of Proposed Meso Scale Model

## 7.1 Introduction

In this chapter, the computational issues associated with performing simulations using the molecular model and bulk property extraction on meso scale systems are discussed. The first section details the performance issued faced with large scale molecular modelling and studies how the computational demands change as the system size increases. This section also highlights the importance of the consideration of density when considering large scale molecular simulations.
The second section contains a study of the flow along a slit pore of meso scale dimensions. Simulations contain between $20,000$ and $100,000$ molecules and the impact this increased number of molecules and increased density has on the performance of the computation, and the behaviour of the fluid is discussed.

## 7.2 Issues in Using Large Numbers of Molecules

In general, as the number of molecules increases in the system the computational time and resources required also increases. The number of molecules in a system can change in two ways, as a result in a change in density, as a change in volume, or both. Up to this point in this thesis, molecular simulations have been performed within cells of a maximum dimension of $15nm$, with a max-

imum of 5104 molecules. This has been to allow validation of the molecular model, and the ability to explore the abilities of the bulk property extraction method with low numbers of molecules, where the method is weakest. In this section the resulting impact on the computational resources is discussed as a result of increasing the size of the molecular system to achieve meso scale dimensions.
Firstly, the effect of an increase in the number of molecules at constant density (increased volume) is discussed.

### 7.2.1 Processing Large Number of Molecules

An increase in the system size has a number of knock on effects within a molecular simulation. By increasing the number of molecules, the time to process the molecules and their interactions increases as well the memory needed to store their positions and lists of neighbours. Additionally, information on each molecules position, velocity, and resultant force in all three dimensions must be stored during each time step.
In order to simulate meso scales systems which contain large (up to 100,000) numbers of molecules, the computational requirements of the simulation must be fully understood. To explore the limits of a molecular model, performance tests are performed to gain an understanding of the computational requirements in two ways. Firstly, the effect of a simple increase in system size is tested by comparing the processing time of simulations with different numbers of molecules of the same density (volume altered). Secondly these results will be compared to simulations of varying density in systems of the same volume. These tests will help our understanding of the issues important in simulating large molecular systems, and the limits faced. These simulation tests are performed with a small number of molecules, between 14 and 5104 molecules. It is hoped that these small molecular numbers will display some overhead processing time, of the standard computations and operations performed giving a minimum computation time.

#### Constant Density Simulations

The simulations performed at constant density, were performed using a cubic cell with periodic boundary conditions in all three dimensions. The side of the

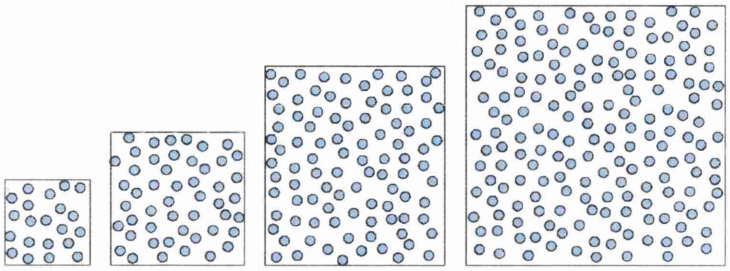

Figure 7.1: Simulations performed at constant density, over a range of volumes and numbers of molecules, to test computational requirements.

cubes tested were $1nm$, $2nm$, $3nm$, $4nm$, $5nm$, $6nm$, $7nm$, which contained 14, 114, 385, 913, 1783, 3080, and 5104 molecules respectively, as shown in Figure 7.1. This test explores the scalability of the molecular model, and the extra requirements needed to simulate at large molecular numbers. For each system, the time taken to reach $1ns$ of simulation time was recorded, along with the average number of neighbour interactions per molecule. In a molecular simulation, as the number of molecules increases, so does the size of the arrays required to the store position, velocity of all the molecules. The size of these arrays is a constant amount of memory required for every additional molecule in the system and is of little interest. However, the size of the neighbour list arrays depends on the number of neighbour pairs in the simulation and changes with the number of molecules and the density of the simulation. The neighbour lists can be far longer than the molecular properties arrays, and because of their dependance on the number of molecules as well as the system parameters, can capture behaviour that may further increase the computational time and memory requirements.
Figure 7.2 shows a plot of the number of molecules against the average number of neighbours possessed by molecules within the system, over the different system volumes at constant density.

This graph shows a constant 72.6 neighbours per molecule for simulations with above 385 molecules, and hence for systems with sides greater than $3nm$. The low number of neighbours for 14 ($1nm$) and 114 ($2nm$) molecules are due to the neighbour list cutoff radius being greater than 2 times the length of the periodic cell, as only a one image buffer is considered in each dimension. However, this constant relationship is to be expected beyond the $3nm$ system,

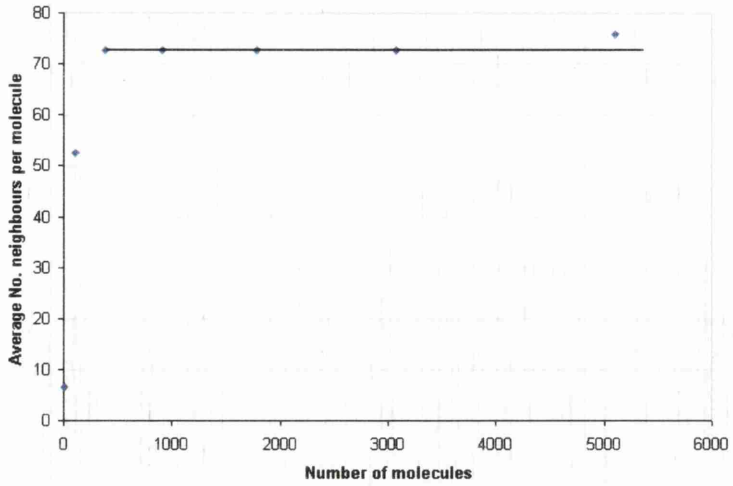


Figure 7.2: Plot of number of molecules against average number of neighbours per molecule for the constant density simulations.

due to the constant density. This presents a linear relationship between the

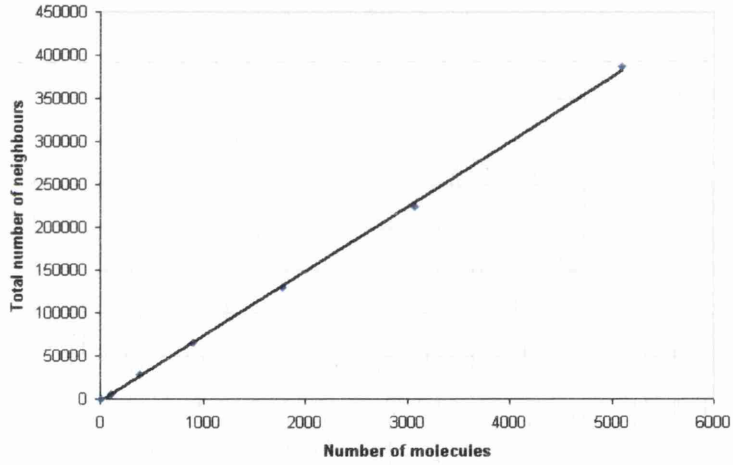


Figure 7.3: Plot of total number of neighbours against number of molecules for the constant density case

number of molecules and the total number of neighbour pairs (Figure 7.3), steadily increasing the computational time needed to process all the neighbour interactions.

Figure 7.4 shows a plot of the number of molecules against the time taken for the simulation to reach $1ns$. This graph shows a smooth relationship between the time needed to process the simulation and the number of molecules.

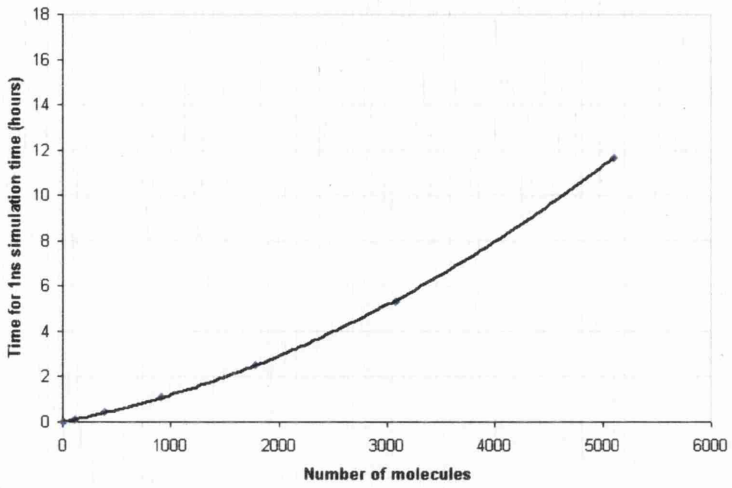


Figure 7.4: Plot of number of molecules against time taken to reach $1ns$ of simulation time for the constant density simulations.

The time increase added for each molecule added increases with the number of molecules. As shown in Figure 7.2 the number of neighbours per molecules is constant for the larger systems, however in this case extra time is spent searching through the extra molecules constructing and processing the neighbour list interactions. Neighbour searches are performed periodically as described in Chapter 2 but the searches are performed over the whole system. By adding one extra molecule to a system of $N$ molecules, the number of search evaluations being performed increases by $N$, and at this density the number of extra interactions to process increases by approximately 72.
Such computational costs can be reduced by implementing another stage of search/sorting that can be performed over smaller areas frequently, and over the whole system less frequently. This however, would require more memory, trading off memory against computation time.

### Constant Volume Simulations

To aid as a comparison with the above results for system sizes at constant density, simulations were performed over a range of molecular numbers at constant volume. Simulations were performed over a range of densities (Figure 7.5) within a constant volume cube of side $5nm$, and periodic boundary conditions in all three dimensions.

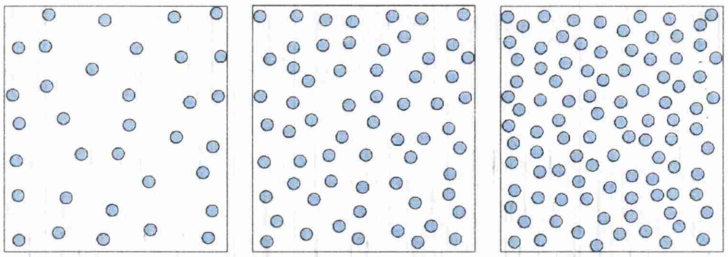

Figure 7.5: Simulations performed for different numbers of molecules at the same volume, with varying densities to test the additional computational resources required for high density systems.

The densities tested were 2.984, 24.29, 82.05, 194.6, 380.0, 656.4, and 1087.$kg/m^3$ with 14, 114, 385, 913, 1783, 3080, and 5104 molecules of methane, respectively. In these simulations, the number of molecules increases which increases the time required to process and move the system molecules, and are subject to all the issues raised about computational time and resources as the constant density tests above. However these simulations are performed at increasing density, which when compared to the results above, isolate the effect of increasing the length of the neighbour lists.

Figure 7.6 shows a plot of the number of molecules against the average number of neighbours per molecule possessed by each molecule in the simulation.
The graph shows a linear increase in the number of neighbours with the increase in number of molecules present. This means that the neighbour lists are no only getting longer due to the increased number of molecules, as was shown in the constant density test results, but the length of the neighbour lists is also increasing because the number of neighbours possessed by each molecule in the system is increasing. This further increases the number on pairwise force evaluations needing to be evaluated, extending the demand on memory storage and CPU processing.
Figure 7.7 shows a plot of the number of molecules against the time taken for the simulation to reach one nano second, for a range of system densities as specified above. Simulations were performed on a 3GHz processor PC with 2GB RAM.
The graph for the constant volume simulations (Simulations of varying density,

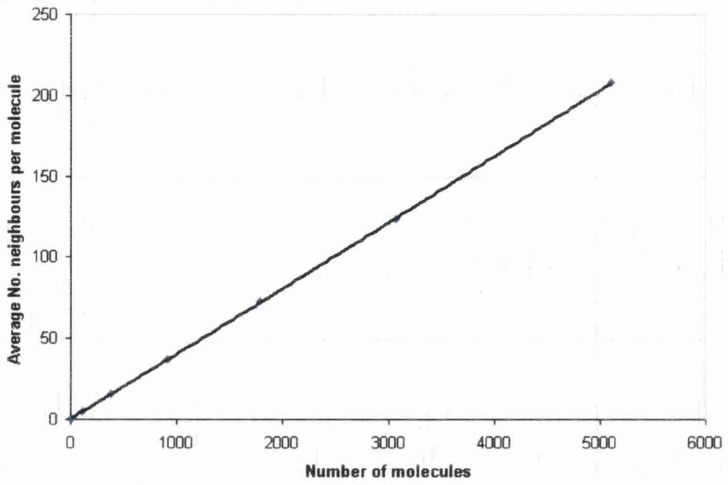


Figure 7.6: Plot of number of molecules against the average number of neighbours per molecule.

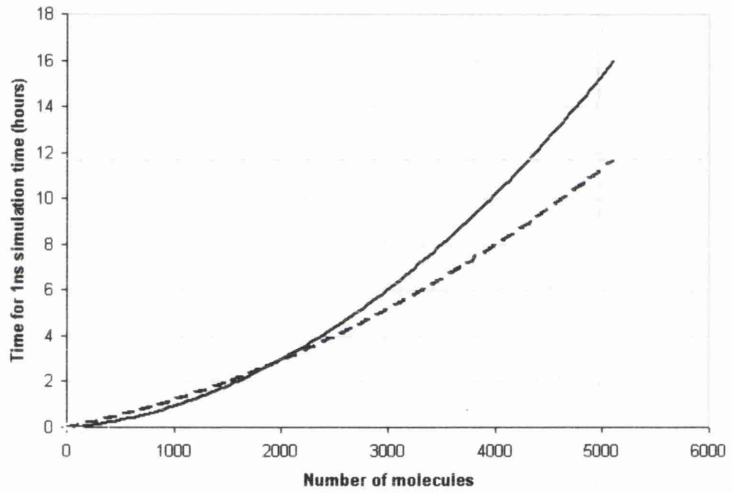


Figure 7.7: Plot of number of molecules against time taken to reach $1ns$ of simulation time for the constant density simulations for constant volume simulations (solid line) and constant density simulations (dashed line, Figure 7.4)

solid line) is shown against the results for processing time of the constant volume simulations (dashed line, Figure 7.4). The constant density simulations were performed in a $5nm$ cube, and the range of numbers of molecules used was the same in both constant density and volume simulations. As a result, the two resulting curves intersect at the system containing 1783 molecules. This however creates an interesting point on the graph in Figure 7.7, where

systems larger than 1783 molecules (Constant density simulations performed at $380.0kg/m^3$) show the higher density simulations (solid line) to require more computational time than the simulations containing the same number of molecules at a lower density(from the constant density simulations). This is due to the extended length of the neighbour lists and the number of extra interactions needing processing per molecules. However, for the simulations with less than 1783 molecules, systems with lower densities than the constant density simulations, display a shorter length of processing time is needed to process the interactions within the system, as the neighbour lists are shorter. This demonstrated the importance of considering the density of a molecular simulation when considering the resources required by a simulation.

The above study highlights this issues present in simulating large numbers of molecules. Although simulations have been using a maximum of 5104 molecules, they show the behaviour of the system at different volumes and densities. It is particularly important to understand these concepts with small system sizes, as the only difference between these tests and large-massive systems (apart from larger numbers) is the reduced proportion of time spent of overhead calculations and linear operations.
These results highlight the importance of considering the density of the simulation as well as the number of molecules being processed, as a high density simulation (or one with high density regions) can significantly increase the processing time and memory requirements. Also highlighted, is the tradeoff that is possible between CPU resources and memory, that can be made during the search routines. This can utilise a larger memory usage to speedup the time taken searching for neighbouring pairs within the simulation domain with a tree like search structure.
These issues are key, as these results indicate that there is a limit on the available simulation domain at meso scales in terms of both molecular numbers and density, which depend on the computing power available.

### 7.2.2 Boundary Conditions

In this molecular model, the solid molecular boundaries have been replaced with an approximating continuous wall to remove solid molecules from the simulation in order to reduce computational cost. These diffuse boundary condi-

tions replicate the scattering/corrugation effect of a molecular wall over a large number of collisions by thermalising a proportion of the colliding molecules. As the characteristic length and time of the system increases, the number of collisions occurring with the wall over this time and length scale increases. As a result, the wall approximation is being performed over a larger number of collisions, and provides a much better approximation. The boundary conditions have been validated against fully molecular walls at molecular scale dimensions with results published by Sokhan *et al* [66], in Chapter 5. This validation of the model with a low collision rate over the time and length scale of the simulation, gives us the confidence in the validity of the boundaries at larger scales where the collision rate is higher.

### 7.2.3 Bulk Property Extraction

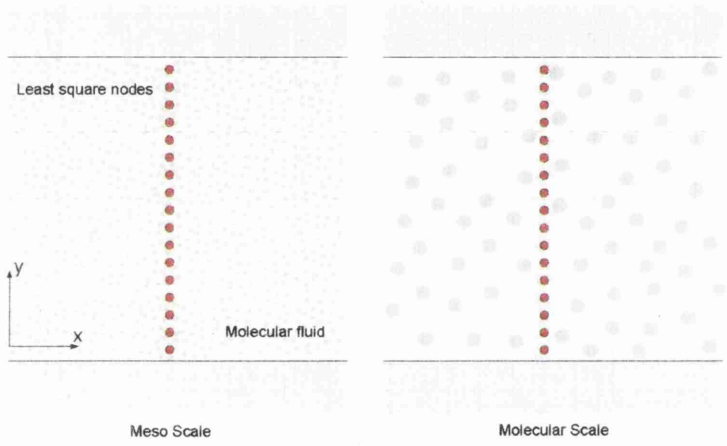


Figure 7.8: Extracting bulk properties from systems with high number of molecules (left) and low number of molecules (right)

At meso scale dimensions, bulk properties become much more defined and stable as their definition improves and importance rises, but are still below the limit at which they can be evaluated by the continuum governing equations. The parametric study performed in Chapter 5 highlights that the ensemble averages of properties collected, is improved by sampling the widest range of available phase space positions. A molecular system with meso scale dimensions containing a large number of molecules allows for a greater number of molecules to be included in the influence zone of each node as the resolution

of the system moves up to meso scale resolutions, when compared to a system of molecular scale dimensions of the same density (Figure 7.8).

## 7.3 Meso Scale Simulations

The small scale tests performed up to now have tested the lower limits of this method for extracting bulk ensemble properties from molecular simulations. The results may be less accurate because the ensemble averages have low numbers of molecules. Never the less, the method provides a framework which allows the characterisation of bulk effects from a molecular model. These bulk fluid properties have a definitive meaning above the molecular scale over large numbers of molecules. The bulk properties have a definite definition on a continuum scale, however there are a wide range of governing equations that can predict bulk fluid behaviour at these scales. The aim of this method is to capture the behaviour of these properties at meso scales where they have meaning but cannot be characterised by continuum equations. It is particularly important to characterise fluid in terms of meaningful properties relevant to solving engineering problems occurring at meso scale. In this section Simulations are performed at meso scale dimensions to examine the way in which the behaviour of this method, and the dynamics of the molecular model, change when a large number of molecules is used.

The system used is similar in form to the slit channel used previously to aid with comparison with smaller systems, this is shown in Figure 7.9. The slit channel is approximated by two parallel sheets of graphite separated by $93nm$, with modified boundary potentials to approximate an infinite solid comprised of parallel graphite layers. The walls themselves were approximated using the diffuse boundary conditions with a tangential momentum accommodation coefficient of $f = 0.029$ [66,67]. Periodic boundary conditions are applied in the $x$ and $z$ at $93nm$ and $40nm$ respectively. An acceleration of $1 \times 10^{13} m/s^2$ is used to simulate a pressure driven flow in the $x$ direction.

The available volume between the graphite walls was filled with methane molecules interacting with Lennard-Jones potential with a collision radius of $\sigma = 3.81A$ and a well depth of $\epsilon = 148.1K$. A range of densities was investigated of 1.58, 3.15, 4.73, and $7.89 kg/m^3$, corresponding to 20,000, 40,000,

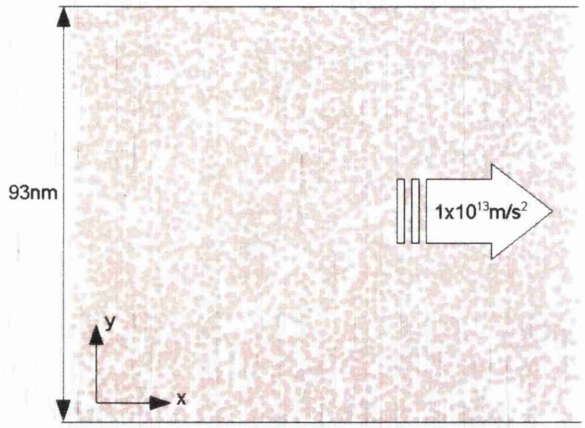


Figure 7.9: Approximated slit pore - flow of methane molecules between parallel graphite planes.

60,000 and 100,000 molecules respectively. All simulations were performed with a fluid and wall temperature equal to $300K$. This model generates a flow of molecules along the slit pore, the behaviour of which was observed using a one dimensional series of 46 nodes placed perpendicular to the direction of flow, in the $y$ direction. The nodes, spaced at $2nm$ intervals captured the streamwise component of velocity.

The nodes collected molecular properties of molecules within a radius of influence of $2.5nm$, using the Gaussian weighting function in the least squares approximation. The Gaussian weighting function was shown to be the most capable in the parametric study in Chapter 5, and the nodal radius was chosen to allow for high resolution, to allow the boundary layers at the solid interfaces to be captured.

The time step used was $2fs$ and samples were taken every 100 time steps. The ensemble averages were calculated over all nodes every 2,000 time steps. The parametric study also captured that larger times between samples and ensembles gave the best results, but for these simulations relatively short times were chosen to capture the development of the steady state solution.

Figure 7.10 shows the development of the solution for the low density system containing 20,000 molecules. This graph clearly shows the systems progress to developing a steady state solution from $t = 0$ where the velocity of the system is zero, to the final equilibrium state after 90,000 time steps at $t = 180ps$. At

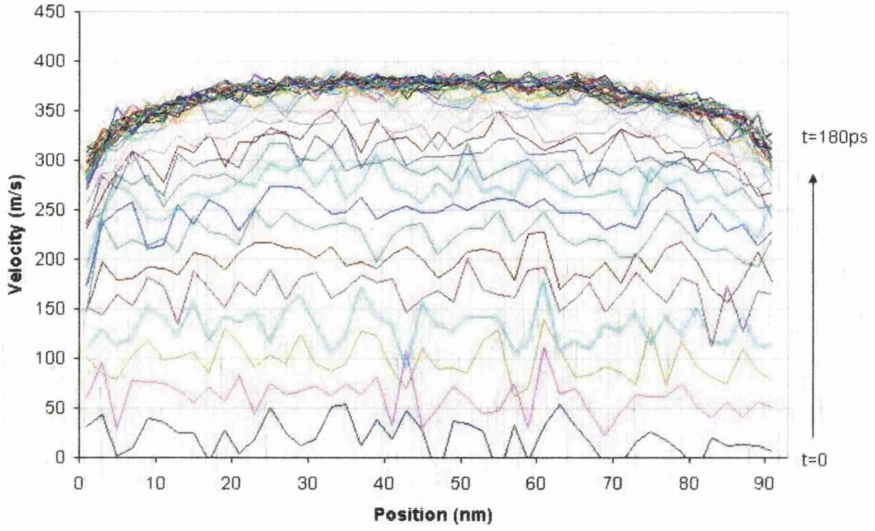


Figure 7.10: Bulk ensemble velocity profiles taken at $2ps$ intervals. At $t = 0$ the fluid is at rest.

$t = 0$, the initial velocity increase in between ensembles is large and the data contains a lot of variation, however as the simulation progresses the change in velocity between successive profiles reduces until the equilibrium state is reached. Once equilibrium has been reached, the successive velocity profiles are almost identical and show significantly less variation than at the start of the simulation, where diffusion is a higher component of the resultant velocity of the molecules.

The above simulation was repeated for systems of the same volume containing $40,000$, $60,000$ and $100,000$ to examine the effect that a density increase had on large systems in terms of both the fluid behaviour, and the performance of the simulation. All simulations were performed with the same approximated pressure gradient of $1 \times 10^{13} m/s^2$, and using the same parameters for collecting the ensemble properties.
The resulting steady state profiles are shown in Figure 7.11 for the four different densities. The average of four extracted profiles is shown with variation in each case of $\pm 7m/s$. From this graph the difference between the simulations of different densities can be seen. All of the results show boundary layer effects at both walls, however the velocity at the wall is slightly higher on the right hand side of the graph. This is due to the distance between the nodes and the solid boundary, which is $1nm$ on the left of the graph and $3nm$ on the right. This

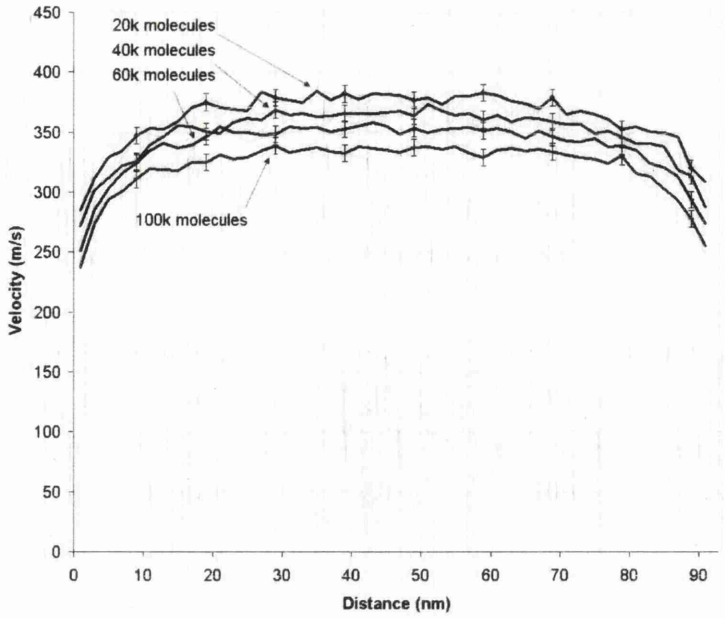


Figure 7.11: Steady state velocity profiles for slit channel systems with $20,000$ (top) $40,000$ (middle top), $60,000$ (middle bottom) and $100,000$ (bottom) molecules, corresponding to densities of 1.58, 3.15, 4.73, and $7.89kg/m^3$. For clarity the average profile is shown with $\pm 7m/s$

has been done to highlight the errors that are introduced at the boundaries. If a nodes 'zone of influence' extends beyond the boundaries of the fluid only a proportion of its available area may contain molecules, hence there are fewer molecules from which to sample the local behaviour. This leads to an increase in the variation in the results, as fewer points in the available phase space are sampled, an effect that can be clearly seen when comparing the results of the four simulations on the left and right hand sides of the graphs. Here, the node placed at $3nm$ from the boundary is has its $2.5nm$ 'zone' fully within the fluid domain and shows a clear distinction between the four sets of results. The final node on the left, placed at $1nm$ from the boundary shows more variation as more of the nodes 'zone' is outside the fluid domain. However, this node captures a lower velocity at the boundary than the node on the right. This is an important effect to consider when placing nodes within the domain, as nodes closer to the boundaries give better information about the behaviour at the boundary but only if the information is within an acceptable tolerance. This effect is minimised when the number of molecules is increased and as the percentage difference between the number of molecules in boundary nodes

and the number of molecules in other nodes is reduced.
As the density of the simulation is increased, the average velocity in the channel decreases. In continuum terms, increasing the density of a simulation increases the Reynolds number however at molecular scales, the concept of Reynolds number is not well defined due to the variation of flow properties. A flow with a higher Reynolds number could potentially mean higher losses within the system, and Chapter 6 highlighted that higher losses were found in systems with high diffusion of energy and lower diffusion of mass. Higher density simulations exhibit an increased number of collisions due to the increased number of neighbouring molecules.

### 7.3.1 Performance of Meso Scale Simulations

These meso scale simulations at different densities contain large numbers of molecules, from 20,000 to 100,000. The performance tests performed earlier in this chapter highlighted the high demand of high density simulations, and as a result these tests were performed at relatively low densities. All simulations in this section were performed on a Xeon 3.2GHz processor with 6GB RAM. To examine the performance similar data to previous tests was extracted, in the form of neighbour pairs and simulation time.
Figure 7.12 shows a plot comparing the number of molecules in the simulation against the number of neighbour pairs per molecule. The graph shows the same linear relationship to that shown by the smaller scale variable density simulations in Figure 7.6, although in these tests the density is much lower (small scale density simulations were performed at a density of $72.8kg/m^3$).
Figure 7.13 shows a plot of the simulation rate of the variable density simulations at meso scales. From this, an exponential decrease on the number of time steps that can be performed per hour as the number of molecules in the system increases. In the 20,000 molecule case 3483 time steps could be completed in an hour, but by increasing the number of molecules by a factor of 5, the number of steps that can be processed decreases by a factor of 21.4 to 163 per hour. This demonstrates the high cost of large systems of molecules. The computational cost could increase significantly for systems of higher densities.

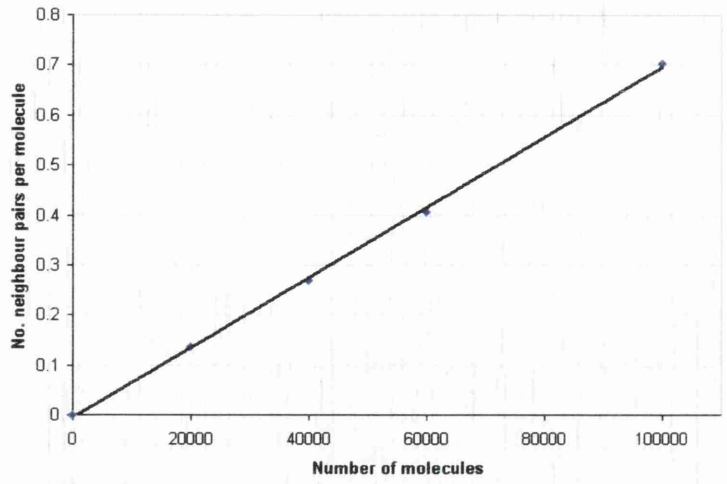


Figure 7.12: Number of molecules plotted against number of neighbour pairs per molecule for the meso scale density simulations.

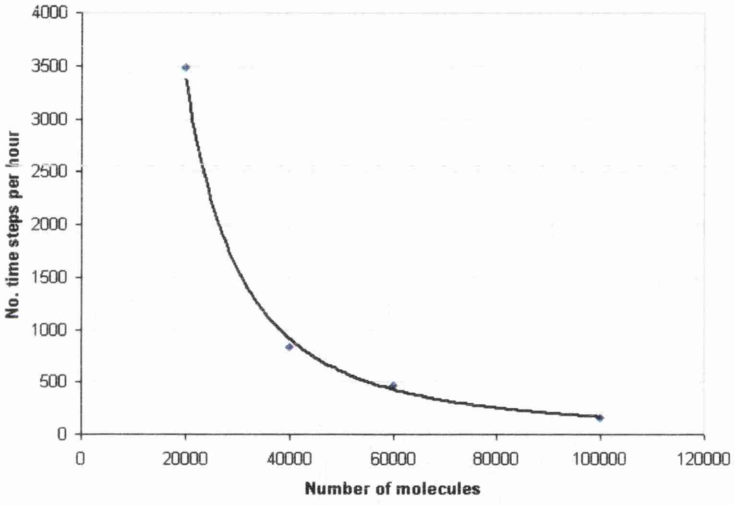


Figure 7.13: Plot of number of time steps achieved per hour against the number of molecules in the meso scale variable density simulations

### Predictions

Using the data collected in the above section, it is possible to predict the consequences of dramatically increasing the number of molecules. Figure 7.14 shows a plot of the number of molecules against the number of neighbour pairs for the same, constant volume, examples shown above. In this figure, the line of best fit has been extended to predict the number of neighbours present if there were one million molecules in the same volume. The figure shows that

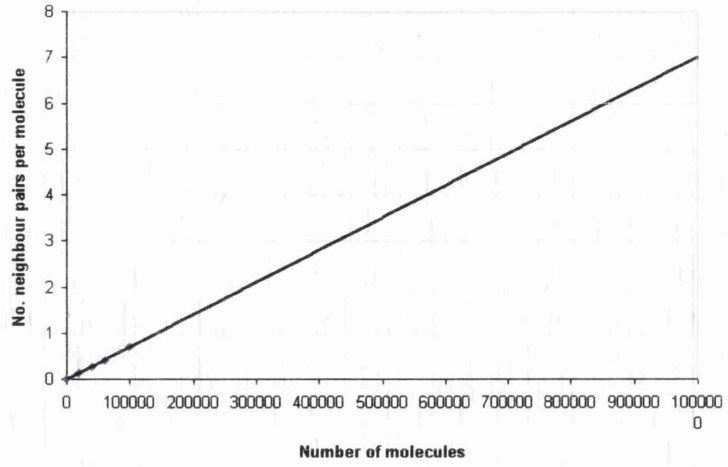


Figure 7.14: Plot predicted from previous data of number of molecules plotted against number of neighbour pairs per molecule for up to $1M$ molecules

on average there would be approximately seven neighbour pairs per molecule. As has been shown above, the density of the system impacts strongly on the CPU time and resources required to complete each time step. Figure 7.15 shows a plot of the number of molecules against the number of time steps that can be completed per hour. This figure has used the line of best fit to predict the number of time steps completed per hour for a system containing one million molecules. The plot shows that approximately 2.2 time steps can be

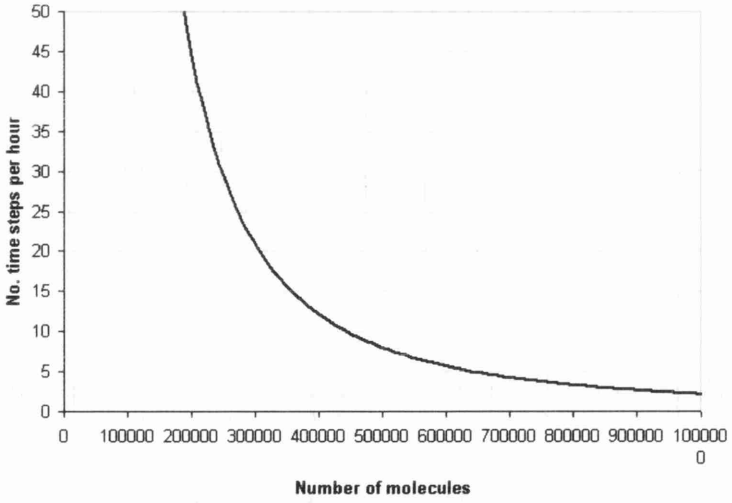


Figure 7.15: Plot predicted from previous data of number of time steps achieved per hour against the number of molecules up to $1M$

completed per hour. This dramatic reduction is due to the time processing the movement of such a large number of molecules, the time searching through the domain for neighbouring molecules, and the evaluation of the forces between neighbour pairs (which is also increased as the high density of the system generates a larger number of force interactions to be processed). To perform the same $180ps$ equilibration time with a one million molecule simulation would take approximately 4.6 years of continuous simulation time. This time could be seriously reduced with the implementation of parallel processing, and by performing searches for neighbour pairs over smaller subdomains rather than over the global system.

## 7.4 Summary

This chapter has presented a large number of issues associated with modelling meso scale systems with a molecular model. At meso scales, the number of molecules begins to prohibit the range of systems that can be simulated. The limit on the molecular model is no in terms of scale and dimensions but in terms of the number of molecules and the density of the system. The penalty in terms of increased computational cost increases exponentially as the number of molecules or density increases.

From the bulk property extraction method point of view, as the number of molecules increases over the length scale of the simulation, the better the definition and the more stable the ensemble averages of the bulk properties become. A greater number of molecules improves the phase space sampling at each of the nodes allowing for a better resolution in time as well as space compared to the length scale of the simulation.

# Chapter 8

# Conclusions and Future Work

## 8.1 Summary and Conclusions

The work presented in this thesis demonstrates the developed method for simulating fluid behaviour of meso scale systems. This method provides a versatile environment with which to investigate fluid flow systems in the region of $1\mu m$ to $50nm$ where molecular physics play a substantial part in fluid behaviour or complex molecular effects are present which cannot be considered by generalised governing equations.
The work undertaken has focused on the following points:

- *Mesoscopic description of fluid.* Meso scale systems, by their nature, can neither be fully defined by continuum not molecular mechanics. The continuum governing equations and existing mesoscopic methods fail to account for the in depth detail of the molecular scale effects that alter the behaviour of the flow [45]. Molecular models include the correct physics for simulations of fluid systems but the bulk effects are not characterised from the molecular behaviour. Several schemes have been developed to couple molecular regions to continuum with some success (Chapter 4) but these deal with small molecular regions, including the molecular information into the boundary conditions or as a correction. This approach deals with meso scale systems directly, using the ensemble descriptions of large scale fluid properties to extract and characterise the bulk effects occurring within the fluid.
  In this method the molecular model for the fluid behaviour is over-

looked by a system of nodes placed within the domain, which collect local ensemble averages for bulk fluid properties. This presents a versatile environment for meso scale fluid investigation, as any fluid property which can be described as an ensemble can be extracted as a distribution within the flow field. Examples have been shown for temperature and bulk velocity, but other properties can also be easily implemented such as density and pressure.

The parametric study performed in Chapter 5 has demonstrated the versatility of this approach, allowing for easy implementation for a wide variety of different systems. For equilibrium systems, the bulk properties can be initially taken over short time periods to observe the approach to equilibrium, and then either lengthened to achieve stable property distributions or averages taken of shorter ensembles. These sample and ensemble parameters, along with the radius of the nodes can be used to tailor the simulation to the exact requirements of the system of interest.

- *Mesoscopic molecular fluid model* The above bulk properties are extracted from a molecular model. The computation of the molecular model represents a large computational load, and a fully molecular simulation would be very computationally expensive, especially for common engineering applications the include complex geometries. A molecular model was developed especially to operate in the meso scale region. This model employed simplifications at the boundaries that allowed all solid molecules to be removed from the simulation, allowing the computational effort to focus more on the internal fluid interactions. Also implemented was an approximation for a pressure driven flow, where a uniform acceleration is applied to all molecules. This approximation must be balanced by a thermostat to balance the system energy as the application of the acceleration adds energy to the molecules artificially. This approximation allows only the area of interest to be simulated where all molecules are participating in the construction of the resulting ensemble averages.

  This mesoscopic model for fluid behaviour is however still limited by the computation of the molecules within the system. The model has been validated against existing work [66] using a well developed, fully molecular fluid model, and extensive testing has been performed to identify the issues in using this model with large numbers of molecules. This high-

lighted the importance of considering system density, and the increased load associated with it. Theses studies showed that using this meso scale molecular model systems within the meso scale could be reached with up to 100,000 molecules being simulated easily on a server or high end desktop machine.

These two tools combine to generate a powerful and versatile method for the simulation of meso scale fluid systems. The method represents the first step to developing a complete meso scale engineering simulation environment, which presents a large scope for future work.

## 8.2 Future Work

The work presented in this thesis demonstrates how this method has been developed and implemented. The focus had been on developing a versatile and powerful engineering tool for meso scale systems, and presents large scope for future work. Recommended directions for future development are discussed below:

- *Search efficiency.* Much of the time spent processing the molecular model is spent searching for neighbours within the domain. As the system size increases as compared to the interaction radius of the individual molecules and the number of molecules increases, the proportion of time spent searching throughout the domain for neighbour pairs. This efficiency could be significantly increased by the implementation of a second level of search routine, where frequent neighbour searches are performed over smaller subdomains of the flow field.

- *Parallel implementation.* To allow the meso-molecular model access to larger systems containing upward of 1,000,000 molecules, this method would require parallelisation to take advantage of multiple processor machines to allow the storage of more molecules, and longer neighbour lists, and reduce the computation time per molecule. This is also compatible with methods of improving search routines as a form of domain decomposition would be required.

- *Meso scale boundary conditions* For most engineering problems, the typical periodic boundary condition used in MD simulations, that the fluid

properties must be identical on opposite sides of the simulation cell, is unrealistic, as illustrated in Figure 8.1. The figure on the left shows the type of system that can be simulated using periodic boundary conditions. The limitation of these conditions is that the fluid at opposite

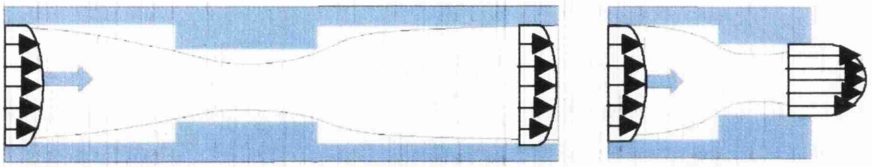

Figure 8.1: **Left:** Flow restriction modelled with current periodic boundary conditions, molecular energy conserved **Right:** Modified boundaries allow a different type of problem to be simulated

sides of the simulation cell must be at identical states to prevent violation of thermodynamic laws. In order to simulate the change in fluid properties at intermediate sections e.g. a restriction, the inlet and outlet conditions will need to be exactly same and hence, far away from the restriction to apply periodic boundary conditions. This means that independent conditions cannot be applied to the boundary to solve common fluid flow situations that occur in engineering problems. For example, the boundary condition as shown in Figure 8.1 (right), cannot be evaluated using periodic boundaries. However, maintaining the invisibility of the boundary to the fluid molecules presents a significant challenge.

- *Investigate and develop energy/temperature controls* This thesis has identified that the current temperature controls are insufficient to deal with increases in temperature due to changing internal dynamics. This needs more investigation and possibly a new method for applying system controls.

# References


[1] S. Gosh, A. Sood, and N. Kumar. Carbon nanotube flow sensors. *Science*, 299:1042, 2003.

[2] R. Karnik, R. Fan, M. Yue, D. Li, P. Yang, and A. Majumdar. Electrostatic control of ions and molecules in nanofluidic transistors. *Nano Lett.*, 5:943–948, 2005.

[3] Y. Park, K. Nam, S. Ha, P. Pai, C. Chung, and S. Lee. Porous poly(l-lactide) membranes for guided tissue regeneration and controlled drug delivery: membrane fabrication and characterization. *J. Cont. Rel.*, 43:151–160, 1997.

[4] M. Riegelman, H. Liu, and H. Bau. Controlled nanoassembly and construction of nanofluidic devices. *J. Fluid Eng.*, 128:6–13, 2006.

[5] H. R. Wu, Y. L. He, G. H. Tang, and W.Q. Tao. Lattice boltzmann simulation of flow in porous media on non-uniform grids. *Prog. Comp. Fluid Dyn.*, 5(1/2):97–103, 2005.

[6] P. J. Hoogerbrugge and J. M. Koleman. Simulating microscopic hydrodynamic phenomena with dissipative particle dynamics. *Europhys. Lett.*, 19:155, 1992.

[7] J. F. Douglas, J. M. Gasiorek, J. A. Swaffield, and L.B. Jack. *Fluid Mechanics.* Pearson Education, 5th edition, 2005.

[8] J. M. Haile. *Molecular Dynamic Simulation, Elementary Methods.* Wiley-Interscience, 1997.

[9] Sir. J. Jeans. *An Introduction to the Kinetic Theory of Gasses.* Cambridge, 1967.

[10] *Oxford English dictionary.* Oxford Uni. Press, 2nd edition, 1989.

[11] O. Reynolds. An experimental investigation of the circumstances which determine whether the motion of water shall be direct or sinuous, and of the law of resistance in parallel channels. *Roy. Soc.*, (44):52–105, 1883.

[12] A. G. Malan. *Investigation into the Continuum Thermodynamic Modeling of Investment Casting Shell-Mould Drying.* PhD thesis, Uni. Wales Swansea, 2002.

[13] J. D. Van Der Waals. *On the Continuity of the Gaseous and Liquid States.* Dover Publications, 2004.

[14] F. London. On centers of van der waals attraction. *J. Phys. Chem.*, 46:305–317, 1942.

[15] M. Massimi. *Pauli's Exclusion Principle.* Cambridge University Press, 2005.

[16] G. Dharmadurai. Solid state density equations if state for fluids. *J. Phys. III France*, 6:505–509, 1996.

[17] D. Keffer. Thermodynamic properties of a single component fluid. *Uni. Knoxville*, March 2001.

[18] D. Frenkel and B. Smit. *Understanding molecular simulation*, volume 1. Accademic Press, 2002.

[19] M. Lewerenz. *Monte Carlo Methods: Overview and Basics*, volume 10. John von Neumann Institute for Computing, 2002.

[20] N. Metropolis, A. Rosenbluth, M. Rosenbluth, Teller A, and Teller E. Equation of state calculations by fast computing machines. *J. Chem. Phys.*, 21:1087–1092, 1953.

[21] C. Pangali, M. Rao, and B. Berne. On a novel monte carlo scheme for simulating water and aqueous solutions. *Chem. Phys. Lett.*, 55:413–417, 1978.

[22] H. Gould, J. Tobochnik, and W. Christian. *Introduction to Computer Simulation Methods:Applications to Physical Systems.* Addison-Wesley, 3rd edition, 2006.

[23] D. Levesque, A. Gucquel, F. Lamari Darkrim, and S. Beyaz Kayiran. Monte carlo simulations of hydrogen storage in carbon nanotubes. *J. Phys: Cond. Matt.*, 14:2985–9293, 2002.

[24] D. N. Blauch. Kinetic molecular theory. http://www.chm.davidson.edu /ChemistryApplets/KineticMolecularTheory/ Maxwell.html, May 2006.

[25] R. Radhakrishnan and K. Gubbins. Effect of fluid-wall interaction on freezing of confined fluids: Towards the development of a global phase diagram. *J. Chem. Phys.*, 112(24):11048–11057, 2000.

[26] K. Travis and K. Gubbins. Computer simulation of isothermal mass transport in graphite slit pores. *Mol. Sim.*, 27:405–439, 2001.

[27] R. Tuzun, D. Noid, B. Sumpter, and R. Merkle. Dynamics of fluid flow inside carbon nanotubes. *Nano. Tech.*, 7:241–246, 1996.

[28] R. Cracknell, D. Nicholson, and N. Quirke. Direct molecular dynamic simulation of flow down a chemical potential gradient in a slit shaped micropore. *Phys. Rev. Lett.*, 74(13):2463–2466, 1995.

[29] C. Bing-Yang, C. Min, and G. Zeng-Yuan. Rarefied gas flow in rough micro channels by molecular dynamic simulation. *Chin. Phys. Lett.*, 21(9):1777–1779, 2004.

[30] F. Ercolessi. A molecular dynamics primer. international school for advanced studies, 1997. Italy.

[31] B. Yoon. Anisotropic phase transition of hard spheres confined in hard walls. *Bull. Korean Chem. Soc*, 22(12):1375, 2001.

[32] B. Yoon. Analytical expressions for the radial free space distribution function of the hard sphere system and the phase transition. *Chem. Phys. Lett.*, 243(1-3):35–38, 1995.

[33] B. Peterson, K. Gubbins, G. Heffelfinger, U. Marconi, and Swol F. van. Lennard-jones fluids in cylindrical pores: Nonlocal theory and computer simulation. *J. Chem. Phys.*, 88:6487, 1988.

[34] R. Radhakrishnan and K. Gubbins. Quasi-one-dimensional phase transition in nanopores: Pore-pore correlation effect. *Phys. Rev. Letts*, 79(15):2847.

[35] M. Meyer and H. Stanley. Liquid-liquid phase transition in confined water: A monte carlo study. *J. Phys. Chem. B*, 103:9728–9730, 1999.

[36] P. Poole, U. Essmann, F. Sciortino, and H. Stanley. Phase diagram for amorphous solid water. *Phys. Rev. E*, 48(6):4605–4610, 1993.

[37] S. Gatica, G. Stan, M. Calbi, J. Johnson, and M. Cole. Axial phase of quantum fluids in nanotubes. *J. Low Temp. Phys.*, 120(5/6):337–359, 2000.

[38] G. Stan and M. Cole. Low coverage adsorption in cylindrical pores. *Surf. Sci.*, 395:280–291, 1998.

[39] J. Dash, M. Schick, and O. E. Vilches. Phases of helium monolayers: search and discovery. *Surf. Sci.*, 299:405–414, 1994.

[40] M. Cole, V. Crespi, G. Stan, C. Ebner, Hartman J, Moroni S, and Boninsegni M. Condensation of helium in nanotube bundles. *Phys. Rev. Lett*, 84:3883, 2000.

[41] M. Miyahara and K. Gubbins. Freezing/melting phenomena for lennard-jones methane in slit pores: A monte carlo study. *J. Chem. Phys*, 106(7):2865–2880, 1997.

[42] M. Maddox and K. Gubbins. A molecular simulation study of freezing/melting phenomena for lennard-jones methane in cylindrical nanoscale pores. *J. Chem. Phys.*, 107(22):9659–9667, 1997.

[43] H. Kim and W. Steele. Computer simulation study of the phase diagram of the methane monolayer on graphite: Corrugation effects. *Phys. Rev. B*, 45(11):6226–6233, 1992.

[44] L. Gelb. *The Ins and Outs of Capillary Condensation in Cylindrical Pores.* Florida State Univ., 2002.

[45] K. Travis, B. Todd, and D Evans. Departure from navier-stokes hydrodynamics in confined liquids. *Phys. Rev. E*, 55(4):4288–4295, 1997.

[46] E. Lauga, M. Brenner, and H. Stone. *Handbook of experimental fluid dynamics.* Springer, 2005.

[47] C. J. Maxwell. On stresses in rarefied gasses arising from inadequacies of temperature. *Phil. Trans. RoS I*, 170:231–256, 1897.

[48] M. Von. Smoluchowski. Ueber wrmeleitung in verdnnten gasen. *Annalen der Physik und Chemi*, 64:10130, 1898.

[49] M. Gad el Hak. The fluid mechanics of microdevices - the freeman scholar lecture. *Fluids Eng.*, 121:5–33, 1999.

[50] M. Gad el hak. *Liquids: The holy grail of microfluidics modelling.* Virginia Commonwealth University, 2004.

[51] W. Loose and S. Hess. Rheology of dense model fluids cua non-equilibrium molecular dynamics: shear thinning and ordering transition. *Rheologica Acta*, 28:91–101, 1989.

[52] J. Pfahler, J. Harley, and B. Bau. Liquid transport in submicron channels. *Sensors and Actuators*, A21-A23:431–434, 1990.

[53] H. Rafii-Tabar, L. Hua, and M. Cross. A multi-scale atomistic-continuum modelling of crack propagation in a two-dimensional macroscopic plate. *J. Phys: Cond. Mat.*, 10:2375, 1998.

[54] G. Ayton, S. Bardenhagen, P. McMurtry, D. Sulsky, and G. Voth. Interfacing molecular dynamics with continuum dynamics in computer simulation: Toward an application to biological membranes. *IBM J. Res. and Dev.*, 45(3/4):417–426, 2001.

[55] F. Abraham. Dynamically spanning the length scales from the quantum to the continuum. *J. mod. Phys. C*, 11(6):1135–1148, 2000.

[56] A. L. Garcia, J. B. Bell, W. Y. Crutchfield, and B. J. Alder. Adaptive mesh and algorithm refinement using direct simulation monte carlo. *J.Comp. Phys.*, 154,:134–155, 1999.

[57] X. Nie, S. Chen, W. E, and M. Robbins. A continuum and molecular dynamics hybrid method for micro- and nano-fluid flow. *J. Fluid Mech.*, 500:55–64, 2004.

[58] E. S. Boek, P. V. Coveney, H. N. W. Lekkerkerker, and P. van der Schoot. Simulating the rheology of dense colloidal suspensions using dissipative particle dynamics. *Phys. Rev. E*, 55(3):3124, 1997.

[59] P. V. Coveney and K. E. Novik. Computer simulations of domain growth and phase separation in two-dimensional binary immiscible fluids using dissipative particle dynamics. *Phys. Rev. E*, 54(5):5134–5141, 1996.

[60] A. G. Schlijper, P. J. Hoogerbrugge, and C. W. Manke. Computer simulation of dilute polymer solutions with the dissipative particle dynamics method. *J. Rheol.*, 39(3):567–579, 1995.

[61] J. Tolke, M. Krafczyk, M. Schulz, and E. Rank. Lattice boltzmann simulations of binary fluid flow through porous media. *Philos Transact A Math Phys Eng Sci*, 360(1792):535–545, 2002.

[62] M. M. Dupin, I. Halliday, and C. M. Care. Multi-component lattice boltzmann equation for mesoscale blood flow. *J. Phys. A*, 36:8517–8534, 2003.

[63] S. Naris, D. Valougeorgis, F. Sharipov, and D. Kalempa. Discrete velocity modelling of gasious mixture flow in mems. *S.Latt and M.Struct*, 35:629–643, 2004.

[64] R. Qin. Dl meso. http://www.ccp5.ac.uk/dlmeso/DL MESO.html, Sept. 2006.

[65] M. P. Allen and D. J. Tildesley. *Computer simulation of liquids.* Oxford, 1997.

[66] V. Sokhan, D. Nicholson, and N. Quirke. Fluid flow in nanopores: an examination of hydrodynamic boundary conditions. *J. Chem. Phys.*, 115:3878, 2001.

[67] G. Arya, H. Chang, and E. Maginn. Knudsen diffusivity of a hard sphere in a rough slit pore. *Phys. Rev. Lett.*, 91(2):026102, July 2003.

[68] E. Clementi. Global scientific and engineering simulations on scalar, vector and parallel lcap-type supercomputers. *Phil. Trans Roy. Soc. A*, 326:445470, 1988.

[69] K. G. Wilson and J. B. Kogut. The renormalization group and the $\epsilon$ expansion. *Phys. Rep.*, 12:77–199, 1974.

[70] E. B. Tadmor, M. Oritz, and R. Phillips. Quasicontinuum analysis of defects in crystals. *Phil. Mag. A*, 73:1529–1563, 1996.

[71] V. B. Shenoy, R. Miller, E. B. Tadmor, R. Phillips, and M.Oritz. Quasicontinuum models of interfacial structure and deformation. *Phys. Rev. Lett.*, 80:742, 1998.

[72] V. B. Shenoy, R. Miller, E. B. Tadmor, D. Rodney, R. Phillips, and M. Oritz. An adaptive finite element approach to atomic-scale mechanicsthe quasicontinuum method. *J. Mech. Phys. Solids*, 47:611, 1999.

[73] D. Rodney and R.Phillips. Structure and strength of dislocation junctions: An atomic level analysis. *Phys. Rev. Lett.*, 82:1704, 1999.

[74] R. Miller, M. Oritz, R. Phillips, V. Shenoy, and E. B. Tadmor. Quasicontinuum models of fracture and plasticity. *Eng. Frac. Mech.*, 61:427, 1998.

[75] L. B. Lucy. A numerical approach to the testing of the fission hypothesis. *Astro. J.*, 82:1013–1024, 1977.

[76] J. Feldman. *Dynamic refinement and boundary contact forces in Smoothed Particle Hydrodynamics with applications in fluid flow problems.* PhD thesis, School of Engineering, Swansea University, June 2006.

[77] J. J. Monaghan. Smoothed particle hydrodynamics. *ARAA*, 30:543–74, 1992.

[78] E. Fasshauer. Toward approximate moving least squares approximation with irregularly spaced centers. *Illinois inst. of Technology*, 2003.

[79] J. Liao and S. Yip. Coupling continuum to molecular dynamics simulation: Reflecting particle method and the field estimator. *Phys. Rev. E*, 57(6):7259–7267, 1998.

[80] S. Shen and S. Atluri. Computational nano-mechanics and multi-scale simulation. *CMC*, 1(1):59–90, 2004.

[81] R. E. Rudd and J. Broughton. Coarse-grained molecular dynamics and the atomic limit of finite elements. *Phys. Rev. B*, 58:5893, 1998.

[82] L. Verlet. Computer experiments on classical fluids. i. thermodynamical properties of lennard-jones molecules. *phys. rev.*, 159:98, 1967.

[83] M. Sun and C. Ebner. Molecular dynamics simulation of compressible fluid flow in two dimensional channels. *Phys. Rev. A*, 46(8):48134818, October 1992.

[84] C. W. Gear. The numerical integration of ordinary differential equations of various orders. Technical Report 7126, Argonne National Laboratory, 1966.

[85] C. W. Gear. *Numerical initial value problems in ordinary differential equations.* Prentice-Hall, 1971.

[86] S. Cooper, B. Cruden, and M. Meyyappan. Gas transport characteristics through carbon nanotubes. *Nano Lett.*, 4(2):377–381, 2004.

[87] S. Bhatia, H. Chen, and D. Sholl. Comparisons of diffusive and viscous contributions to transport coefficients of light gasses in single walled carbon nanotubes. *Univ. Queensland.*

[88] V. Sokhan, D. Nicholson, and N. Quirke. Fluid flow in nanopores: Accurate boundary conditions for carbon nanotubes. *J. Chem. Phys.*, 117(18):8531–8539, 2002.

[89] D. Evans, W. Hoover, B. Failor, B. Moran, and A. Ladd. Non equilibrium molecular dynamics via gauss's principle of least constraint. *Phys. Rev. A*, 28(2):1016–1020, 1983.

[90] D. J. Evans and G. P. Morriss. *Statistical mechanics of non equilibrium liquids.* Theoretical Chemistry Monograph Series. Academic Press, London, 1990.

[91] A. Branka and K. Wojciechowski. Generalisation of nosé and nosé-hoover isothermal dynamics.

[92] S. Nose. Constant-temperature molecular dynamics. *J. Phys.: Cond. Matt.*, 2:SA115–SA119, 1990.

[93] S. Nosé. A unified formulation of the constant temperature dynamics methods. *J. Chem. Phys*, 81(1):511–519, 1984.

[94] M. Tuckerman and M. Parrinello. Integrating the carparrinello equations. i. basic integration techniques. *J. Chem. Phys.*, 101(2):1302, 1994.

[95] W. Smith, T. R. Forester, I.T. Todorov, and M. Leslie. *THE DL_POLY 2 USER MANUAL*, volume 2.16. CCLRC Daresbury Laboratory, Daresbury, Warrington WA4 4AD, UK, March 2006.

[96] G. H. L. Hagen. Ueber die bewegung des wassers in engen cylindrischen rohren. *Poggendorfs Annalen der Physik und Chemie*, 16, 1839.

[97] H. Darcy. Recherches experimentales relatives au movement de leau dans les tuyaux. *Paris: Imprimerie Nationale*, 1857.

[98] F. McMurry. *chemistry*, volume Prentice-Hall Inc. fourth edition edition, 2004.

[99] A. Guinier. *The Structure of Matter.* Edward Arnold Inc., 1984.

[100] S. Chapman and T. G. Cowling. The mathematical theory of non uniform gasses. *Cambridge university press*, 1961.

[101] D. Heyes, J. Baxter, U. Tuzun, and R. Qin. Discrete element method simulations: From micro to macro scales. *Phil. Trans. R. Soc. Lon. A*, 362:1853–1865, 2004.

[102] J. Liao and S. Yip. Nearly exact solution for coupled continuum/md fluid simulation. *J. Comp. Aid. Mat. Des.*, 6:95–102, 1999.

[103] J. Bonet and J. Peraire. An alternating digital tree (adt) algorithm for 3d geometrical searching and intersection problems. *Int. J. Num. Methods in Eng.*, 31:1–17, 1991.